PERMEABILITY WITHIN BASALTIC OCEANIC CRUST

Andrew T. Fisher
Earth Sciences Department and Institute of Tectonics
University of California, Santa Cruz

Abstract. Water-rock interactions within the seafloor are responsible for significant energy and solute fluxes between basaltic oceanic crust and the overlying ocean. Permeability is the primary hydrologic property controlling the form, intensity, and duration of seafloor fluid circulation, but after several decades of characterizing shallow oceanic basement, we are still learning how permeability is created and distributed and how it changes as the crust ages. Core-scale measurements of basaltic oceanic crust yield permeabilities that are quite low (generally 10^{-22} to 10^{-17} m^2), while in situ measurements in boreholes suggest an overlapping range of values extending several orders of magnitude higher (10^{-18} to 10^{-13} m^2). Additional indirect estimates include calculations made from borehole temperature and flow meter logs (10^{-16} to 10^{-11} m^2), numerical models of coupled heat and fluid flow at the ridge crest and within ridge flanks (10^{-16} to 10^{-9} m^2), and several other methods. Qualitative indications of permeability within the basaltic oceanic crust come from an improved understanding of crustal stratigraphy and patterns of alteration and tectonic modification seen in ophiolites, seafloor samples and boreholes. Difficulties in reconciling the wide range of estimated permeabilities arise from differences in experimental scale and critical assumptions regarding the nature and distribution of fluid flow. Many observations and experimental and modeling results are consistent with permeability varying with depth into basement and with primary basement lithology. Permeability also seems to be highly heterogeneous and anisotropic throughout much of the basaltic crust, as within crystalline rocks in general. A series of focused experiments is required to resolve permeability in shallow oceanic basement and to directly couple upper crustal hydrogeology to magmatic, tectonic, and geochemical crustal evolution.

1. INTRODUCTION

1.1. Permeability and Fluid Flow Within Oceanic Crust

Permeability is the most important hydrologic parameter influencing the movement of fluids through Earth's crust. Fluid flow within basaltic oceanic crust transports heat and solutes, modifies the physical state of the crust and the overlying ocean, and impacts processes as diverse as seismicity at ridges and subduction zones, the chemistry and occurrence of arc volcanism, and the distribution of seafloor biological communities. Despite its importance, we presently have a limited understanding as to how permeability is distributed within upper oceanic basement. This understanding is based largely on direct measurements in a few boreholes and an eclectic collection of indirect estimates. Each approach incorporates specific spatial and temporal scales, as well as assumptions regarding the form of permeability, making it difficult to integrate the interpretations into a single model.

This paper summarizes recent studies that directly or indirectly address the distribution of permeability in the upper igneous oceanic crust, places results in context, and suggests where future work might be directed. Numerous excellent reviews of fluid flow in Earth's crust [e.g., *Cathles*, 1990; *Lowell*, 1991; *Garven*, 1995; *Person et al*., 1996] and the extent and influence of hydrothermal circulation within the seafloor [e.g., *Lowell et al*., 1995; *Humphris et al*., 1995; *Alt*, 1995] have been published in the last few years. The present review is not intended to duplicate these comprehensive summaries, although there is limited overlap, but instead focuses on the magnitude and distribution of permeability within basaltic oceanic crust, how it is established and modified, and how measurements scale, and on assumptions about fluid flow influence our current understanding.

The significance of fluid flow within the oceanic crust has been appreciated since some of the earliest seafloor heat flow studies identified areas containing both high and low values, often over young, thinly sedimented oceanic crust [*Von Herzen and Uyeda*, 1963; *Lee and Uyeda*, 1965; *Lee and Uyeda*, 1965; *Elder*, 1965]. With the development of analytical cooling models of the lithosphere [*McKenzie*, 1969; *Sclater and Francheteau*, 1970], it soon became apparent that much of the expected conductive heat flow through young oceanic crust was missing and that the discrepancy between models and observations might be attributed to hydrothermal circulation [e.g., *Le Pichon and Langseth*, 1969; *Lister*, 1972]. While the magnitude of the total seafloor heat flow anomaly (the extent of deviation from a conductive reference model) is contentious [e.g., *Stein and Stein*, 1992, 1994], it is widely accepted that a significant fraction of oceanic crustal heat loss occurs advectively when

Reviews of Geophysics, 36, 2 / *May 1998*
pages 143–182
8755-1209/98/97RG-02916*$15.00*
Paper number 97RG02916

the crust is young [e.g., *Williams and Von Herzen*, 1974; *Wolery and Sleep*, 1976; *Sclater et al*., 1980] and that advection of heat from the crust generally diminishes as the crust ages, reflecting the blanketing effects of the thickening sediment layer, the blocking of pores by the deposition of hydrothermal precipitates and physical crustal consolidation, and a reduction in heat flow into the base of the crust [*Anderson et al*., 1977; *Stein and Stein*, 1994].

This paper focuses on the basaltic oceanic crust because that is where most direct measurements have been made. In addition, many of the indirect methods used to infer permeability in the oceanic crust (seafloor heat flow, numerical modeling, geophysical surveys, alteration patterns) are insensitive to hydrogeologic properties deeper than 1–2 km below the seafloor. We eventually need to understand lower crustal hydrogeology as well, but quantifying properties below the basaltic layers will require many more direct measurements.

In the remainder of this introduction, I present a brief overview of common hydrogeologic terminology and describe the general stratigraphy of the upper oceanic crust, developed through several decades of seismic, drilling, coring, dredging, and ophiolite studies. Subsequent sections summarize direct and indirect estimates of permeability within the basaltic oceanic crust, discuss whether the wide range of values might be reconciled, and suggest how several remaining questions could be resolved through carefully planned experiments.

1.2. Definitions

The following digression into terminology and basic hydrogeology will be unnecessary for readers familiar with fluid flow phenomena in porous and fractured systems. However, many others interested in permeability and fluid flow in the upper oceanic crust may be unfamiliar with the derivation of these terms and their formal meanings; in several cases the distinctions between similar terms are subtle but important.

The word "permeability" appears frequently in discussions of seafloor physical properties and fluid and mass fluxes, but its historical use has been inconsistent. The empirical work by *Darcy* [1856] related the volume flux of water through a porous medium (a column of sand packed into a cylindrical tube) to the gradient in head (energy per unit weight of water) and the cross-sectional area of the medium perpendicular to flow. The steady state volume flux, geometry of the apparatus, and force driving the flow were related through a constant of proportionality commonly known as "hydraulic conductivity," K. The dimensions of K [L T^{-1}] can be determined through consideration of the dimensions of the other terms in the volume-flux form of the Darcy equation:

$$Q = -KA \frac{dh}{dx} \tag{1}$$

The negative sign indicates that flow occurs in the direction opposite to the gradient in head. Later investigators [e.g., *Wyckoff et al*., 1934; *Hubbert*, 1940] demonstrated that hydraulic conductivity comprises the properties of the flowing fluid as well as the properties of the porous medium,

$$K = k \frac{\rho g}{\mu}$$

where k is rock or soil permeability (or "intrinsic permeability"), ρg is the specific weight of the fluid, and μ is fluid dynamic viscosity. Once again, the dimensions of k [L^2] are readily determined through an analysis of the other terms in the equation. The observation that permeability has dimensions of area might suggest that it is a measure of the equivalent cross-sectional area of an pipe or channel through which the same volume flux would occur, given an equivalent head gradient [*Gueguen et al*., 1996]. The use of permeability rather than hydraulic conductivity for describing the transmissive properties of oceanic basement is appropriate, as fluid viscosity and density are highly dependent on temperature, pressure, and composition.

Many workers have derived expressions for the permeability of porous media directly from first principles or from additional laboratory observations, typically by relating permeability to grain size and grain size distribution, the shapes of intergranular pores, or the tortuosity of flow paths [e.g., *Walsh and Brace*, 1984], but it has been difficult to find a universal set of relations that can be applied a priori to all hydrogeologic systems. The fundamental problem is that geological materials are complex and heterogeneous; subtle differences in grain size distribution or diagenesis profoundly influence permeability. Understanding and predicting permeability is even more difficult where flow follows discrete channels, as the shape, distribution, and orientation of individual pathways must be determined, as described below.

An alternative form of the Darcy equation describes the volume flux per cross-sectional area:

$$q = \frac{Q}{A} = -K \frac{dh}{dx} \tag{2}$$

where q is the "specific discharge" (or "Darcy velocity," a confusing alternative) and has the same dimensions as velocity [L T^{-1}]. The true fluid velocity through a rock depends on the details of the pore structure and the flow path followed by each particle, but a common approach for determining the average linear velocity is to divide specific discharge by the effective porosity, the interconnected void space through which fluids travel. The average linear velocity will always be greater than the specific discharge, and actual fluid velocities along irregular paths are generally greater than the linear average [*Freeze and Cherry*, 1979].

Equations (1) and (2) are one-dimensional, steady-state versions of what is widely recognized to be a multidimensional, transient process. Permeability is a tensor property, having as many as nine components

[*Bear*, 1972]. Where directions of principal permeability anisotropy coincide with coordinate axes, the tensor can be reduced to three components: k_x, k_y, and k_z. Only in the isotropic case can permeability be considered to have a single value independent of direction. Similarly, since head can be described in terms of a scalar field, the gradient in head that drives fluid flow is more properly noted as ∇h. There is no reason why the steepest descent along ∇h in a natural system should coincide with one of the principal anisotropy directions in permeability, although they are often assumed to coincide for simplicity. A head gradient oblique to the direction of greatest permeability will often drive significant flow along this direction, particularly when anisotropy is large [e.g., *Hubbert*, 1940]. Because of the tendency for fluids to follow the most permeable path, the distribution and form of permeability will often dominate the direction and intensity of flow in natural systems [*Norton and Knapp*, 1977].

Two additional terms, transmissivity and storativity, appear frequently in literature describing saturated water-rock systems, particularly in the context of water resource development and aquifer test analysis. Transmissivity is the vertically averaged product of hydraulic conductivity and aquifer thickness for two-dimensional (horizontally oriented) aquifers, $T = Kb$, and has dimensions of $[L^2\ T^{-1}]$. It is essentially a measure of the ability of an aquifer to transmit fluid. Storativity is a vertically averaged measure of the ability an aquifer to store or release fluid in response to a change in head,

$$S = \frac{\Delta V/V}{\Delta h} b$$

where ΔV is water production (positive or negative) from a unit volume V of aquifer resulting from a unit change in head (Δh). Within saturated seafloor systems, storativity comprises two primary components: aquifer (pore) compressibility and fluid compressibility. Rock grain compressibility is generally assumed to be sufficiently small to be neglected. Both fluid compressibility (isothermal) and fluid expansivity (isobaric) contribute to storativity in systems undergoing changes in pressure and temperature. All water that comes out of (goes into) a seafloor aquifer must come out of (go into) storage, unless there is a recharge (discharge) source. At steady state, flows into and out of an aquifer balance, and there will be no net change in storage; within transient systems the difference between input and output must be balanced by a change in storage.

Permeability varies over many orders of magnitude within natural geological systems, from $<10^{-21}$ m^2 in shales and massive crystalline rocks to $>10^{-12}$ in fractured rocks and clean, well-sorted sandstones [e.g., *Freeze and Cherry*, 1979; *Clauser*, 1992; *Neuzil*, 1994]. Variations in permeability of several orders of magnitude are common over length scales of centimeters or less, making it difficult to assess this fundamental hydrologic parameter. Hydrogeologists often deal with small-scale heterogeneity through adoption of a continuum approach, including the selection of a representative elemental volume (REV). The REV is (modified from *Bear* [1993]) a rock volume of sufficient size and shape such that (1) the REV contains both rock and void space in consistent proportions no matter where the REV is applied in the domain, (2) a sample (rock or fluid property) taken at a single point within the REV is characteristic of the entire REV, and (3) there would be no statistical change in properties of the REV if the volume was incrementally changed. The last requirement provides both upper and lower bounds on REV size. Selection of an appropriate REV depends on the timescale and length scale of interest, as well as on the nature of the fluid, heat, or solute transport problem under consideration.

Another difficulty in determining permeability in the igneous oceanic crust is that the basalt comprising the shallowest volcanic basement is often fractured. *Norton* [1988, p. 610] described permeability within fractured hydrothermal systems as being "a measure of the geometric properties of percolation networks that control the magnitude of flow." Flow in fractured and fractured-porous rocks may be considered in terms of an equivalent REV (within which some porous medium is assumed to adequately represent the fractured system), through analysis of discrete flow channels (ignoring flow through the remaining rock within the system, assumed to be insignificant), through a combination approach (dual porosity, dual permeability) that incorporates components of porous and fractured flow systems, with limited or free exchange between the two [e.g., *Pinder et al*., 1993; *Kohl and Hopkirk*, 1995; *Dershowitz and Miller*, 1995], or as a percolation network [e.g., *Gueguen et al*., 1991; *David*, 1993]. As will be described later, the first two approaches are by far the most common to have been applied to the basaltic oceanic crust.

One common approach for representing permeability within fractured rock is based on the Navier-Stokes equations for viscous flow between two parallel plates [e.g., *Snow*, 1968; *Norton and Knapp*, 1977], resulting in an equivalent permeability of $k = Na^3/12$, where a is fracture aperture and N is the number of fractures per unit length of rock exposure perpendicular to flow. Modifications to the "cubic" rule include replacing the fracture aperture term with mean aperture or hydraulic (effective) aperture terms [e.g., *Brown*, 1987; *Zimmerman and Bodvarsson*, 1996]. A similar approach for representing a single fracture (distinct from the surrounding rock) is to cast constitutive flow equations in terms of fracture transmissivity,

$$T = a^3 g/12\nu$$

where g is gravitational acceleration and ν is kinematic viscosity [e.g., *Keller et al*., 1995]. Application of these cubic rules often involves predicting equivalent porous

medium permeability or fracture transmissivity from measured fracture parameters (size, distribution, roughness, and occurrence of asperities). The equivalent porous medium approach has a firm theoretical basis for idealized geometries, but applicability to natural systems has been rigorously tested in only a few cases [e.g., *Gale and Raven*, 1980; *Tsang*, 1984; *Keller et al*., 1995], and often found to be unreliable [e.g., *Lee and Farmer*, 1993].

The discrete channel approach presents additional challenges. The Darcy equation has been found to apply consistently only under laminar flow conditions, when the Reynolds number (ratio of viscous forces to inertial forces) is very low. *Bear* [1972] demonstrated that nonlinear flow behavior within porous systems may occur well below the Reynolds number criterion for turbulence, and *Zimmerman and Bodvarsson* [1996] suggest that the critical Reynolds number for development of nonlaminar flow within rough-walled channels could be lower by a factor of 10^3 than that within smooth channels. Perhaps of greater practical difficulty, one must know in advance the geometry and properties of particular flow channels or have a good statistical understanding of the distribution and properties of the natural fracture set [e.g., *Dershowitz and Miller*, 1995; *Mattison et al*., 1997; *Glover et al*., 1997]. Because seafloor mapping of fracture paths is limited to outcrop and borehole exposures, attempts to describe permeability in the basaltic oceanic crust in terms of discrete channels have generally been limited to idealized "fracture loop" models [e.g., *Lowell*, 1975; *Strens and Cann*, 1982]. Ophiolites provide additional opportunities to map fracture patterns in multidimensional detail, but by the time these rocks are exposed on land, many of the fractures are sealed and it is difficult to know when they were open [*van Everdingen*, 1995].

1.3. Igneous Oceanic Crustal Stratigraphy

The primary, layered stratigraphy of upper oceanic crust was first defined through marine seismic surveys and by analogy with ophiolites [*Raitt*, 1963; *Shor et al*., 1971; *Moores and Vine*, 1971; *Cann*, 1974]. Subsequent work has revealed additional architectural complexity and raised questions as to how crustal evolution may change correlations between seismic and lithologic boundaries [e.g., *Houtz and Ewing*, 1976; *Purdy and Detrick*, 1986; *Wilkens et al*., 1991].

Oceanic crustal seismic layer 1 is associated with sediments and is absent at most seafloor spreading centers, where sedimentation rates are typically millimeters per thousand years. Sediments accumulate, thicken, and gain continuity with age as the crust spreads and subsides. Seismic layer 2 is upper basement with a mean *P* wave velocity V_p less than about 6.5 km s^{-1} [e.g., *Houtz and Ewing*, 1976] and relatively high velocity gradients [e.g., *Carlson and Herrick*, 1990]. There is general agreement that the top of seismic layer 2 is composed of extrusive basalt (pillows and flows) and that the base of layer 2 is intrusive basalt (sheeted dikes), but the identification and lithologic associations of sublayers remain controversial [*Jacobson*, 1992; *Carlson and Jacobson*, 1994; *Christeson et al*., 1994; *Carbotte et al*., 1997]. One model divides the extrusive basaltic crust into three sublayers: porous pillows, flows and breccias (layer 2A) overlying a less porous extrusive zone and transition (layer 2B), with sheeted dikes at the base (layer 2C). The boundary between layers 2A and 2B is thought to reflect differences in fracturing or hydrothermal alteration [e.g., *McClain et al*., 1985; *Becker et al*., 1989; *Wilcock et al*., 1992]. Another model confines the extrusive crust entirely to layer 2A and places the underlying dikes in layer 2B [e.g., *Francheteau et al*., 1992; *Harding et al*., 1993; *Kappus et al*., 1995].

The top of seismic layer 3 ($V_p \sim 6.7$ km s^{-1}) is commonly attributed to a lithologic transition from sheeted dikes to gabbro, although measurements in Deep Sea Drilling Project/Ocean Drilling Program (DSDP/ODP) Hole 504B and comparison to ophiolite properties suggests that layer 3 velocities may be found within the sheeted dikes [*Carlson and Herrick*, 1990; *Detrick et al*., 1994; *Salisbury et al*., 1996]. Difficulties in correlating universally between seismic and lithologic boundaries in oceanic crust may reflect different scales of measurement [*Swift et al*., 1996] as well as regional and local heterogeneity. While the primary stratigraphy of the upper igneous crust is established close to the ridge crest [*Macdonald*, 1982; *Purdy and Detrick*, 1987; *Pezard et al*., 1992], subsequent modifications reflect crustal alteration [e.g., *Jacobson*, 1992; *Lowell et al*., 1995] as well as tectonic and magmatic processes [e.g., *Karson and Rona*, 1990; *Johnson et al*., 1993; *Christeson et al*., 1994; *Kappus et al*., 1995].

Total oceanic crustal thickness does not seem to vary significantly with seafloor spreading rate [*Chen*, 1992], but it may vary with mantle temperature below the ridge [*Su et al*., 1994], and it is known to vary in association with structural and magmatic boundaries such as propagating rifts [*Hey et al*., 1980], fracture zones [*Karson and Dick*, 1983], and along-ridge discontinuities [*Macdonald et al*., 1988]. Pillow basalts seem to be more common within slow-spreading crust [*Bonatti and Harrison*, 1988], although other studies suggest that the upper igneous crust is lithologically variable over a range of spreading rates [e.g., *Macdonald et al*., 1989; *Smith and Cann*, 1992; *Head et al*., 1996].

Igneous oceanic crust is not exposed at the ridge axis at sedimented spreading centers, where a high sedimentation rate prevents normal igneous crustal accretion. Magma rises from depth, spreads laterally below the seafloor, and cools to form an upper oceanic crust comprising interlayered sills and altered sediment. Two sedimented spreading centers explored through drilling, Guaymas Basin, Gulf of California [*Curray and Moore*, 1982] and Middle Valley, northern Juan de Fuca Ridge [*Davis et al*., 1992b] have this upper crustal structure, as has the seafloor within other marginal basins drilled near large sediment sources (e.g., Yamato Basin, Japan Sea

[*Tamaki et al*., 1990]). It is at least as difficult to correlate seismic and lithologic boundaries within crust formed at sedimented spreading centers as within normal oceanic crust, and making additional associations between seismic and hydrologic properties is challenging in all settings.

2. DIRECT MEASUREMENTS

Permeability can be measured through application of Darcy's law, a conservation of mass equation for the experimental geometry, and appropriate initial and boundary conditions. Flow is induced and changes in head are monitored, or a head gradient is established and flow is monitored. These laboratory tests and in-situ determinations of permeability within basaltic oceanic crust are considered to be "direct measurements" and are summarized in this section.

2.1. Laboratory Measurements

Laboratory measurements of basalt permeability involve cutting a subsample of rock with a specific geometry, encasing the sample in a test chamber, and monitoring changes in fluid pressure or flow rate under controlled conditions. Experimental uncertainties of laboratory measurements are relatively low, perhaps 10% or less for repeated tests of a single sample, although determining the reliability of such measurements for accurate spatial characterization would require a large number of regularly spaced samples.

The first laboratory permeability measurements of oceanic crustal basalt samples collected during DSDP drilling were made with material recovered from Holes 417D and 418A in 110 Ma basement of the western North Atlantic Ocean. One-inch (2.54 cm) diameter cores of fresh basalt and basalt breccia had permeabilities of 10^{-20} to 10^{-16} m^2 [*Johnson*, 1980a; *Hamano*, 1980]. Basalt samples containing significant diagenetic smectite had lower permeabilities, 10^{-22} to 10^{-20} m^2, thought to result from clogging of microcracks by clay particles [*Johnson*, 1980a]. Permeabilities were not found to vary consistently with porosity or electrical resistivity [*Hamano*, 1980].

Karato [1983a] tested basalt cores from the upper few hundred meters of basement in DSDP Hole 504B, in 5.9 Ma crust south of the Costa Rica Rift, with the samples exposed to confining pressures of 5–15 MPa (equivalent to about 200–500 m below seafloor). Permeabilities tended to fall as confining pressures increased to 5 MPa, but were little influenced by subsequent increases. Permeabilities measured at confining pressures greater than 7 MPa had a geometric mean of 5×10^{-20} m^2. *Karato* [1983a] related core-scale permeability to porosity and electrical resistivity measured on the same samples and noted that the apparent hydraulic radius (the "effective" size of the pore throats) for the samples was considerably smaller than the observed pore size (0.01–0.1 μm versus >10 μm). Additional tests conducted on upper basement samples from 1.0 Ma crust on the south flank of the Galapagos Spreading Center yielded similar core-scale permeabilities [*Karato*, 1983b].

Christensen and Ramananantoandro [1988] tested the permeability of basalt samples cored from the interiors of pillow lavas recovered from the Juan de Fuca Ridge and from a vesicular basalt sample recovered from the Tonga-Kermadec region, under confining pressures of 5–40 MPa (500–1500 m below seafloor). The greatest measured permeability for Tonga-Kermadec basalt was 1.5×10^{-18} m^2, while the greatest measured permeability for Juan de Fuca basalt was 3.0×10^{-19} m^2 [*Christensen and Ramananantoandro*, 1988]. *Aksyuk et al*. [1992] tested core samples collected from DSDP Hole 345, in 28 Ma crust of the Arctic Ocean, over a range of pressures and temperatures. Core-scale basalt permeabilities increased (up to 7×10^{-18} m^2) as samples were heated to 600°C under confining pressures of 30–100 MPa, but more typical values at room temperatures and low confining stresses were 10^{-19} to 10^{-18} m^2 [*Aksyuk et al*., 1992], consistent with previous measurements.

2.2. In Situ Measurements

Measurements of bulk formation permeability have been made in oceanic basement holes using drill string packers, which use inflatable rubber elements to temporarily isolate part of a borehole during testing [*Becker*, 1986]. A packer is attached to the drill string and lowered into a previously drilled hole in the seafloor. Packers can be set either in casing or in open hole, although the latter requires that the hole be of an appropriate diameter and that the formation provide both mechanical and hydrologic seals. When the packer is set in casing, the entire open hole below the casing is subjected to testing, as is the cement bond between the casing and the formation. A packer can also be set with two inflatable elements, either with the elements placed next to each other (to assure a good seal) or with the elements separated by one or more sections of drill pipe (to allow testing between the elements), but this second kind of test has never been completed in a DSDP or ODP borehole. Rig floor and downhole gauges record pressures during all packer operations.

Two main kinds of packer tests have been used to estimate in situ properties: pressure slug tests and constant-rate injection tests. A slug test is initiated with a rapid increase in fluid pressure in the borehole below the packer, and the decay with time of this excess pressure is monitored. An injection test is conducted by pumping fluid into the isolated zone at a constant rate and monitoring the rise in fluid pressure with time. After a period of continuous injection (typically 20–30 min in DSDP and ODP boreholes), pumping is stopped and the pressure recovery of the formation is monitored to make an additional estimate of hydrologic properties. Time series observations from all tests are compared with one or more idealized aquifer models to estimate formation properties, as described below. Although multihole

aquifer tests are common in terrestrial hydrogeology and petroleum engineering practice, only single-hole packer tests have been conducted to date in oceanic basement.

The standard hydrologic methods used to analyze packer data are based on fitting time series pressure observations to analytical solutions of a mass conservation, radial flow equation, using appropriate boundary and initial conditions. All interpretations of DSDP and ODP packer tests in basement have been based on the following assumptions: the permeable zone is horizontally oriented, of infinite lateral extent and of constant thickness; prior to pumping, head is the same everywhere in the permeable zone; the well has a small diameter relative to the depth of influence of the test and is 100% efficient, with no "skin" or damaged zone resulting from drilling or other operations; the well fully penetrates the aquifer, which has hydrologic properties that are isotropic and homogeneous; fluid flow to and from the well is radial, horizontal, independent of azimuth, and laminar; and fluid properties do not vary with time or location during each test. These assumptions incorporate an application of the REV concept described earlier, in that the test interval is assumed to be large in relation to the size and distribution of flow channels in the rock, and to be effectively represented by a porous medium having homogeneous, isotropic properties. Packer experiments do not indicate how zones of high and low transmissivity are distributed within the tested intervals, and the results of these tests must be considered to reflect idealized formation properties [*Becker*, 1990a]. The permeability values estimated from these tests are for an equivalent porous medium and are commonly referred to as "bulk permeabilities" [e.g., *Becker*, 1989]. This term is restricted in the present review to results of borehole testing.

DSDP and ODP slug tests have been analyzed using the method of *Bredehoeft and Papadopulos* [1980] for low-permeability formations, a modification of the method described by *Cooper et al*. [1967] and *Papadopulos et al*. [1973]. The relative pressure change with time is related to two dimensionless parameters α and β by the integral function $F(\alpha, \beta)$. The α parameter includes storativity, while the β parameter includes transmissivity (see section 1.2). Normalized pressure data are plotted against log-time and compared to a family of type curves of $F(\alpha, \beta)$ versus log β, for values of α spanning many orders of magnitude. The time axis of the data is shifted relative to the type curves to find a good match, and the corresponding transmissivity and storativity values are calculated. The type curves for different values of α are similar, making it difficult to constrain storativity to better than about an order or magnitude, even under ideal conditions [*Cooper et al*., 1967; *Bredehoeft and Papadopulos*, 1980]. In contrast, estimates of bulk formation permeability are generally more reliable, accurate to within a factor of 2–3 if the data are of high quality, but subject to the assumptions listed above.

The quantitative interpretation of slug test data requires that the initial pressure pulse be of a short duration relative to the subsequent decay. Typically during DSDP and ODP slug tests, 250–1000 L of fluid is pumped into a sealed hole in 30–60 s, producing a pressure rise of 0.5–2.0 MPa (depending on formation properties and the thickness of the isolated zone). If the pressure rise is small and decays quickly (within a few to a few tens of seconds), then the formation is too permeable for slug testing, and injection tests must be used to assess bulk permeability.

The standard solution to the radial flow equation applied to constant-rate injection testing in aquifers [*Theis*, 1935] relates head changes following the start of pumping to an integral function $W(u)$, often called the "well function" [*Freeze and Cherry*, 1979]. The dimensionless parameter u contains formation transmissivity and storativity, time since pumping started, and the radial distance to the observation point from the pumping well. Observations are compared to a type curve of $W(u)$ versus $1/u$ in log-log space, the abscissa and ordinate of the data plot are shifted to match the type curve, and corresponding values for transmissivity and storativity are calculated.

The method most commonly applied to interpretation of ODP injection tests [*Becker*, 1990a] is analogous to the increase in sediment temperature surrounding a thin probe containing a heat source, as used in thermal conductivity measurements [*Von Herzen and Maxwell*, 1959]. This approach has been used extensively in petroleum reservoirs [*Horner*, 1951; *Matthews and Russell*, 1967] and can be justified by representing the function $W(u)$ as a truncated series expansion, valid for small values of u (long times since the start of pumping or short distances from the pumping well) [*Cooper and Jacob*, 1946]. Another method used for interpretation of injection tests in oceanic basement [*Zoback and Anderson*, 1983] was based on the steady state Glover formula [*Snow*, 1968], useful after the pressure increase within the isolated interval becomes stable during continued pumping.

Interpretation of formation recovery data following the end of injection is accomplished by noting that the cessation of pumping is equivalent to the superposition of a phantom well in the same location, with fluid pumped out of the formation at a rate equal to that used during injection. The net flux into the formation is then zero, and the linear solutions for flow in and out of the formation may be superimposed and matched to observations, essentially using the transient methods described above for interpretation of injection tests. Multiple tests conducted in the same well that do not allow for full recovery between slugs or injection periods must also be corrected for residual decay from earlier tests. The fitting of borehole test data to type curves has traditionally been accomplished by eye, although procedures for interpretation of ODP data have become standardized [*Becker*, 1990a].

The validity and significance of the assumptions used

TABLE 1. Summary of in Situ Packer Measurements of Bulk Permeability in Deep Sea Drilling Project and Ocean Drilling Program Holes in Basaltic Oceanic Crust

Hole	*Location*	*Crustal Age, Ma*	*Depth Range, Into Basement, m*	*Bulk Permeability, m^2*	*References*
395A	Mid-Atlantic Ridge, west flank	7.3	303.0–513.0	1.5×10^{-14} [a]	*Becker* [1990b]
			423.0–513.0	$\leq 1.5 \times 10^{-14}$ [a]	*Becker* [1990b]
			490.0–571.0	6.0×10^{-18}	*Hickman et al*. [1984a]
504B	Costa Rica, Rift, south flank	5.9	42.0–214.5	3.7×10^{-14}	*Anderson and Zoback* [1982], *Zoback and Anderson* [1983]
			199.0–214.5	2.6×10^{-15} [b]	*Anderson et al*. [1985a, b]
			211.5–214.5	1.9×10^{-15} [b]	*Anderson et al*. [1985a, b]
			264.0–1013.0	1.4×10^{-17} [c]	*Anderson et al*. [1985a, b]
			264.0–1013.0	≤ 1.4–7.5×10^{-16} [e]	*Becker* [1996]
			661.5–1132.3	2.3×10^{-17} [a]	*Becker* [1989]
			961.5–1273.0	4.6×10^{-18} [a]	*Becker* [1989]
801C	Pigafetta Basin, western Pacific	157.4–166.8	39.4–132.4	8.0×10^{-14}	*Larson et al*. [1993]
			48.4–66.4	4.0×10^{-13} [d]	*Larson et al*. [1993]
858G	Middle Valley, Juan de Fuca Ridge	≤0.2	11.0–173.6	8.0×10^{-14}	*Becker et al*. [1994]
			61.0–91.0	2.5×10^{-13} [f]	*Becker et al*. [1994]
896A	Costa Rica Rift, south flank	5.9	16.0–290.0	5.0×10^{-14} [g]	*Becker* [1996]
			16.0–54.0	2.0×10^{-13} [h]	*Becker* [1996]
			54.0–290.0	1.4×10^{-14} [a]	*Becker* [1996]
			206.0–290.0	1.1×10^{-14} [a]	*Becker* [1996]
			54.0–206.0	1.3×10^{-14} [h]	*Becker* [1996]

[a] Arithmetic mean of most reliable values.
[b] Original interpretation presented by *Anderson and Zoback* [1982] and *Zoback and Anderson* [1983] revised by *Anderson et al*. [1985a, b] based on new seawater viscosity calculation. *Becker* [1989] subsequently noted a possible underestimate of bulk permeability because of underestimate of system compressibility.
[c] An underestimate of system compressibility may have led to an underestimate of bulk permeability. Data reinterpreted by *Becker* [1996].
[d] Smaller test interval based on the assumption that the most permeable zone included the region of extreme hydrothermal alteration, as indicated by geophysical logs illustrated by *Larson et al*. [1993].
[e] Reinterpretation of packer experiments conducted by *Anderson et al*. [1985a, b] assuming a system compressibility for slug tests more typical of ODP packer testing in this setting.
[f] Smaller test interval based on hypothesis of *Becker et al*. [1994] that most transmissivity is concentrated within a thin zone defined by geophysical and spinner–flow meter logs.
[g] Most reliable injection test.
[h] Inferred bulk permeability for listed interval based on the difference of transmissivities for partially overlapping test intervals.

to interpret borehole packer data in shallow oceanic basement vary from site to site and with the depth intervals and timescales of individual tests. If most of the transmissivity measured in a deep borehole is concentrated within a few discrete fractures located close together, the calculated bulk permeability of the fractured rock will depend on the thickness of the tested interval. If additional geological or geophysical information is available, permeability estimates may be refined, but the bulk values calculated for thick sections of basalt are still useful for comparison. This approach is fairly conventional for in-situ permeability testing in crystalline rock [e.g., *Brace*, 1984], although newer methods developed for interpretation of fractured aquifers [e.g., *Moench*, 1984; *McConnell*, 1993] are becoming increasingly common. Challenges in applying newer methods to DSDP and ODP boreholes arise from the need for knowledge regarding the distribution and importance of individual fractures, the lack of one or more observation wells distinct from the pumping well, and the extremely short duration of oceanic aquifer tests. Results of all DSDP and ODP packer testing in basaltic oceanic crust are listed in Table 1, geographical locations are shown in Figure 1, and the geological settings and test results are summarized briefly below.

The first in situ hydrologic tests in basaltic oceanic crust were completed in 5.9 Ma basement of DSDP Hole 504B. Site 504 is located on the flank of an abyssal hill, where a high sedimentation rate has led to the burial of young igneous crust below several hundred meters of calcareous and siliceous sediment [*Costa Rica Rift United Scientific Team* (*CRRUST*), 1982; *Langseth et al*., 1983]. Packer measurements indicated that the shallowest 200 m of igneous basement were relatively permeable, 10^{-14} to 10^{-13} m^2 [*Anderson and Zoback*, 1982; *Zoback and Anderson*, 1983]. Measurements deeper than 250 m into basement revealed bulk permeabilities near 10^{-17} m^2 [*Anderson et al*., 1985b, c; *Becker*, 1989], although *Becker* [1989, 1996] also noted that system compressibilities may have been underestimated during some of the earlier tests, leading to an underestimate of bulk permeability by as much as an order of magnitude. *Becker* [1996] also processed data from an injection test conducted but not analyzed by *Anderson and Zoback* [1982] (interpreted at that time to indicate failure of the packer element) as indicating bulk permeability possibly as

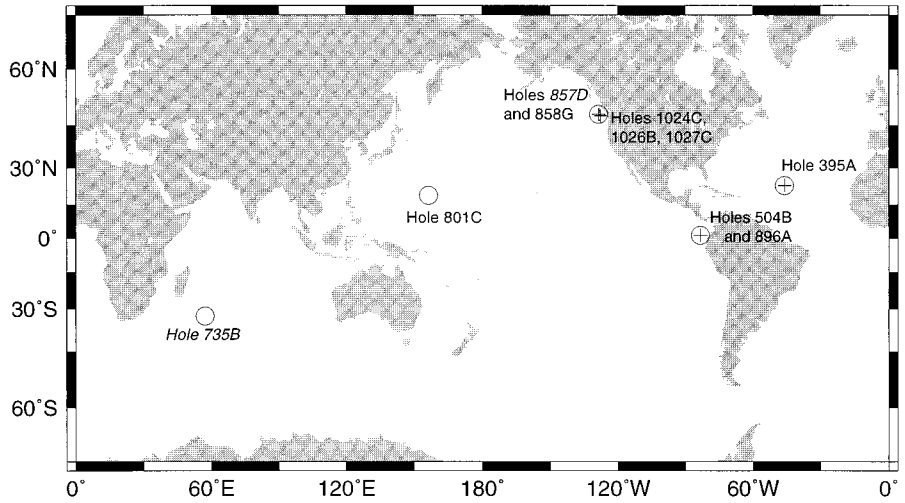

Figure 1. Locations of all DSDP and ODP packer tests (circles) and permeability estimates derived from temperature logs in open boreholes (crosses) in oceanic basement. Hole numbers printed in italics indicate nonbasaltic oceanic basement; see text and Plate 1.

great as 1.4–7.5 $\times$ 10^{-16} m^2 over subbasement depths of 250–1000 m. Thus while the basaltic crust greater than 250 m into basement is considerably less permeable than the shallowest 200 m of basement, the difference in permeability may be as little as two orders of magnitude or as great as four orders of magnitude (Table 1).

ODP Hole 896A was subsequently drilled near the peak of a local heat flow high over a basement ridge about 1 km southeast of Hole 504B, where chemical data from sediment pore fluids indicated fluid upflow from basement at a rate of millimeters per year [*Langseth et al*., 1988; *Mottl*, 1989]. Bulk permeabilities over the upper 290 m into basement in Hole 896A are 10^{-14} to 10^{-13} m^2, similar to that in uppermost Hole 504B [*Becker*, 1996]. Data from Hole 896A do not indicate the abrupt decrease in permeability with depth below 250 m into basement that was apparent in Hole 504B, perhaps reflecting lateral variability.

DSDP Hole 395A was drilled into 7.3 Ma crust on the west flank of the Mid-Atlantic Ridge (MAR). Unlike Sites 504 and 896, Site 395 is located in a region of common basement exposure at the seafloor, where local topographic depressions collect sediment as isolated ponds, typically 1–10 km across and $\leq$500 m thick [*Langseth et al*., 1984]. Hole 395A, located near the eastern edge of one such pond, was drilled 571 m into basement during DSDP Leg 45 and was revisited for downhole experiments during DSDP Leg 78B. *Hickman et al*. [1984a] conducted packer experiments in the lower 80 m of Hole 395A (490–570 m into basement) and measured bulk permeability of about 6.0 $\times$ 10^{-18} m^2. *Becker* [1990b] conducted additional packer tests during ODP Leg 109 and documented significantly greater permeability ($\leq$1.5 $\times$ 10^{-14}) over a depth range of 300–510 m into basement, comparable to the upper 215 m of basement in Hole 504B and the upper 250 m of basement in Hole 896A (Table 1).

Packer experiments were conducted within some of the oldest remaining seafloor, Jurassic oceanic crust of the Pigafetta Basin in the western Pacific Ocean, where 600 m of sediment and 132 m of basement were penetrated during ODP Leg 129 [*Larson et al*., 1992]. A suite of downhole measurements was completed in Hole 801C during ODP Leg 144 [*Larson et al*., 1993]. Packer measurements 40–130 m into basement indicate a bulk permeability of about 10^{-13} m^2; a higher value is indicated if the transmissivity is concentrated within a hydrothermally altered zone about 18 m thick (Table 1), as suggested by drilling conditions, geophysical logs, and basement alteration patterns [*Larson et al*., 1993]. The basement architecture around Hole 801C is unusual compared to most upper oceanic crust being created today, as the hole penetrates 157.4 Ma alkalic (off-axis) basalts overlying 166.8 Ma tholeitic (axial) basalts [*Floyd and Castillo*, 1992; *Pringle*, 1992]. The hydrothermally altered zone containing the greatest permeability is sandwiched between, and may include parts of, these distinct crustal layers. It is not clear how common this crustal character is for Mesozoic oceanic basement, although off-axis volcanism was more common during that period than it is today [*Larson et al*., 1993].

Packer experiments were also conducted in very young basaltic basement at Site 858 in Middle Valley, a sedimented rift at the northern end of Juan de Fuca Ridge [*Becker et al*., 1994]. Hole 858G was drilled through 259 m of sediments and 174 m into a buried basement edifice believed to have been exposed at the seafloor prior to burial by turbidites [*Langseth and Becker*, 1994]. The exact age of upper basement at Site 858 is uncertain, but it is probably $\leq$200 ka [*Davis and Villinger*, 1992]. Packer measurements over a depth interval of 10–175 m into basement in Hole 858G indicate bulk permeability of about 10^{-13} m^2, consistent with upper crustal measurements in more normal settings (Table 1). Spinner flow meter and temperature measurements in Hole 858G suggest that much of the transmissivity may be concentrated within a zone 61–91 m into basement. If so, this zone would have a proportionately greater bulk permeability.

Packer measurements of bulk permeability from two

additional oceanic basement holes are worth noting, although these crustal sections are lithologically distinct from normal basaltic basement. ODP Hole 857D is also located in Middle Valley, 1.6 km south of Hole 858G [*Shipboard Scientific Party*, 1992]. In contrast to Hole 858G, drilled through sediments and into purely igneous basement, Hole 857D was drilled through 470 m of sediments and another 466 m into a sediment-sill sequence [*Langseth and Becker*, 1994]. The intervals of packer testing in Hole 857D comprised the lowermost 180 and 362 m of the hole, entirely within the sediment-sill sequence. Packer measurements indicate a bulk permeability of 10^{-14} m^2 for the lower 180 m of Hole 857D, while measurements including the lower 362 m of the hole indicate a bulk permeability orders of magnitude greater [*Becker et al*., 1994]. Spinner flow meter, temperature, and geophysical logs suggest that much of this permeability is concentrated within one or more thin zones; the zone that appears to be the most transmissive is 5 m thick and is estimated to have a bulk permeability of approximately 10^{-10} m^2 [*Becker et al*., 1994]. Little is known about the structure or lithology within this narrow interval, as core recovery was poor and a large borehole diameter reduced the quality of geophysical logs. The interval is believed to be a fault zone [*Becker et al*., 1994], on the basis of the common occurrence of normal faults in this extensional setting [*Davis and Villinger*, 1992; *Rohr and Schmidt*, 1994] and the apparent structural offset between correlatable sedimentary units at Sites 857 and 858 [*Langseth and Becker*, 1994].

ODP Hole 735B was drilled 501 m into 11.7 Ma gabbroic oceanic crust on a transverse ridge east of the Atlantis II fracture zone, Southwest Indian Ridge. The basement rocks exposed at the seafloor at Site 735 are thought to represent a tectonically unroofed section of the lower oceanic crust [*Shipboard Scientific Party*, 1989; *Dick et al*., 1991]. Packer experiments were conducted at multiple depths and indicate bulk permeabilities of 2×10^{-14} m^2 for the lower 450 m of the hole and 2×10^{-16} m^2 for the lower 111 m of the hole [*Becker*, 1991]. Much of the high transmissivity in Hole 735B is associated with one or more open fractures within sheered gabbros between 170 and 270 m below seafloor [*Becker*, 1991; *Goldberg et al*., 1992]. This interval contains mylonites, variably oriented foliations, and other evidence for synmagmatic deformation, as well as abundant veins and other indications of postemplacement fluid flow and alteration [*Dick et al*., 1991].

The measurements made in Holes 857D and 735B have much in common with others made in oceanic basement. The greatest bulk permeabilities are associated with open fractures and confined to limited depth intervals [*Becker*, 1991; *Von Herzen et al*., 1991; *Becker et al*., 1994; *Langseth and Becker*, 1994]. In addition, when these extremely transmissive zones are excluded, bulk permeabilities within the remaining basement intervals are similar to those determined in the upper 500 m of basaltic oceanic crust, about 10^{-14} to 10^{-13} m^2 [*Becker*, 1991; *Becker et al*., 1994]. Additional packer measurements were recently completed in ODP Holes 1024C, 1026B, and 1027C within the uppermost 50 m into basement in 1.0–3.5 Ma crust on the east flank of Juan de Fuca Ridge [*Davis et al*., 1997b]. Although processing and interpretation of these data is not yet complete, preliminary analyses suggest bulk permeabilities that are broadly consistent with measurements in upper basement in other locations (K. Becker, personal communication, 1997).

Results of packer experiments in DSDP and ODP basement holes are plotted in Plate 1. Bulk permeabilities span seven orders of magnitude, from $\leq 10^{-17}$ m^2 at depths below 500 m into oceanic basement in Holes 504B and 395A, to 10^{-10} m^2 within a thin interval in the sediment-sill sequence of Hole 857D. The data from basaltic crust can be divided into two distinct sections, with relatively high bulk permeabilities ($\geq 10^{-14}$ m^2) extending to about 500 m into basement. There are no values greater than 10^{-13} m^2 that include intervals deeper than 100 m into basement, and intervals extending from 100 to 300 m into basement generally have bulk permeabilities of 10^{-14} to 10^{-13} m^2. While some of the depths at which bulk permeability appears to drop abruptly correlate with lithologic boundaries, these depths also reflect the extent of basement drilling and the thicknesses of the tested intervals. Interpretations based on analysis of open hole temperature logs (also shown in Plate 1) are discussed in the following section on indirect methods.

3. INDIRECT ESTIMATES AND INFERENCES

A wide variety of borehole, seafloor, and ophiolite observations and experiments reflect the nature of permeability within the upper igneous oceanic crust. Discussion of these indirect methods requires more explanation than did discussion of direct methods, and many indirect approaches result in qualitative or semiquantitative constraints on permeability. However, these approaches are extremely valuable, as they reflect observations over wide temporal and spatial scales and the inferences are complimentary to direct measurements. A comprehensive representation of permeability in the basaltic oceanic crust should satisfy both direct and indirect constraints.

Borehole temperatures indicate fluid flow rates to and from upper basement, and flow rates are related to bulk permeability through idealized models of the formation surrounding the borehole. Borehole geophysical logs, fracture analyses based on borehole imaging, fracture studies of seafloor basalt cores and ophiolites, and investigations of basalt structure and alteration from boreholes and cores all reflect hydrologic conditions in basement, although interpreting these data quantitatively is difficult since it requires defining relationships between fracture and flow properties.

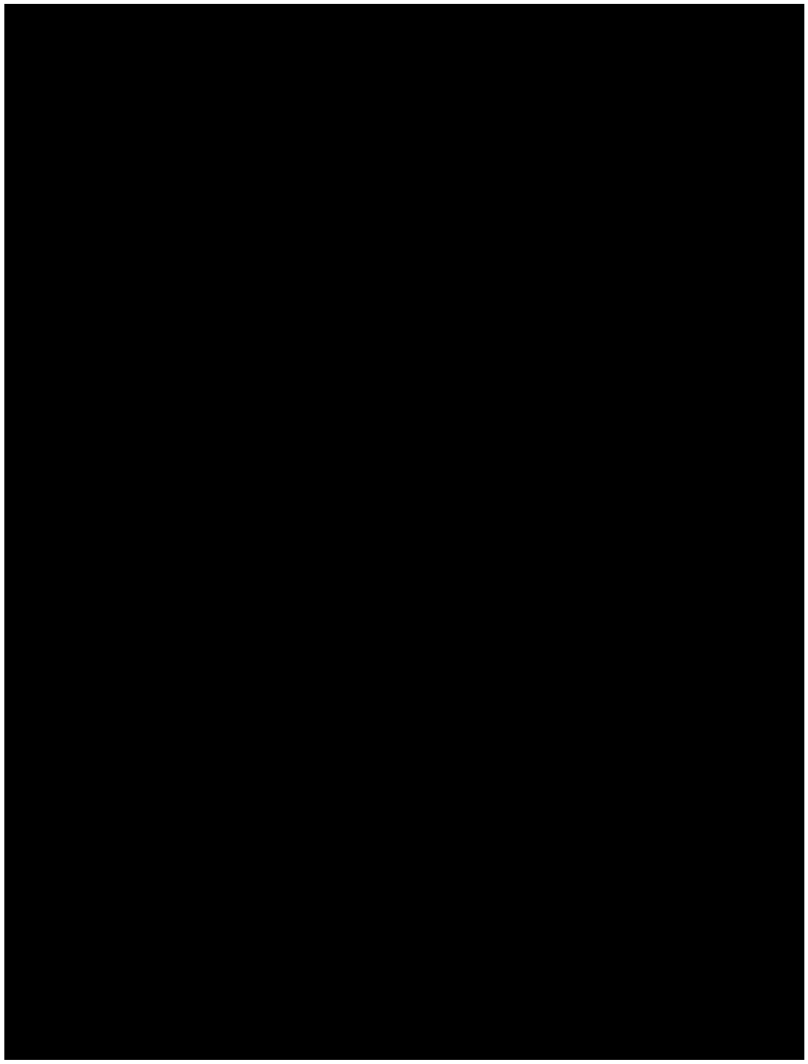

Plate 1. Bulk permeabilities within upper oceanic basement determined with a borehole packer and through analysis of borehole temperature logs. References for the various measurements and calculations are listed with data and depth intervals in Tables 1 and 2. Data from Holes 735B and 857D, while not in basaltic basement, are shown for comparison. The actual depths into "basement" for these measurements are not known, so the data are plotted relative to depth below seafloor (Hole 735B) and depth below the first sill (Hole 857D). The depth ranges for individual measurements indicate the borehole intervals over which the bulk permeability values are attributed. In some cases these represent entire isolated intervals, while in other cases the ranges are based on the differences between transmissivities calculated for overlapping intervals. The range of bulk permeabilities indicated by the width of the boxes reflects differences in values calculated for multiple tests and an estimate of experimental uncertainties. The arrow pointing to the right of the value calculated from an experiment in Hole 504B indicates that this test may have led to an underestimate of the bulk permeability over this thick depth interval because of uncertainties regarding system compressibilities [*Becker*, 1989, 1996]. See text and cited references for discussion of assumptions and analysis methods.

Seafloor heat flow measurements have been used to infer the bulk magnitude and distribution with depth of permeability in underlying basement rocks, with interpretations rooted firmly in conceptual models of circulation geometries. More complex analytical and numerical models have also been used to infer basement hydrologic properties, with models constrained by subseafloor thermal, chemical, and pressure information. Numerous seafloor geological and geophysical observations also reflect permeability within the upper igneous crust. All of these approaches require assumptions regarding permeability distribution, heterogeneity, porous versus fracture flow, flow scale, and other parameters.

3.1. Borehole Thermal Measurements

Of the indirect methods used to estimate upper crustal permeability, borehole thermal data provide the strongest quantitative constraints. Temperature logs in open holes penetrating basement commonly indicate the flow of water into or out of the crust. Seawater often flows down boreholes drilled into upper oceanic basement because the ambient thermal state of the crust, in combination with the thermal expansivity of seawater, causes crustal fluids to have a pressure lower than that of cold seawater in an adjacent borehole. Since cold seawater is introduced into the borehole during drilling, the pressure difference between borehole fluid and formation fluid (referred to herein as "differential pressure") results from a combination of artificial and natural conditions. In contrast, crustal underpressuring or overpressuring relative to ambient hydrostatic conditions is a natural process and may result in fluid flow through basement and overlying sediments at thermally or chemically significant rates even in the absence of a borehole [e.g., *Langseth and Herman*, 1981; *Langseth et al*., 1988; *Davis et al*., 1992a].

Quantitative interpretation of borehole logs to estimate flow rates requires knowledge of the background geothermal gradient, as this provides both initial and boundary conditions for the analysis. Once a flow rate has been calculated from a borehole temperature log, crustal permeability can be estimated on the basis of the measured or calculated differential pressure. Given a correct initial differential pressure, the reliability of permeabilities deduced from temperature logs is essentially the same as that of permeabilities determined from

packer experiments. For this reason, and because many of the assumptions and approximations in the analyses are similar to those used in interpretation of packer data, crustal permeabilities estimated from borehole thermal data are referred to as "bulk permeabilities" in this review. Borehole thermal data may also allow rough assessment of the thickness of the most permeable zone(s), as changes in borehole thermal gradients are often associated with differences in the rate of flow into or out the formation. The shape of the thermal profile is particularly helpful for identifying the base of the deepest zone into which (or from which) fluids flow, as borehole fluids above this depth may be close to isothermal if the flux is sufficiently high. Locations of sites in which basement permeabilities have been estimated using on borehole thermal data are shown in Figure 1, and results of these analyses are summarized in Table 2.

Becker et al. [1983a, b] used the shape of temperature logs in DSDP Hole 504B to estimate the rate at which water flowed down through casing and into upper basement, based on steady state and transient, radial heat exchange models. Open hole thermal data collected 50 days after Hole 504B was drilled indicated that seawater flowed down the hole at about 90 m h^{-1} and that much of this flow entered the formation within a zone 30–100 m thick within uppermost igneous basement [*Becker et al*., 1983a]. Based on a calculated differential pressure [*Anderson and Zoback*, 1982] and a radial flow model, bulk permeability within this upper basement aquifer was estimated to be 6×10^{-14} m^2 to 2×10^{-13} m^2 [*Becker et al*., 1983a, b]. The velocity of flow down Hole 504B was reduced to about 25 m h^{-1}, 2.1 years after penetration of basement (DSDP Leg 83 [*Becker et al*., 1985]), and subsequently to 1 m h^{-1}, 6.9 years after initial drilling (ODP Leg 111 [*Gable et al*., 1989]), suggesting that the differential pressure in basement was being quenched by continued seawater inflow. Surprisingly, the fluid flow rate down Hole 504B increased prior to ODP Leg 137, 11.5 years after penetrating basement, with the flow velocity approaching that estimated 9 years earlier during DSDP Leg 83, before decreasing again a much lower rate as of ODP Legs 140 and 148 [*Gable et al*., 1995; *Guerin et al*., 1996]. The reason for the unexpected increase in flow rate down Hole 504B many years after drilling is unknown, but it seems to require an increase in differential pressure, an increase in bulk permeability, or development of a discharge path leading from the basement borehole to the overlying ocean (as around Hole 395A).

Open hole temperature measurements were made in basement Hole 395A on the west flank of the MAR during DSDP Leg 78B [*Becker et al*., 1984] and ODP Leg 109 [*Kopietz et al*., 1990]. In contrast to conditions in Hole 504B, flow down Hole 395A seems to have continued undiminished for at least 10 years at 10–100 m h^{-1}. Using this range of flow rates and the same heat exchange model used in Hole 504B [*Becker et al*., 1983a], the bulk permeability of the upper 240 m of basement surrounding Hole 395A was estimated to be 10^{-14} to 10^{-12} m^2 [*Becker*, 1990b]. This estimate was refined 4 years later with additional measurements in Hole 395A. Thermal data indicated that flow continued down Hole 395A at approximately the same rate [*Gable et al*., 1992], while a flow meter experiment indicated bulk permeabilities near 10^{-14} m^2 within the upper 350 m of basement [*Morin et al*., 1992a], close to the bulk value determined for the interval 300–500 m into basement using a packer [*Becker*, 1990b]. A much lower value ($\ll 10^{-16}$ m^2) was estimated for the lowermost 200 m of the hole [*Morin et al*., 1992a], also in agreement with earlier packer measurements (Table 2). Additional thermal data were collected in Hole 395A during summer 1997, and the hole was sealed to prevent continued fluid flow into the seafloor. A long-term seafloor observatory will monitor thermal and pressure recovery of the borehole for the next several years (K. Becker, personal communication, 1997), providing additional quantitative constraints on crustal hydrogeology.

Fisher et al. [1997] used the same method as *Becker et al*. [1983a] to calculate the flow rate out of Hole 1026B, drilled into a buried basement ridge in 3.5 Ma crust on the east flank of Juan de Fuca Ridge. Flow out of the formation soon after drilling indicated that the formation was naturally overpressured relative to cold hydrostatic, consistent with two-dimensional models of buried basement ridges in the upper oceanic crust in similar settings [*Fisher et al*., 1990, 1994; *Davis et al*., 1997a]. Although the hole penetrated over 40 m into basement, the temperature data clearly indicated that flow originated from a 10-m-thick zone in the shallowest basalt. The temperatures were consistent with a flow rate of 80–120 m h^{-1}, and on the basis of a likely basement overpressure no greater than 20–30 kPa, bulk permeability within this thin zone is $5–9 \times 10^{-12}$ m^2 [*Fisher et al*., 1997].

Thermal data indicating flow into basaltic basement were also collected in Hole 858G in Middle Valley, north Juan de Fuca Ridge [*Shipboard Scientific Party*, 1992]. Open hole temperature data collected 1.5 days after drilling into basement indicated a flow rate down the hole of about 125 m h^{-1} [*Langseth and Becker*, 1994]. *Davis and Becker* [1994a] estimated that the formation fluid pressure in basement at Site 858 is naturally overpressured by 200–450 kPa relative to hot hydrostatic, a range consistent with long-term measurements in the subsequently sealed borehole (E. E. Davis, personal communication, 1997). There must have been a negative differential pressure at the time the open hole temperature log was collected, however, as these measurements indicated flow down the hole and into the formation. A reasonable upper limit on this differential pressure is the difference between hot and cold hydrostatic at the depth at which fluid entered the formation, calculated to be 600–700 kPa using a standard equation of state [*Haar et al*., 1984] and the predrilling thermal gradient [*Langseth and Becker*, 1994]. This value is close to the 500 kPa

TABLE 2. Selected Indirect Estimates of Bulk Permeability in the Upper Igneous Oceanic Crust

Location	*Crustal Age or Setting*	*Depth Range Into Basement, m*	*Bulk Permeability, m^2*	*References*
		In Situ, Using Temperature and Flow Meter Logs		
Hole 395A, Mid-Atlantic Ridge, west flank	7.3 Ma	19–257	$10^{-14} \times 10^{-12}$ [a]	*Becker* [1990b]
		19–158	3×10^{-14} [b]	*Morin et al.* [1992a]
		158–347	7×10^{-15} [b]	*Morin et al.* [1992a]
		347–571	$\ll 10^{-16}$ [b]	*Morin et al.* [1992a]
Hole 504B, Costa Rica Rift, south flank	5.9 Ma	2–101	6×10^{-14} to 2×10^{-13} [a]	*Becker et al.* [1983a, b, 1985]
Hole 858G, Middle Valley, Juan de Fuca Ridge	≤200 ka	11–174	$1–6 \times 10^{-14}$	this work
		61–91	8×10^{-14} to 4×10^{-13}	this work
Hole 1026B, Juan de Fuca Ridge, east flank	3.5 Ma	10	≤5 to 9×10^{-12} [a]	*Fisher et al.* [1997]
		Ophiolites[c]		
Samail (Oman)	Cretaceous			
Upper Dikes		≥200	10^{-9} to 10^{-8}	*Nehlig and Juteau* [1988a, b]
Lower Dikes		≥1500	10^{-11} to 10^{-10}	*Nehlig and Juteau* [1988a, b], *Nehlig* [1994]
Troodos (Cyprus)	Cretaceous			
Dikes (on-axis)		600–1300	10^{-12} to 10^{-8}	*van Everdingen* [1995]
Dikes (off-axis)		600–1300	10^{-21} to 10^{-18}	*van Everdingen* [1995]
		Models[d]		
Generic ridge crest	young	7000	10^{-16}	*Lister* [1972]
		2000–4000	10^{-14}	*Lister* [1972]
		1000–5000	10^{-11}	*Lister* [1974]
		1000–5000	10^{-7}	*Lister* [1981]
		5000	$\leq 2.5 \times 10^{-15}$	*Fehn and Cathles* [1979]
		unspecified (reaction)	$\leq 10^{-15}$	*Lowell and Rona* [1985]
		unspecified (discharge)	10^{-13}	*Lowell and Rona* [1985]
		1000–2000 (recharge)	$\geq 10^{-12}$	*Cann and Strens* [1989]
		1500 (basalt)	10^{-16}	*Brikowski and Norton* [1989]
		1500–5500 (gabbro)	10^{-17}	*Brikowski and Norton* [1989]
		7000 (discharge)	3×10^{-14}	*Cathles* [1993]
		7000 (recharge)	10^{-16}	*Cathles* [1993]
		unspecified (recharge)	$\geq 10^{-12}$	*Lowell and Germanovich* [1995]
		unspecified (discharge)	10^{-9}	*Lowell and Germanovich* [1995]
Generic ridge crest to ridge flank	unspecified	1500 (basalt)	10^{-15}	*Travis et al.* [1991]
		1500–5250 (gabbro)	2.5×10^{-16}	*Travis et al.* [1991]
		2000–5000	$\leq 10^{-15}$	*Fehn and Cathles* [1986]
Generic ridge flank	unspecified	unspecified	10^{-14}	*Lister* [1981]
Galapagos Spreading Center	0–1 Ma	≥3500	5×10^{-16}	*Ribando et al.* [1976]
	0–2 Ma	2000–5000	5×10^{-15}	*Fehn et al.* [1983]
Juan de Fuca Ridge, crest	unspecified	2000	6×10^{-13} to 6×10^{-12}	*Wilcock and McNabb* [1996]
		1000–3000 (discharge)	10^{-9} to 10^{-10}	*Wilcock* [1997]
Juan de Fuca Ridge, east flank	1 Ma	600	2×10^{-12}	*Davis et al.* [1996]
	1 Ma	600	10^{-13}	*Snelgrove and Forster* [1996]
	3.5 Ma	0–100	10^{-13}	*Fisher and Becker* [1995]
		100–200	5×10^{-15}	*Fisher and Becker* [1995]
		10- to 30-m-thick zones	10^{-9}	*Fisher and Becker* [1995]
	3.5 Ma	0–100	5×10^{-14}	*Yang et al.* [1996]
		100–200	10^{-16}	*Yang et al.* [1996]
		individual fractures	4×10^{-9}	*Yang et al.* [1996]
	3.5 Ma	60	10^{-9}	*Davis et al.* [1997b]
	3.5 Ma	600	10^{-11}	*Davis et al.* [1997b]
East Pacific Rise, west flank	20–50 Ma	unspecified	10^{-12} to 10^{-10}	*Baker et al.* [1991]
Costa Rica Rift, south flank	5.9 Ma	0–100	10^{-13}	*Williams et al.* [1986]
		100–200	$0.4–2.0 \times 10^{-15}$	*Williams et al.* [1986]
		>200	$0.2–1.0 \times 10^{-15}$	*Williams et al.* [1986]
		0–100	10^{-13} to 10^{-12}	*Fisher et al.* [1990]
		100–200	5×10^{-15}	*Fisher et al.* [1990]
		>200	10^{-17}	*Fisher et al.* [1990]
		10- to 30-m-thick zones	10^{-9}	*Fisher et al.* [1994], *Fisher and Becker* [1995]

TABLE 2. (continued)

Location	*Crustal Age or Setting*	*Depth Range Into Basement, m*	*Bulk Permeability, m^2*	*References*
		Models[d] (continued)		
Mid-Atlantic Ridge, west flank	7.3 Ma	300	10^{-13}	*Langseth et al.* [1984]
		Seafloor Geophysical Estimates		
Middle Valley, ridge crest	300 ka	≥1000	10^{-16} to 10^{-14}	*Nobes et al.* [1986]
East Pacific Rise, ridge crest	0–100 ka	1000	5×10^{-12}	*Evans* [1994]

[a] Based on temperature logs and analytical radial fluid flow model around borehole.
[b] Based on flow meter logs and steady state analysis of radial fluid flow model around borehole.
[c] Based on fracture and vein mapping and application of various fracture models.
[d] See individual references for modeling parameters and assumptions regarding the distribution of permeability.

differential pressure observed at the start of packer experiments [*Becker et al.*, 1994] but greater than the differential pressure measured several days later as Hole 858G was sealed [*Davis and Becker*, 1994a]. Using a reasonable range in the initial differential pressure in Hole 858G of 200–600 kPa, and allowing flow rates down the hole of 100–150 m h^{-1} soon after drilling, the bulk formation permeability would be 1 to 6 $\times$ 10^{-14} m^2 if uniformally distributed within the upper 160 m of basement, or 8 $\times$ 10^{-14} m^2 to 4 $\times$ 10^{-13} m^2 if permeability was limited to a zone 61–91 m into basement, as suggested by flow meter and temperature logs [*Becker et al.*, 1983a, 1994] (Figure 2).

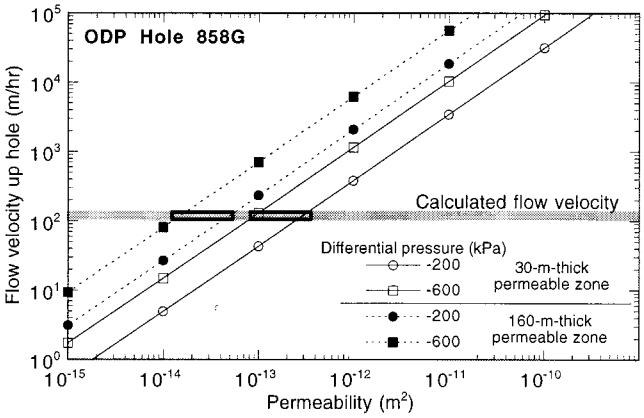

Figure 2. Values of fluid-flow velocity down ODP Hole 858G as a function of bulk formation permeability. Curves are shown for a range of initial differential pressures (pore fluid relative to cold hydrostatic), and different assumed thicknesses of the transmissive zone (solid lines, 30-m-thick permeable zone; dotted lines: 160-m-thick permeable zone). The shaded region indicates a reasonable range of flow velocities estimated using a temperature log collected 1.5 days after penetration of basement [*Langseth and Becker*, 1994]. The boxes indicate likely ranges of flow rates and differential pressures. The limits on the initial differential pressure around Hole 858G are well constrained by observational data and the calculated difference in fluid density over a temperature range of 2°–280°C. The transient diffusive model used to generate these curves is described by *Becker et al.* [1983a] and *Fisher et al.* [1997].

Results of bulk permeability calculations based on borehole thermal data are plotted along with packer results in Plate 1. The borehole thermal data yield values that are consistent with the trends defined by packer measurements, with almost six orders of magnitude of variation over the shallowest 500 m of basement. The estimate of bulk permeability at the top of Hole 1026B is particularly well constrained by the thermal data, which indicate that the hydrologically active part of upper 40 m of basement corresponds to the shallowest 10 m of basalt. Fluid flowing out of this interval of overpressured basement is very similar in chemical composition to fluids flowing out of basement warm springs several kilometers away [*Shipboard Scientific Party*, 1997], suggesting that this shallow crustal interval is laterally extensive and/or chemically homogeneous.

3.2. Other Borehole Estimates of Hydrogeologic Properties

Much of the geophysical logging in oceanic basement holes over the last 20 years was intended to document large-scale formation porosity. While porosity is related to permeability, the nature of this relation depends on the form(s) of porosity. The three primary forms of porosity most commonly present in igneous oceanic crust are [*Pezard*, 1990] (1) vesicles and other primary porosity, likely to be occluded; (2) microcracks having narrow widths and limited lateral extent; and (3) macrofeatures associated with pillow boundaries, collapse structures, and larger-scale tectonic deformation. The first two porosity types can be studied in the laboratory with core samples, while the third requires in-situ measurement and relates most closely to formation-scale permeability. Since there is no way to measure in-situ porosity directly, formation resistivity, density, sonic velocity, and other tool responses are typically related to porosity through theoretical and empirical equations. There are commonly differences between porosity estimates based on different instruments [e.g., *Moos*, 1990], so for the purposes of this review it is perhaps more useful to note relative differences in apparent porosity within a single hole than to rely on absolute values

estimated using any one instrument. As in the case of permeability measurements, geophysical logging of oceanic basement has been largely restricted to the upper 500–1000 m (and generally to the upper 300 m) in a small number of holes.

Kirkpatrick [1979] presented the first suite of conventional geophysical logging data collected in the igneous oceanic crust, with measurements made in the upper 200 m of basement around DSDP Hole 396B, 9 Ma crust, east of the MAR. Porosities in upper basement were of the order of 13% or greater, even in massive units, in contrast to core-scale porosity measurements from nearby sites yielding much lower values [*Hyndman and Drury*, 1976]. Geophysical logging in the upper 100 m of basement in Hole 417D in the western Atlantic Ocean [*Salisbury et al*., 1980] revealed physical properties consistent with the alternation of pillow and massive flow deposits, as delineated by >70% core recovery in basement. Basement porosity was estimated to be about 13%, with 8% attributed to grain boundary porosity and 5% attributed to open macroscale fractures. Both of these in-situ studies revealed layering in basement porosity, with the greatest values associated with breccia and pillow zones tens of meters thick [*Kirkpatrick*, 1979; *Salisbury et al*., 1980].

Large-scale resistivity experiments conducted in DSDP Hole 504B [*Becker et al*., 1982; *Von Herzen et al*., 1983; *Becker*, 1985] revealed a similarly layered structure correlated with basement lithology. Apparent resistivity values were interpreted to indicate a decrease in porosity with depth, from 11–14% in the upper 150 m of basement to 7–10% in the next 500 m, dropping to 1–3% within the transition to sheeted dikes below the upper 700 m of basement [*Becker*, 1985]. *Pezard* [1990] reinterpreted resistivity logs from Hole 504B after a quantitative analysis of the clay and zeolite contribution to electrical conductivity and concluded that while the absolute magnitude of "free water" (water not bound to minerals) porosity may be significantly lower than previously calculated, strong vertical layering remains in the corrected data. In fact, the reinterpreted porosity profile is more consistent with the apparent abrupt decrease in permeability with depth documented during packer experiments [e.g., *Anderson et al*., 1985b, c; *Becker*, 1990b] than was the apparent porosity profile calculated without correcting for cation exchange effects [*Becker*, 1985].

Matthews et al. [1984], *Moos* [1990], and *Carlson and Herrick* [1990] analyzed geophysical logs from the upper 500 m of basement in DSDP Hole 395A, and although data were of variable quality because of deviations in hole size, the resistivity, sonic, and other logs reveal a striking sequence of layers 50–200 m thick. These layers were previously interpreted to reflect magmatic cycles of crustal accretion [*Hyndman and Salisbury*, 1984]. Each layer is defined by low apparent porosity at the base, grading upward to higher porosity (in pillows, breccia, and talus) at the top, thought to represent the last phase of each eruptive sequence. There is good correlation between abrupt changes in gradient in temperature logs collected in Hole 395A [*Kopietz et al*., 1990; *Gable et al*., 1992] and the tops of these petrophysical sequences [*Pezard*, 1990], indicating that the most porous zones contain preferred fluid flow paths. Cyclic porosity variations are also apparent in the values estimated from a large-scale resistivity experiment in Hole 395A, superimposed on an overall decrease in porosity with depth [*Becker*, 1990c].

Anderson et al. [1985a] compared geophysical logs from Hole 504B with those collected in the upper 178 m of basement in DSDP Hole 556, in 17 Ma crust west of the Azores. The upper crust around Hole 556 was well defined by 50% core recovery and includes very thin layers of basalt pillow, breccia, and massive flow units in the upper 90 m of basement, underlain by gabbro, gabbroic breccia, and serpentinized gabbro. Pillow and breccia intervals had the highest and most variable apparent porosity values, with the greatest apparent porosities clustering along boundaries between pillow and breccia units [*Anderson et al*., 1985a].

Broglia and Moos [1988] analyzed borehole logs from the upper 450 m of basement in Hole 418A, 110 Ma crust, in the western Atlantic Ocean. These data also indicate a highly layered porosity structure, although in this case the uppermost 65 m of basement is massive and relatively unaltered, while the underlying 140 m of basement comprises a highly altered pillow and breccia unit with apparent porosities of 5–25%. Natural gamma ray and bulk density logs from Hole 418A indicate a similarly layered structure, with abrupt transitions above and below the altered pillow and breccia intervals [*Broglia and Moos*, 1988; *Carlson et al*., 1988].

Jarrard and Broglia [1991] analyzed borehole geophysical logs from the upper 220 m of basement at Site 768 in the Sulu Sea (18 Ma) and the upper 110 m of basement at Site 770 in the Celebes Sea (42 Ma). These sites are the only representatives within an enormous age gap between other sites of upper basement geophysical logging (essentially 20–110 Ma). In addition, the crust at Site 768 is likely to have formed in a back arc setting [*Jarrard and Broglia*, 1991]. The high-quality logs show consistent patterns of crustal layering. Pillow basalts within the upper 100 m at Site 768 have uniformally low resistivities and compressional velocities, indicating relatively high porosities, in distinct contrast to underlying dolerites and sheet flows. The upper 100 m of logs from Site 770 indicate less variability, but thin intervals of relatively high porosity are associated with pillow and breccia zones identified from cores.

Larson et al. [1993] and *Jarrard et al*. [1995] noted similarly striking layering within the upper 100 m of basement around ODP Hole 801C in the western Pacific Ocean, although in this case the layering reflects a discrete hydrothermal zone incorporating the boundary between axial and off-axis eruptive deposits. Apparent porosity at this site remains high within Jurassic upper basement, much as open porosity remained high at 110

Ma Site 418 [*Salisbury et al*., 1980]. It may be that the isolation of basement rocks in these areas by a thick, relatively impermeable sediment cover has helped to preserve porosity (and permeability) in some of the oldest remaining seafloor by reducing exchange of fluid and solutes with the overlying ocean.

3.3. Borehole Imaging and Core Fracture Analysis

In-situ imaging tools such at the borehole televiewer (acoustic) and formation microscanner (FMS, resistivity) have been used to map out the density, orientation, and borehole apertures of fractures within the upper oceanic crust at several sites. Fracture analyses have also been conducted using basement cores recovered from deep-sea boreholes. Both methods present difficulties: borehole irregularities (washouts, breakouts) and tool malfunctions have resulted in collection of borehole imaging data of variable quality. Core orientation and incomplete and biased recovery present additional challenges. Relating the appearance of fractures on a borehole wall or in a core sample to formation-scale permeability is demanding even under ideal circumstances, as boreholes and cores provide limited views of fracture geometries, hydraulic properties, and regional significance.

The borehole televiewer was first deployed in the upper few hundred meters of oceanic basement rocks in DSDP Hole 504B and nearby Hole 501 [*Anderson et al*., 1983]. Although the quality of the analog images was mixed, distinct lithologic units, fractures, and voids were readily apparent. Only about 25 m of basement data were collected in Hole 501, but the images revealed alternating pillow basalts and massive flows, including one unfractured unit about 8 m thick subsequently correlated to Hole 504B [*Anderson et al*., 1983].

Longer and higher-quality televiewer records were later collected in Hole 504B, revealing more horizontal to subhorizontal fractures in the upper 1 km of basement than would be expected if the hole was drilled into a system having randomly distributed fractures [*Newmark et al*., 1985a, b]. There also appeared to be vertical cyclicity in fracture density on a scale of 10–100 m that tracked variations in conventional geophysical logs. The dominance of subhorizontal fractures and the apparent cyclicity of fracturing continues into the sheeted dikes, although fracture spacing increases with depth [*Newmark et al*., 1985b; *Morin et al*., 1989].

Borehole televiewer logs in MAR flank Hole 395A exposed borehole enlargements and washouts that correlated with lithologically identified breccia zones and the boundaries between pillow and flow units [*Hickman et al*., 1984b]. Additional televiewer data confirmed this correlation, but high logging speeds through upper basement made quantitative analysis of fracture orientation and distribution difficult [*Morin et al*., 1992b].

The formation microscanner provides a microresistivity image of the borehole wall using overlapping arrays of pad-mounted electrodes that are pressed against the formation. FMS images of Hole 504B were collected during ODP Leg 148 and quantitatively analyzed to determine fracture orientation and distribution [*Ayadi et al*., 1996; *Pezard et al*., 1996]. Analysis of 4500 fracture planes within the deepest 200 m of Hole 504B indicated a dominance of vertical fractures and clustering of both horizontal and vertical fracturing within discrete intervals [*Ayadi et al*., 1996]. *Pezard et al*. [1997] analyzed 34,500 fracture planes throughout basement in Hole 504B, noting one zone of highly concentrated fractures within the pillow lavas and breccias of the extrusive basalts, and another zone at the transition between extrusive in intrusive forms.

There have been few detailed studies of rock structure at the hand-sample scale within the basaltic oceanic crust using cores recovered from DSDP and ODP drill holes [e.g., *Choukroune*, 1980; *Agar*, 1994] and only one study that attempted to quantify basement permeability from analysis of fractures in cores [*Johnson*, 1980b]. The lack of such studies reflects difficulties in working with seafloor cores from upper basement, including low and often biased core recovery, and the difficulty of placing data from an individual hole within a broader geological context. *Johnson* [1980b] attempted a quantitative analysis of DSDP core fractures using samples recovered from Hole 418A, documenting fracture depth, width, orientation (relative to horizontal), and fracture-filling material. Crack frequency was found to be extremely variable and to correlate well with lithological classification: cracks were most common within restricted regions identified as breccia zones. Permeability was estimated from crack width and spacing using a parallel plate model to average 10^{-8} m^2, and to be as great as 10^{-6} m^2 within isolated intervals separated by regions of much lower permeability. These values must be gross overestimates of true formation permeability, even before many of the cracks were filled, as effective crack apertures and the extent of lateral continuity are likely to be much lower than has been assumed, and probably not all cracks were open at the same time. The difficulty in converting fracture analyses to quantitative permeabilities is illustrated through a consideration of sites where both borehole fracture imaging and packer measurements have been completed. *Pezard et al*. [1996] identified thousands of fractures in the sheeted dikes surrounding Hole 504B, yet formation bulk permeability within the same interval is apparently of the order of 10^{-18} to 10^{-16} m^2 [*Anderson et al*., 1985b, c; *Becker*, 1989, 1996]. This difficulty is not unique to the upper oceanic crust; measurements within metamorphic rocks at 2 km depth in the Cajon Pass well along the San Andreas fault also identified numerous fractures [*Barton and Moos*, 1988] within a zone having a bulk permeability of the order of 10^{-18} m^2 [*Coyle and Zoback*, 1988].

3.4. Seafloor Heat Flow Measurements

The distribution of seafloor heat flow values is related to upper crustal permeability, as the combination of high crustal permeability, fluid heat capacity, and heating

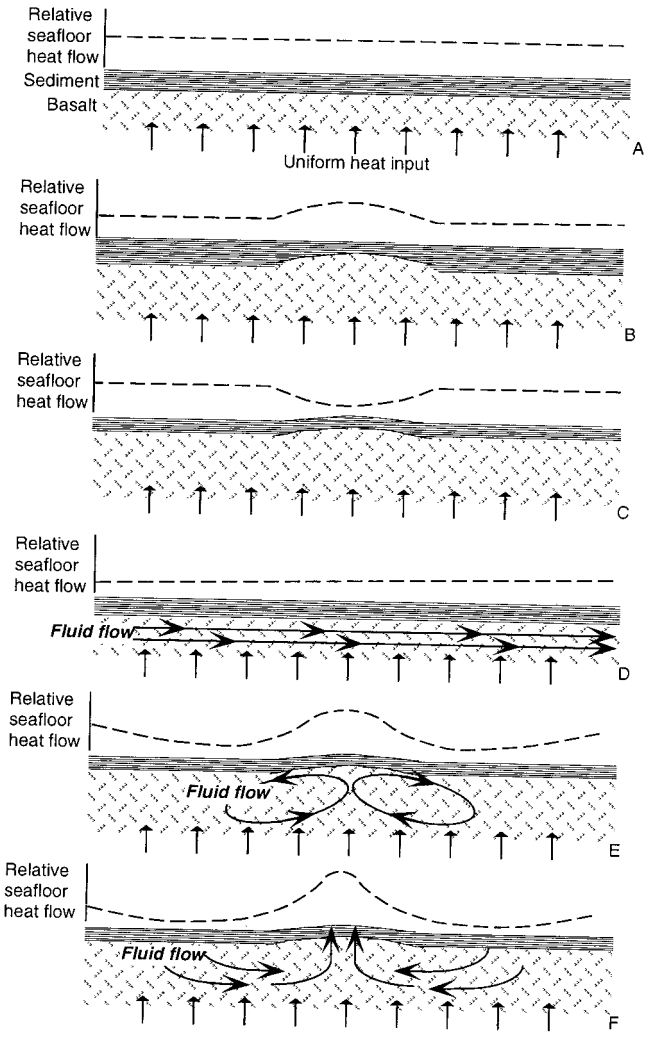

Figure 3. Steady state seafloor heat flow patterns resulting from idealized conductive and advective conditions within oceanic basement and sediments. Heat input at the base of the crust is assumed to be constant and uniform; seafloor heat flow relative to that input at the base of the crust is shown by the dashed line above the schematic crustal section. (a) Seafloor heat flow is uniform and equal to input at the base of the crust when sediments and basement are flat lying, sediment thickness is constant, there are no heat sources within the crust, and heat flow is purely conductive. (b) Seafloor heat flow is elevated above a buried basement ridge below flat sediments because greater basement thermal conductivity channels heat to flow out through the basement ridge. (c) Seafloor topography leads to conductive refraction at the seafloor, making heat flow lower over a seafloor and basement high. (d) Lateral fluid flow within basement may result in an overall lowering of conductive heat flow at the seafloor, as heat is advected laterally away from the site. The system requires a recharge area, and the advected heat must eventually exit the crust. (e) Cellular convection confined to basement results in local to regional redistribution of heat, but there is no net regional, advective heat loss from basement to the overlying ocean. (f) Cellular convection including local or regional recharge may result in elevation of seafloor heat flow in discharge areas and suppression of seafloor heat flow in recharge areas. The net conductive heat flux is depressed in relation to the heat input at the base of the crust.

from below leads to significant heat advection through the seafloor. Understanding advective interpretations of heat flow requires a brief review of conductive heat flow and common causes of seafloor thermal anomalies. This approach is most widely applicable on ridge flanks, as it was not possible until recently to measure conductive heat flow through exposed basalt [*Johnson and Hutnak*, 1996]. Heat flow patterns have been mapped in detail at the ridge crest only at sedimented spreading centers [e.g., *Lonsdale and Becker*, 1985; *Davis and Villinger*, 1992; *Davis and Becker*, 1994b] and on single hydrothermal mounds [e.g., *Becker et al*., 1996].

Seafloor heat flow is considered to be anomalous when it deviates from a conductive lithospheric cooling reference [e.g., *Parker and Oldenberg*, 1973; *Davis and Lister*, 1974; *Parsons and Sclater*, 1977]. Where basement is flat, the sediment layer has uniform thickness, and thermal transport is purely conductive, seafloor heat flow should vary only with heat input at the base of the crust (Figure 3a). If the seafloor is well sedimented and flat, but there is significant basement relief below the sediment layer, heat flow may be higher over basement ridges because the greater thermal conductivity of basalt relative to shallow sediments (usually about 1.5:1 to 2.0:1) will channel heat (Figure 3b). If there is seafloor relief with a uniform sediment layer draped over basement topography, thermal refraction will decrease heat flow over basement and seafloor ridges and increase heat flow over troughs [*Birch*, 1967; *Lee*, 1991]. The relative magnitudes of conductive focusing versus conductive refraction will depend on the size of the thermal conductivity contrast, the amplitude and wavelength of relief, and sediment thickness and variability. Given typical abyssal hill relief of several hundred meters and the relatively modest contrast between the thermal conductivity of sediment and upper basement, seafloor refraction will often overwhelm conductive focusing, making conductive heat flow lower over local seafloor highs, even if sediment thins slightly over basement ridges (Figure 3c).

Conductive anomalies may be overshadowed by advective effects, which reflect crustal hydrogeological properties. Ridge flanks host hydrothermal circulation responsible for most of the advective heat loss from oceanic crust [*Sclater et al*., 1980; *Stein and Stein*, 1994], as well as significant chemical exchange [*Mottl and Wheat*, 1994; *Kadko et al*., 1995; *Elderfield and Schultz*, 1996]. Even where sediment cover appears to be continuous, advective or nonhomogeneous conditions in basement may cause local heat flow anomalies [e.g., *Sclater et al*., 1976]; in fact, many ridge flank measurements judged previously to be "most reliable" on the basis of local sediment thickness and continuity actually may be no more reliable than those made in areas of incomplete sediment cover [*Stein and Stein*, 1994].

Fluids flowing laterally through basement can remove much of the heat conducted from the base of the lithosphere before it reaches the seafloor (Figure 3d). This

advected heat must leave the crust somewhere, perhaps at a basement exposure or through permeable conduits such as faults. Seafloor heat flow over crust through which heat is being laterally advected may be suppressed relative to the conductive reference, and there may be a subtle "downstream" increase in heat flow, depending on the flow rate in basement, depth of flow, and other conditions. Advective heat loss at a lateral scale of kilometers apparently occurs along lightly sedimented areas and isolated sediment ponds on the north flank of the Galapagos Spreading Center [*Sclater et al*., 1974; *Anderson et al*., 1976] and on the west flank of the MAR [*Langseth et al*., 1984, 1992]. The same process apparently occurs at a greater lateral scale on the east flank of the Juan de Fuca Ridge [*Davis et al*., 1992a; *Fisher et al*., 1996; *Shipboard Scientific Party*, 1997], in the Brazil Basin west of the MAR [*Langseth and Herman*, 1981], in the Guatemala Basin [*Abbott et al*., 1984], and on the west and east flanks of the East Pacific Rise (EPR) [*Sclater et al*., 1976; *Baker et al*., 1991; *Langseth and Silver*, 1996].

Hydrothermal circulation in basement can also redistribute seafloor heat flow without resulting in a regional loss of measurable heat, as documented over oceanic crust having a range of ages [e.g., *Anderson et al*., 1977, 1979; *Embley et al*., 1983; *Langseth et al*., 1988; *Noel and Hounslow*, 1988]. If fluid circulation is sufficiently vigorous, upper basement may become thermally homogenized [e.g., *Davis et al*., 1989; *Fisher et al*., 1990; *Shipboard Scientific Party*, 1997], resulting in heat flow values that are higher over basement ridges and lower over basement troughs (Figure 3e). In this case, the net regional heat flux will match the lithospheric reference, but conductive seafloor heat flow will be locally elevated or depressed.

Another form of off-axis hydrothermal circulation is essentially a mixture of the last two types, combining local convection in basement and advective loss of heat to the overlying ocean (Figure 3f). This form of hydrothermal circulation is most common over young oceanic crust [e.g., *Lister*, 1970; *Anderson et al*., 1977; *Hobart et al*., 1985; *Davis et al*., 1992a] but may continue out to greater age if permeability is sufficiently high. This form of hydrothermal circulation may result in both regional suppression of seafloor heat flow below that expected based on crustal age, and local heat flow anomalies reflecting the extent of basement thermal homogenization, basement relief, sediment thickness, and the presence of fluid venting or recharge sites. These last two forms of hydrothermal circulation (Figures 3e and 3f) have been called "cellular convection" because of the hypothesized shape of the fluid convection cells [e.g., *Lister*, 1972; *Davis et al*., 1992a], although in the present discussion no particular flow geometry is assumed. Cellular convection appears to occur commonly in oceanic basement, on the basis of a review of data from many older surveys, although navigational uncertainties and widely spaced measurements made it difficult to interpret these correlations with confidence [*Fisher and Becker*, 1995]. Some thermal homogenization of upper basement is required to explain many of these observations, as thermal refraction would otherwise lead to the opposite correlation between seafloor relief and heat flow (Figure 3c), and the magnitude of many heat flow anomalies is too great to be explained by conductive focusing alone (Figure 3b).

As is clear from this brief overview, distinct conductive and advective processes can lead to similar deviations in seafloor heat flow. The first heat flow studies along ridge flanks that included relatively closely spaced measurements arranged along orderly transects identified distinct regions of higher and lower heat flow [e.g., *Lister*, 1972; *Williams et al*., 1974], often forming elongate patches parallel or subparallel to the ridge crest, with a cross-strike wavelength of one to several kilometers. These observations led to an inferred wavelength of hydrothermal circulation cells in the upper crust, with regions of higher heat flow indicative of rising fluids. The Rayleigh number Ra was used to relate the onset of convection in particular areas to equivalent porous-medium permeability:

$$Ra = \frac{\alpha g k H \Delta T}{\nu \kappa_m} \tag{3}$$

where α is fluid expansivity, k is permeability (isotropic and homogeneous), H is the thickness of the porous medium, ΔT is the difference in fixed temperature boundary conditions at the top and bottom of the permeable layer, ν is kinematic viscosity, and κ_m is the thermal diffusivity of the fluid-saturated porous medium. The Rayleigh number is a measure of the tendency of fluid within a porous system to convect as a result of buoyancy forces, when advection will be more efficient than conduction in transporting heat vertically from the bottom to the top boundary. Convection will occur when a critical Rayleigh number is exceeded, typically a value of about 40 ($4\pi^2$) for fixed-temperature boundary conditions [*Lapwood*, 1948; *Nield*, 1968]. The convection cells formed as a result of Rayleigh instability within an isotropic, homogeneous, porous medium tend to have a low aspect ratio (width to height), as confirmed by Hele-Shaw cell experiments [e.g., *Hartline and Lister*, 1981]. A common application of (3) to seafloor hydrothermal systems has been to assign reasonable values for all parameters except permeability on the right-hand side, assume that permeability is isotropic and homogeneous, and calculate the permeability required to initiate Rayleigh instability.

Since porous media models suggested that homogeneous, isotropic systems tend to host thermal convection cells with low aspect ratios, the apparent spacing of several kilometers of seafloor heat flow anomalies suggested a depth of penetration on a similar scale, constraining the apparent permeability of the upper several kilometers of oceanic crust [*Williams et al*., 1974; *Ander-*

son and Hobart, 1976; *Anderson et al*., 1977; *Cathles*, 1990]. Similar reasoning has been applied to shorter-wavelength variations in seafloor heat flow [*Davis et al*., 1992a, 1996; *Snelgrove and Forster*, 1996]. The resulting conceptual models of ridge crest and ridge flank hydrothermal circulation were consistent with the first direct measurements of upper crustal permeability (bulk values of 10^{-13} to 10^{-14} m^2) but inconsistent with many subsequent measurements made below the upper few hundred meters of basement (bulk values below 10^{-16} m^2) [e.g., *Hickman et al*., 1984a; *Anderson et al*., 1985b, c; *Becker*, 1990b].

The idea that hydrothermal circulation penetrates to several kilometers at the ridge crest is supported by geological and geochemical evidence from ophiolites [e.g., *Gregory and Taylor*, 1981; *Nehlig and Juteau*, 1988a, b], the need for a thin boundary layer above a magma chamber to supply sufficient heat to support ridge crest vents [*Lister*, 1974; *Cann and Strens*, 1982] and the presence of a seismic reflector at many spreading centers thought to represent the top of a magma chamber [e.g., *Detrick et al*., 1987; *Calvert*, 1995], and geobarometry of hydrothermal vent fluids [*Campbell et al*., 1988] and fluid inclusions [*Vanko*, 1988]. While the evidence is compelling for high-temperature ridge crest hydrothermal systems, the depth extent of ridge flank hydrothermal flow is not well constrained by observations. *Lister* [1974, 1980] noted the difficulty in using seafloor heat flow values to infer the depth extent or magnitude of permeability within the oceanic crust, and others have expressed similar concerns [e.g., *Fisher et al*., 1990; *Fisher and Becker*, 1995; *Davis and Chapman*, 1996]. Yet the idea that the lateral scale of seafloor heat flow variations provides some indication as to the depth of circulation remains strongly rooted in conceptual models of how these systems behave [e.g., *Davis et al*., 1980, 1996; *Fehn et al*., 1983; *Cathles*, 1990, 1993].

While large-scale lateral convection (Figure 3d) and cellular convection (Figures 3e and 3f) modify the thermal structure of the uppermost crust, deep convection is not required unless one assumes that circulation cells have a low aspect ratio. For example, *Davis et al*. [1992a, 1996] initially suggested that fluid convects in low-aspect-ratio cells in 1 Ma crust along an east Juan de Fuca flank profile, within an isotropic, permeable layer 600 m thick. Shallow basement reflectors subparallel to seafloor heat flow anomalies were subsequently recognized in multichannel seismic data from the site, suggesting the possibility of a permeability-controlled circulation geometry in upper basement [*Davis and Chapman*, 1996]. Consideration of the total conductive heat loss from 1 Ma oceanic crust along this profile also seems to require a component of large-scale lateral flow (e.g., Figure 3d), as seafloor heat flow is well below that expected on the basis of crustal age [*Fisher and Becker*, 1995] despite being tens of kilometers from the nearest known basalt outcrops that might allow entry of cold seawater and exit of warmed fluids [*Davis et al*., 1992a].

Langseth and Herman [1981] used an idealized heat-exchange model to estimate lateral specific discharge within the upper igneous crust of $1–2 \times 10^{-8}$ m s^{-1} in the Brazil Basin, and noted that measured permeabilities in uppermost Hole 504B were consistent with this flow rate and a lateral pressure gradient of 0.05–0.5 MPa km^{-1}. *Langseth et al*. [1984] estimated equivalent porous-medium permeability of about 10^{-13} m^2 for the upper 300 m of basement below a sediment pond west of the MAR, using a lateral-flow analytical model and measured seafloor heat flow values 70–90% below that predicted for conductively cooling crust. *Baker et al*. [1991] applied a larger-scale lateral-flow model (originally introduced by *Langseth and Herman* [1981]) to calculate the apparent permeability in basement within the west flank of the EPR, estimating values of 10^{-10} to 10^{-12} m^2 over lateral distances of 200–20 km, respectively. Application of the same model along a 75-km transect across the Guatemala Basin would result in similarly high permeabilities, as heat flow is 50–90% below that predicted by lithospheric cooling models [*Abbott et al*., 1984].

Heat flow highs at ridge flank sites are often associated with normal faults on the margins of abyssal hills [e.g., *Lister*, 1972; *Williams et al*., 1974, 1979; *Green et al*., 1981; *Johnson et al*., 1993]. This observation suggests that faults may act as conduits or barriers to flow within the upper oceanic crust (as do geological observations at ridge crests) but the significance of faults in channeling large-scale circulation is unclear. For example, a recent multichannel seismic survey around DSDP Site 504 indicated that many normal faults in basement penetrate the seafloor [*Kent et al*., 1996]; these faults cannot be major conduits for fluid flow through the sediments, since there is no regionally "missing" heat flow, but the faults could be hydrologically important within basement. Since faults are often associated with seafloor abyssal topography [*Macdonald et al*., 1996], determining their role relative to that of basement relief in directing fluid flow is difficult. However, subvertical faults in the upper oceanic crust cannot be responsible for transporting significant quantities of fluid and heat laterally across strike unless the faults rotate at depth or otherwise connect intervals of high subhorizontal permeability.

Borehole heat flow values at depth in Hole 504B also may reflect upper crustal permeability, although such an interpretation is speculative. Heat flow within the deepest kilometer of the hole has repeatedly been determined to be about 120 mW m^{-2}, 40% lower than the 200 mW m^{-2} measured within the sediment section in nearby Hole 504C [*Becker et al*., 1983a] and predicted by conventional lithospheric cooling models for 5.9 Ma crust [e.g., *Parsons and Sclater*, 1977]. This reduction in heat flow with depth is difficult to explain because the mean value at the seafloor is close to the predicted lithospheric value [*Langseth et al*., 1988; *Fisher et al*., 1990], so that there can be no net advective heat loss regionally. *Gable et al*. [1989] and *Fisher and Becker*

[1991] discussed the possibility of borehole convection contributing to the apparent reduction in heat flow with depth, while *Guerin et al*. [1996] described an alternative explanation: regional conductive heat flow of 120 mW m^{-2} and lateral fluid flow along a listric normal fault located about 525 m into basement [*Agar*, 1991; *Pezard et al*., 1997], at the top of the transition zone between extrusive and intrusive basalts. A two-dimensional numerical model of coupled heat and fluid flow provided a good match to the thermal data measured deep in Hole 504B when fault zone permeability is about 10^{-15} m^2 (significantly greater than that measured by *Anderson et al*. [1985b, c], but close to the upper end of the range reinterpreted by *Becker* [1996] from the same packer measurements; see Table 1), but a large lateral pressure gradient of unknown origin is required to drive sufficient fluid flow, as is a separate flow system capable of maintaining much higher heat flow at the seafloor.

In summary, heat flow data provide useful constraints on fluid circulation parameters (depth, fluid velocity, temperature, driving forces, permeability, etc.), but quantitative interpretations require assumptions regarding the geometry and distribution of flow. Measurements of seafloor heat flow indicating nonconductive conditions within upper basement (Figures 3d to 3f) require that there be fluid circulation, and thus significant permeability, but seafloor thermal data do not constrain the depth of circulation or the hydrologic properties of the upper crust, except where remaining parameters are independently estimated.

3.5. Hydrothermal Circulation Models

The use of hydrothermal circulation models of the upper oceanic crust to estimate permeability (magnitude and depth extent) is described in this section, with discussion of selected models and a listing of quantitative inferences in Table 2. In addition to estimating permeability values for the upper oceanic crust, these models provide insight as to the form and origin of permeability. This review is divided into ridge crest and ridge flank models. Hydrothermal circulation models also fall into two general methodological groups [*Lowell et al*., 1995]: porous/fractured media and fracture loop. In the former, the large-scale properties of the upper oceanic crust are represented through use of the REV concept described earlier, Darcy's law is assumed to apply, and zones containing fractures are represented through localized increases in porosity and permeability. Fluid and rock conditions within the porous-flow system are generally assumed to be at equilibrium within individual subdomains (mesh cells or elements). While it is not strictly possible to verify complex numerical results [e.g., *Oreskes et al*., 1994], model output can be examined for consistency with independent observations (other than those used to construct the model).

In fracture loop models, the flow path is considered to be an open channel, and interactions with the surrounding rock occur across the wall of the channel, more readily incorporating nonequilibrium conditions between the fluid and rock. Fracture loop models are generally single pass, with seawater entering at the seafloor, exchanging heat and solutes with the surrounding formation at depth, and then venting into the ocean. Some fracture loop models include distinct upflow and downflow channels [e.g., *Bodvarsson and Lowell*, 1972; *Lowell*, 1975] while others incorporated flow longitudinally along a single channel [e.g., *Strens and Cann*, 1982].

3.5.1. Models of ridge crest circulation. Modeling ridge crest hydrothermal circulation is considerably more difficult than modeling ridge flank circulation. Ridge crest vent temperatures may exceed 350°C [*Von Damm*, 1995], and hydrologic properties may change on short timescales [*Baker et al*., 1989; *Lowell and Germanovich*, 1995], while ridge flank systems include much lower temperatures and conditions that change more slowly and are less spatially variable [*Mottl and Wheat*, 1994]. In addition, some high-temperature hydrothermal fluids undergo phase separation during flow [e.g., *Butterfield et al*., 1990, 1994], greatly complicating the physics that must be simulated [e.g., *Bischoff and Rosebauer*, 1984, 1989]. There are no direct measurements of crustal permeability at normal ridge crests, and much of the permeability within these systems is probably dominated by fractures. Fluids within high-temperature vent systems probably flow turbulently, at least within parts of upflow zones, creating additional difficulties in modeling. Diffuse flow may dominate some hydrothermal fluxes at ridge crests [*Schultz et al*., 1992; *Rona and Trivett*, 1992; *Ginster et al*., 1994], but the geometries of distinct convection systems are poorly understood. Fortunately, these difficulties have not discouraged several generations of modelers from attempting to simulate ridge crest hydrothermal circulation, and the results of these models provide numerous estimates of hydrologic properties within upper oceanic basement.

Pioneering analytical models of *Lister* [1972, 1974] were essentially one dimensional and weakly coupled, as fluid flow and heat flow components were considered separately within a single conceptual model that included stress state, crack propagation, and transient magmatic input and heat loss. Inferences regarding permeability were assumed to apply broadly to ridge crests and flanks. *Lister* [1972] initially assumed crustal permeability of 10^{-16} m^2 extending to depths as great as 7 km, although he recognized the potential importance of lateral variability in permeability, seafloor topography, and the presence of a low-permeability sediment layer in guiding fluid circulation. Permeabilities as great as 10^{-14} m^2 for the upper several kilometers of crust were also considered [*Lister*, 1972, 1974], with the assumed depth of fluid penetration based mainly on microseismic observations associated with geothermal activity in Iceland and observations of products of hydration reactions within the gabbroic and deeper sections of ophiolites [*Lister*, 1974]. *Lister* [1974, 1977, 1980] developed a theoretical basis for the establishment of relatively high

permeability in the upper oceanic crust: the formation and migration of a cracking front as cold ocean water circulated into much warmer rock. *Lister* [1974] suggested that vertical permeability would be twice as great as horizontal permeability, given the expected distribution and orientation of cracks, and proposed that permeability would vary with time, falling by a factor as great as 10^4 because of fatigue failure or thermal stresses.

Bodvarsson and Lowell [1972] and *Lowell* [1975] examined the dependence on crack width of venting temperature and duration. *Lowell* [1975] modeled viscous flow in a flat, rectangular channel and noted that expected flow rates were extremely sensitive to fracture widths, with turbulent flow for fracture widths >1 cm but widths of 3 mm considered to be more typical. Fractures of varying widths and depths distributed throughout the upper crust were hypothesized to explain observed seafloor variability in heat flow. *Lowell and Rona* [1985] constructed a series of fracture loop models to examine how the nature of crustal heat sources and permeability might influence the formation of sulfide deposits within upper basement. The necessary heat could be extracted through the thin lid of a replenished magma chamber if permeability within a 1-km-thick reaction zone is about 10^{-15} m^2, with permeability in the crustal upflow zone being 10^{-13} m^2. Permeability within the reaction zone would be considerably greater if the reaction zone is thinner [*Lowell and Rona*, 1985].

Strens and Cann [1982, 1986] considered fluid upflow and downflow within a single fracture along strike of the ridge crest. *Strens and Cann* [1982] restricted the discharge from their fracture loop systems to pass through a small number of thin "pipes" in order to generate realistically high temperatures at the seafloor. These models did not explicitly include rock permeability, as flow was restricted to individual open fractures, but flow was required to extend to 500–1000 m below the seafloor to tap sufficient heat from an axial magma chamber. *Strens and Cann* [1986] compared the efficiency of a 40-cm-wide fracture and a porous medium having a cross-sectional width of 2 km, and noted that a porous medium would need to have a permeability of about 10^{-8} m^2 to allow the same mass flux, given conditions appropriate for a black smoker hydrothermal vent. *Cann et al*. [1985] conducted additional studies of sulfide formation at a mid-ocean ridge environment, modeling flow channels as open pipes containing turbulent flow to a depth of 1.5–2.0 km.

Cann and Strens [1989] explored the causes of megaplume events along mid-ocean ridges, with a low-permeability recharge zone and a more restricted, high-permeability discharge zone connected through a reaction zone at depth. The authors envisioned a complex pore and crack structure within the seafloor, including turbulent flow within open channels, clogging of cracks through hydrothermal precipitation, and the transient formation of a low-permeability cap within the seafloor discharge zone. A sudden increase in discharge permeability would result from crustal extension and/or hydrofracturing following an abrupt increase in fluid pressure above hydrostatic, as has been observed in terrestrial hydrothermal systems [e.g., *Fournier*, 1991]. A model simulating the formation of a megaplume event included recharge permeabilities of 10^{-13} to 10^{-11} m^2, with values of at least 10^{-12} m^2 apparently required to allow sufficient fluid flow.

In contrast, *Cathles* [1993] argued that a low-permeability cap and high recharge permeabilities are not needed to generate megaplumes. These models included circulation to the base of the crust (~7 km) and a similar circulation width. Upflow to hydrothermal vents occurred within a thin zone along the edge of a large magmatic intrusion (a 5-km-high cylinder of 2-km radius) at the ridge axis. Consideration of the heat output of a megaplume event and the geometry of the upflow zone then required that upflow permeability need be only about 3×10^{-14} m^2, provided that recharge permeability is no less than 10^{-16} m^2 [*Cathles*, 1993].

Lowell and Germanovich [1995] explored the implications of dike injection at spreading centers for upper crustal permeability and the formation of megaplumes with a fracture loop model applicable to either along-strike or across-strike, single-pass circulation. The model did not require penetration of a previously impermeable cap or previously existing hydrothermal activity at the megaplume site, but it did require that initial permeability within the hydrothermal recharge zone be $\geq 10^{-12}$ m^2 [*Lowell and Germanovich*, 1995]. An effective permeability for the upflow zone, based on application of the cubic rule for an equivalent porous medium, was calculated to be about 10^{-9} m^2. Such high permeabilities would be unusual and could explain why megaplumes do not always accompany dike injection, even where there is preexisting black-smoker venting. In addition, cracks would take years to seal through deposition of silica [*Lowell et al*., 1993; *Lowell and Germanovich*, 1995], preventing the immediate continuation of black smoker venting following megaplume discharge. *Wilcock* [1997] suggested that an abrupt increase in upflow permeability, to 10^{-9} to 10^{-10} m^2, as well as high permeability within a reaction zone reservoir at depth, could result in a massive transient plume following fluid decompression.

Wilcock and McNabb [1996] used an analytical model for fluid flow at a ridge crest to estimate the large-scale permeability of the upper igneous crust, with the Endeavor segment of the Juan de Fuca Ridge providing observational constraints. High-temperature venting was considered in terms of the loss of fluid from crust at depth that must be recharged from the surface. Seafloor vent clusters were thus envisioned as overlying point sinks for mass at depth, and the resulting pressure gradients and fluid flow necessary to replace this loss constrained a range for effective permeability, 6×10^{-13} to 6×10^{-12} m^2 for a homogeneous, isotropic upper crust. Additional calculations based on an anisotropic model

(with greater permeability along strike than across strike) yield similar values for along-strike permeability and values of 3×10^{-14} to 2×10^{-12} m^2 for across-strike permeability.

Ribando et al. [1976] noted that the observations of *Williams et al*. [1974] close to the Galapagos Spreading Center were consistent with the concept of two-dimensional cellular convection within the oceanic crust, and attempted to simulate the observed variability in seafloor heat flow using a range of possible boundary conditions and permeability distributions within a two-dimensional, porous-media model. The apparent wavelength of the heat flow highs and lows (7 km) was used to infer the depth of penetration of the circulation cells, 3.5 km in the case of constant permeability, and greater depth of penetration in the case of exponentially decreasing permeability. Isotropic permeability was estimated to be of the order of 4.5×10^{-16} m^2 and was considered to represent a fractured medium having crack widths of 0.05 mm and crack spacing of 1–10 m [*Ribando et al*., 1976].

The two-dimensional models of *Fehn and Cathles* [1979, 1986], *Fehn et al*. [1983] and *Fehn* [1986] included a heat flow contribution from the spreading center as well as heating from below the crust. Initial simulations represented a system 5–10 km thick with a uniform permeability of $2.5–5.0 \times 10^{-16}$ m^2, as well as a permeability distribution that decreased exponentially with depth from 2.5×10^{-15} m^2 at the surface. *Fehn and Cathles* [1979] also introduced a vertically oriented 500-m-wide zone of relatively high permeability to explore the possible influence of fractures or "shear zones" and found that such permeability enhancements were necessary to produce seafloor regions having large negative heat flow anomalies. The tendency of these more permeable zones to concentrate fluid flow, upward or downward, depended on the location of the zones relative to kilometer-scale convection cells. The *Fehn et al*. [1983] models were completed following the first in-situ measurements of bulk permeability in DSDP Hole 504B [*Anderson and Zoback*, 1982], and it was recognized that there was a discrepancy between the magnitudes of inferred "crustal scale" permeabilities ($\sim 10^{-15}$ m^2) used in many numerical models and measured values 5–50 times greater measured within the shallowest basaltic crust. The difference was attributed to the measurements being in the shallowest crust.

Rosenberg et al. [1993] modeled ridge crest hydrothermal circulation within horizontally and vertically layered systems and suggested that the imposition of a more permeable layer overlying a less permeable layer may cause focusing of discharge without a narrow zone of elevated permeability near the seafloor. The models did not include venting at the seafloor through orifices tens of centimeters across, however, so it is not clear that self-organization can account for this frequently observed manifestation of high-temperature flow. *Travis et al*. [1991] completed some of the first three-dimensional models of ridge-crest hydrothermal circulation, including isotropic permeability within thick layers of basalt, gabbro, and upper mantle. Basaltic pillows, flows, and dikes were represented by a single layer, 1.5 km thick, with effective permeability of 10^{-15} m^2. Regions of upwelling and high heat flow were relatively restricted, and transient effects following intrusion at the ridge crest were also simulated.

Several ridge crest models included aspects of transient permeability development such as precipitation of mineral phases that clog cracks [*Wells and Ghiorso*, 1991], thermal stresses associated with hydrothermal cooling [*Lister*, 1974; *Lowell*, 1990; *Germanovich and Lowell*, 1992], or both [*Lowell and Germanovich*, 1994; *Lowell et al*., 1993]. *Wells and Ghiorso* [1991] incorporated porosity changes in fluid upflow zones due to silica precipitation, with permeability calculated using an empirical relation developed for porous media, and calculated that hydrothermal flows may be limited by low permeability on a decadal scale. *Lowell and Germanovich* [1994] demonstrated that high-temperature venting could not be sustained on decadal timescales unless heat was supplied at the base at a rate equal to the hydrothermal extraction rate, or a permeable cracking front penetrated to greater depth with time, as precipitation of hydrothermal silica would clog open fractures and pores. Coupled models are intriguing and have been applied extensively to continental systems [e.g., *Lichtner*, 1985; *Ortoleva et al*., 1987]. More work will be required to demonstrate understanding of both positive and negative feedback mechanisms influencing seafloor hydrothermal systems and to constrain reaction kinetics, crustal stress and strain rates, and the distribution of basement permeability.

3.5.2. Models of ridge flank circulation. The *Fehn and Cathles* [1986] and *Fehn et al*. [1983] studies also included ridge flanks, and permeability was assumed to remain constant or to decrease exponentially with depth. *Fehn and Cathles* [1986] suggested that smooth lateral variations in seafloor heat flow on ridge flanks could not be explained by large-scale convection that was controlled by a heterogeneous permeability distribution. *Fehn and Cathles* [1986] also tested exponentially decreasing permeability distributions and found that significant fluid flow penetrated to depths having permeability $\geq 10^{-15}$ m^2. These models contained additional features consistent with geochemical and geological observations in boreholes and ophiolites, including the formation of distinct primary and secondary convection systems, the transport of ridge flank convection cells with the spreading crust, and across-strike seafloor heat flow anomalies.

Williams et al. [1986] conducted a radial, two-dimensional study of ridge flank convection near DSDP/ODP Hole 504B and demonstrated that the observed decrease with time of fluid flow into the hole could be explained by a transient loss in fluid underpressuring in basement. These models included a thick sediment layer having

extremely low permeability overlying 1 km of basalt, with permeabilities in basement being greater than 2×10^{-15} m^2 only within the upper 100 m. *Fisher et al*. [1990] conducted two-dimensional simulations of the Site 504 region using models having significant permeability within only the upper few hundred meters of basement. These models included idealized seafloor and basement relief and differential sediment thickness, with thinner sediments draped over basement ridges. Observations successfully simulated included basement differential pressures, heat flow highs over basement ridges, and vertical and lateral fluid flow within overlying sediments. The original models also included localized heat flow highs over seafloor troughs, in contrast with many observations, but these were attributed to numerical inefficiencies resulting from a rectilinear representation of the upper oceanic crust [*Fisher et al*., 1990].

Localized heat flow highs over basement troughs were eliminated through the use of curvilinear elements that allowed more efficient lateral heat and fluid transport and through additional concentration of permeability within one or more thin zones. The geometric mean permeability within the upper 100 m of basement was 10^{-13} m^2, in agreement with packer and borehole temperature measurements (Plate 1), but most of the permeability was concentrated within thin layers of upper basement [*Fisher et al*., 1994; *Fisher and Becker*, 1995]. The effect of including these thin, very permeable zones, represented in the models by elongated, curvilinear elements, was to impose extreme lateral anisotropy in upper crustal permeability. Perhaps the most important conclusion drawn from these studies was that significant permeability was not required at depths greater than those measured during packer experiments in order to allow chemically and thermally significant fluid flow within the uppermost crust, provided that sufficient permeability concentration and anisotropy allowed for efficient lateral transport.

These simulations also suggested that basement relief could strongly influence the pattern and intensity of hydrothermal convection [e.g., *Lister*, 1972], as well as seafloor heat flow. *Lowell* [1980] and *Hartline and Lister* [1981] showed that the influence of basement topography should not extend to depths much greater than the amplitude of relief, interpretations consistent with the shallow circulation models of *Fisher et al*. [1990, 1994] and *Fisher and Becker* [1995]. Basement relief of a few hundred meters would be much less important to flow geometries if free convection extended 1 km or more below the top of an isotropic basement.

Rosenberg and Spera [1990] and *Rosenberg et al*. [1993] examined the importance of anisotropy and permeability distribution on ridge flank hydrothermal circulation, with horizontal transport in a shallow layer enhanced by horizontal anisotropy (k_x/k_z) values as large as 10. Permeability anisotropy was intended to reflect pervasive horizontal fracturing within the shallowest basement as well as vertically oriented structure associated with diking in deeper basalt [*Rosenberg and Spera*, 1990]. Greater anisotropy tended to reduce the number of convection cells, while the absolute magnitude of permeability controlled the depth extent of significant flow.

Davis et al. [1996] and *Snelgrove and Forster* [1996] completed simulations of hydrothermal circulation within young crust on the east flank of Juan de Fuca ridge. The most permeable upper basement layer in their simulations was flat-lying and 600 m thick, based on the calculated depth of a seismic reflector [*Rohr et al*., 1994] and the expectation that low-aspect-ratio convection cells within an isotropic porous medium would explain seafloor heat flow variations. *Davis et al*. [1996] found that an upper crustal permeability of either 3×10^{-14} or 2×10^{-12} m^2 provided the appropriate thermal homogenization of upper basement, with the higher value being favored. *Fisher and Becker* [1995] suggested that the same seafloor heat flow pattern could be explained by hydrothermal convection within a thin layer in the upper crust, with small-scale basement or aquifer topography influencing the pattern of flow. *Snelgrove and Forster* [1996] assumed porous medium permeability of 10^{-13} m^2 within the upper 600 m of basalt and completed a detailed parametric study of the importance of sediment permeability on the form and thermal effect of circulation within basement.

Davis et al. [1997b] conducted additional simulations of ridge flank hydrothermal circulation in a parametric study of the thickness and permeability of the basement aquifer and the importance of basement relief beneath a flat seafloor. These analyses suggested that very high crustal permeabilities may be required to allow thermal homogenization at the sediment-basement interface as well as the generation of fluid overpressures within basement ridges. The porous-medium permeabilities required to match inferred thermal conditions were $\geq 10^{-9}$ m^2 for a 60-m-thick permeable zone and $\geq 10^{-11}$ m^2 for a 600-m-thick permeable zone. Equivalent permeability values for upper basement were estimated using a high-conductivity proxy to simulate thermally efficient convection, as steady state simulations with very high permeabilities proved to be unstable. The *Davis et al*. [1997b] models required extremely vigorous, chaotic convection to homogenize basement temperatures, while chaotic conditions were not required within the thin layers modeled by *Fisher et al*. [1994] and *Fisher and Becker* [1995].

Wang et al. [1997] completed additional parametric studies of basement topography, aquifer thickness, and permeability in the upper oceanic crust, noting that the direction of flow within basement depended on a combination of crustal parameters and initial conditions. Unstable convection was likely to develop at Rayleigh numbers greater than 10 times the critical value. The possibility of unstable convection within an isotropic porous medium heated from below has been recognized for some time [e.g., *Horne and O'Sullivan*, 1974], but its

occurrence in the upper oceanic crust remains to be confirmed.

Yang et al. [1996] modeled the east flank of Juan de Fuca ridge as well but incorporated vertical and horizontal fractures into a porous-medium model of coupled heat and fluid flow, suggesting that the representations of permeability in the models of *Fisher and Becker* [1995] and *Davis et al*. [1996] were geologically unjustified. Primary models included background permeabilities of about 5×10^{-14} m^2 and 10^{-16} m^2 for the upper two layers of basement (each 100 m thick), and randomly distributed horizontal and vertical fractures having an aperture of 0.22 mm. Each fracture was simulated as a discrete layer or column having local permeability of 4×10^{-9} m^2 using an equivalent-permeability relationship. Since fracture spacing was allowed to be no closer than 10 m, the overall equivalent porous-medium permeability of the fractured layers was no greater than 9×10^{-14} m^2 and was lower where fractures were more widely spaced. No specific geological mechanisms or observations constrained the number or distribution of fractures in these simulations, but the resulting seafloor heat flow pattern did match the amplitude and wavelength of observations without including basement relief, differential sediment thickness, or a thick permeable zone. The subsequent presentation by *Davis and Chapman* [1996] of upper basement reflectors that are subparallel to seafloor heat flow patterns suggested that the distribution of basement permeability may influence flow geometry in this setting, but the *Yang et al*. [1996] models illustrate the potential importance of wide-scale fracturing in the upper crust.

3.6. Additional Geological, Geophysical, and Crustal Alteration Constraints

Seafloor crustal morphologies and the location of sulfide deposits, geophysical properties at ridge crests, bulk chemical compositions within ophiolites, and other aspects of ocean crustal geology have additional implications for the distribution of permeability within shallow basement, although much of the associated discussion is speculative and qualitative. It is difficult to quantify the results of these experiments and observations in terms of hydrogeology, but selected examples help to complete a picture of permeability formation and evolution within basaltic oceanic crust.

3.6.1. Geological studies. Although mapping of the global ridge system is far from complete, the typical spacing between hydrothermal vent sites appears to be inversely proportional to spreading rate [*Lowell et al*., 1995]. Faster spreading ridges presumably have greater overall magmatic and energy budgets, so vents would need to draw heat from a shorter lateral distance. Spreading rate and the dominance of tectonic versus magmatic forces may also influence the magnitude, directionality, and continuity of permeability with upper basement. One might expect more extensive vertical upper crustal permeability at a spreading ridge that is dominated by tectonic rather than magmatic processes; this idea is crudely consistent with a comparison of permeability estimates from Holes 395A and 504B (Table 1, Plate 1). More continuous lateral permeability would also accompany crust formed at a ridge crest dominated by frequent effusive flows [*Fornari and Embley*, 1995].

The morphologies of massive sulfide deposits also seem to reflect the distribution of permeability within shallow basement [*Hannington et al*., 1995]. A 100-m-diameter network of channels below a sulfide mound at the Galapagos Rift may indicate the passage of reacted fluids through pervasively permeable pillow lava and hyaloclastite deposits [*Embley et al*., 1988]. This system appears to have been relatively open to mixing with seawater, as was the upper crust around the trans-Atlantic geotraverse (TAG) hydrothermal mound, where there is a wide range of vent temperatures [*Humphris et al*., 1996]. In contrast, tall sulfide structures along the Endeavour Segment of the Juan de Fuca Ridge tend to be narrower and to vent fluids at 350°C or more, suggesting that the deposits formed from fluids that rose from depth with little or no interaction with cold seawater [*Delaney et al*., 1992; *Hannington et al*., 1995]. High-temperature sulfide deposits also seem to be generally larger at slower spreading ridges (compare TAG on the MAR or deposits in Middle Valley with numerous smaller deposits along the faster spreading EPR), suggesting that the longevity of hydrothermal sites may also be related to the stability of crustal permeability [*Fornari and Embley*, 1995; *Wilcock and Delaney*, 1996].

Seafloor hydrothermal activity tends to cluster along structural trends, both at the ridge crest [e.g., *Karson and Rona*, 1990; *Haymon et al*., 1991; *Embley and Chadwick*, 1994; *Wilcock and Delaney*, 1996] and along some ridge flanks [*Lonsdale*, 1977; *Green et al*., 1981; *Rona et al*., 1990]. Intense alteration along the edges of fault blocks in western Troodos suggests that faults may focus hydrothermal solutions during subseafloor circulation [*Varga and Moores*, 1985]. Deep penetration of hydrothermal fluids at the ridge crest may also be enhanced along discrete, subvertical fractures. An alternative explanation is that widely distributed, high-temperature flow within the upper crust becomes concentrated to discharge through a small number of isolated conduits close to the seafloor [e.g., *Goldfarb and Delaney*, 1988], but a mechanism capable of focusing flow to the necessary extent has not been identified.

Ridge-parallel alteration trends in the sheeted dike complexes of ophiolites suggest that permeability within this part of the upper crust may be concentrated along faults or fractures, with fluids entering the high-temperature system between magmatic centers, along strike of the ridge [*Haymon et al*., 1991]. This fluid would move along vertically oriented fractures and fracture networks and discharge at the seafloor above the regions of having the greatest heat input [e.g., *Lowell*, 1975; *Wilcock and Delaney*, 1996]. In contrast, the shallower parts of the

upper crust would be more pervasively permeable but would be dominated by lower-temperature, lower velocity flows. Segregation between these two hydrothermal systems would result from an extreme contrast in permeability (dropping abruptly below the top of the sheeted dikes) as well as a difference in the form of permeability (horizontally layered versus concentrated along subvertical fractures). This conceptual model is consistent with limited direct measurements of bulk permeability in the upper kilometer of oceanic crust [e.g., *Anderson and Zoback*, 1982; *Becker*, 1990b, 1996], although high permeability along fractures within the sheeted dikes has not been observed to date. If these fractures are vertical to subvertical and if they are distributed at the typical abyssal hill spacing of several kilometers, they might be difficult to locate, penetrate, and test using a vertical drill hole.

Nehlig and Juteau [1988a, b] and *Nehlig* [1994] conducted fracture and vein analyses of the Samail ophiolite, including sheeted dikes and deeper parts of the crust, as the extrusive section is thin and discontinuous in this region. Mapping of fractures having apertures of $\geq$2 mm (often with a spacing of 10 cm of less) and application of the parallel plate model resulted in calculated permeabilities approaching 10^{-8} m^2 in the upper sheeted dikes and 10^{-10} m^2 in the lower sheeted dikes [*Nehlig and Juteau*, 1988a, b]. *Nehlig* [1994] subsequently suggested that permeabilities at the base of the sheeted dikes were lower (10^{-11} to 10^{-12} m^2) but strongly anisotropic and heterogeneous when these systems were most active. *Nehlig and Juteau* [1988a] suggested that permeability within the shallowest basaltic crust should be highly anisotropic, with higher horizontal permeabilities in the extrusives (reflecting the depositional character of pillow lavas and massive flows) and higher vertical and along-strike permeabilities in the sheeted dikes (reflecting the orientation of stresses and associated fracturing as the crust forms and ages). *Van Everdingen* [1995] similarly suggested that fracture permeability within the sheeted dikes of the Troodos ophiolite must have been highly anisotropic, but fracture distribution and orientation within the extrusive crust displayed no preferential fabric. Permeability within the sheeted dikes while the crust was on axis (assuming all cracks were open) was estimated to be 10^{-12} to 10^{-8} m^2, while fractured rock containing calcite-filled veins was calculated to have an off-axis permeability of 10^{-21} to 10^{-18} m^2 [*van Everdingen*, 1995].

Agar [1994] suggested that cooling fractures associated with primary crustal accretion may eventually help to nucleate faults within the basaltic oceanic crust. This would be consistent with the axial and off-axis formation of enhanced permeability within both extrusive and intrusive sections of the upper crust, but with distinctly different anisotropies: the extrusive section would tend to form subhorizontal brittle failure surfaces, while the intrusive dikes would tend to form subvertical arrays of fractures. Additional subhorizontal failure surfaces may be associated with major lithological boundaries such as the dike-pluton boundary at the base of the basaltic crust [*Agar*, 1991, 1994]. *McClain et al*. [1987] proposed that the uppermost crust develops porosity and permeability as it moves away from the neovolcanic zone, where magmatic intrusion would not accompany continued tectonic extension. Off-axis tectonic activity would lead to enhancement of upper crustal permeability and the formation of detachments. A similar suggestion was proposed for zones of enhanced fracturing within the upper kilometer of Hole 504B [*Pezard et al*., 1997]. Localized fracturing might not lead to a significant increase in crustal porosity and would be difficult to detect with large-scale seismic experiments [*McClain et al*., 1987]. Such an increase in crustal porosity with age might counteract the porosity loss associated with clogging of cracks and pores, as has been interpreted to result in an increase in crustal seismic velocities with age [e.g., *Wilkens et al*., 1991].

Systematic mapping and hydrologic testing of terrestrial fault zones [e.g., *Forster and Evans*, 1991; *Barton et al*., 1995; *Caine et al*., 1996] unfortunately cannot be duplicated with the same detail and geological control on the seafloor. Continental faults zones in crystalline rock frequently contain complex geometries and fabrics [e.g., *Logan and Decker*, 1994; *Caine et al*., 1996]. The fault core often contains gouge and other relatively low permeability material, while a surrounding zone of fractured and damaged country rock may have considerably greater permeability. For example, the permeability of core-scale samples from crystalline thrust faults in Wyoming typically fell in the range of 10^{-18} to 10^{-16} m^2 for fault gouge, while values of 10^{-16} to 10^{-14} m^2 were typical for the damaged zone around the faults [*Forster et al*., 1994]. Many lower values for fault gouge permeability in crystalline rocks (10^{-22} to 10^{-18} m^2) were tabulated by *Smith et al*. [1990]. Fault zones within crystalline rocks may also be highly heterogeneous in their hydrologic properties over short distances [e.g., *Davison and Kozak*, 1988], making regional characterization of faults difficult.

The geometries and properties of fault structures may lead to increased permeability parallel to the fault, while across-fault permeability is reduced; the appropriate hydrogeologic representation of a fault system depends on the setting and deformational style [*Smith et al*., 1990; *Caine et al*., 1996]. The effective permeability of particular fault or fracture zones within crystalline rock also depends on fracture roughness [e.g., *Brown*, 1987], the relation between fault geometry and ambient stress field [e.g., *Tsang and Witherspoon*, 1981; *Bruhn*, 1994; *Barton et al*., 1995, 1996], and the extent of fracture connection over the length scale of interest.

3.6.2. Geophysical studies. *Nobes et al*. [1986] conducted a seafloor electrical resistivity experiment near Middle Valley to evaluate the distribution of porosity with depth. Basement properties were not well constrained below one site close to the center of the

valley, but at another site on the flank of the valley the porosity of the upper 1000 m of basement was estimated to be about 8%, and permeability was estimated to be 10^{-16} to 10^{-14} m^2 [*Nobes et al*., 1986].

Evans et al. [1991] conducted a similar experiment on the EPR at 13°N, and *Evans* [1994] subsequently combined these results with seismic data from the same location [*Harding et al*., 1989] to estimate the porosity of the upper 1 km of basement within zero-age and 0.1 Ma crust. The resistivity structure with depth was essentially identical at the two sites, suggesting porosities of about 15–20%, with an abrupt decrease near 1 km subsurface. In contrast, seismic velocities appear to increase at about 500 m subsurface at the older site relative to the younger site, illustrating the difficulty in associating seismic properties with crustal porosity. *Evans* [1994] related resistivity values directly to permeability using an empirical porous media model and calculated a value for the upper 1 km of 5×10^{-12} m^2. Apparent permeability dropped abruptly to 3×10^{-17} m^2 below this depth.

Holmes and Johnson [1993] and *Stevenson et al*. [1994] conducted seafloor gravity studies on the northern and southern Juan de Fuca Ridge, respectively, and concluded that total porosities within the shallowest crust may be 20–25%, with local values as great at 30%. Such high values presumably reflect the formation of collapse and pillar structures and other large-scale voids [e.g., *Applegate and Embley*, 1992; *Gregg and Chadwick*, 1996], as well as the irregular distribution of volcanic centers along many spreading centers [e.g., *Smith and Cann*, 1992; *Bryan et al*., 1994]. *Haymon et al*. [1993] noted the common formation of lava tubes along the fast spreading EPR, and *Fornari and Embley* [1995] suggested that such structures have the potential to greatly enhance horizontal permeability within the upper crust created at fast and superfast ridges.

Crustal seismic velocity and anisotropy are also responsive to differences in porosity and pore shape, although these relations are strongly nonlinear [e.g., *Wilkens et al*., 1991; *Moos and Marion*, 1994; *Sohn et al*., 1997]. *White and Clowes* [1990, 1994] noted seismic velocity and attenuation anomalies below the Juan de Fuca Ridge crest, interpreted to represent regions of increased fracture porosity at the layer 2–layer 3 boundary. Calculated porosities at depths of 1.0–1.5 km are essentially zero, except within a narrow zone directly below the ridge axis. Restricted fracturing in the basalt dikes of layer 2 would lead to hydrothermal flows along strike, with both recharge and discharge along the ridge axis. Other studies at the ridge crest [*Caress et al*., 1992; *McDonald et al*., 1994] and on flanks [e.g., *Stephen*, 1981, 1985] also indicated seismic anisotropy within the upper crust, perhaps indicative of preferred fracture orientation.

3.6.3. Crustal alteration. The geochemical state of oceanic crust comprises the integrated effects of fluid interaction over a range of temperatures, chemistries, and time scales. For example, radiometric dating of alteration minerals from upper oceanic basement has yielded values spanning tens of millions of years in both ophiolite and seafloor samples [*Peterson et al*., 1986; *Gallahan and Duncan*, 1994]. While the lateral extent of variability in alteration is difficult to assess from seafloor cores, except in the few locations where upper crustal sections have been sampled at adjacent sites [*Natland*, 1979; *Muehlenbachs*, 1980; *Alt et al*., 1996], ophiolites provide opportunities to map out two- and three-dimensional alteration patterns [e.g., *Gillis and Robertson*, 1988, 1990; *Haymon et al*., 1989; *Valsami-Jones and Cann*, 1994] and, together with seafloor samples, help to define consistent trends in upper crustal alteration and associated water-rock interaction.

The alteration of upper oceanic crust is intimately linked to the primary stratigraphy of the crust. The uppermost pillows, flows, and breccias are typically characterized by low-temperature oxidation and alkali fixation reactions [*Gillis and Robinson*, 1988; *Alt et al*., 1986a, b], starting when the crust is young and continuing for tens of millions of years [*Staudigel et al*., 1981; *Gallahan and Duncan*, 1994]. Alteration within the upper basement is not uniform, but varies over centimeter- and meter-scale distances [see *Alt*, 1995, Figure 7]). *Gallahan and Duncan* [1994] suggested that the heterogeneous distribution of low-temperature alteration products in the uppermost basaltic crust of the Troodos ophiolite is inconsistent with any particular flow geometry being favored for low-temperature hydrothermal circulation. Instead, discontinuous sealing of cracks would cause irregular redirection of fluid flow throughout basaltic extrusives. *Gillis and Robinson* [1988, 1990] mapped the distribution of alteration in the lavas and dikes of Troodos, defining distinct vertical alteration zones and extensive lateral variability. Variations in the forms of pillows, flows, hyaloclastites, and breccias suggested that permeability was heterogeneously distributed, as did local preservation of fresh glass immediately adjacent to regions of intense alteration [*Gillis and Robinson*, 1990]. Such geochemical variability is consistent with patterns described in other ophiolites [*Stern and Elthon*, 1979; *Harper et al*., 1988] as well as in rocks collected in seafloor boreholes [*Alt et al*., 1996]. Alteration minerals reflect abrupt increases in temperatures with depth from the lower volcanics (100°–150°C) to the upper dikes (250°–350°C), with apparent temperature differences of 100°–250°C over tens of meters [*Alt et al*., 1986a, b; *Gillis and Robinson*, 1990]. The geochemistry of the uppermost sheeted dikes from both Hole 504B and from the MAR indicate low water/rock ratios [*Alt and Emmermann*, 1985; *Gillis and Thompson*, 1993], although there are veins, breccias, and pillow rims that indicate locally greater water-rock interaction [*Alt et al*., 1985, 1986a, b; 1989].

Calculation of geochemical water/rock ratios can provide a semiquantitative indication as to the mass or volume of fluid that has passed through the upper oceanic crust during alteration, although these values also

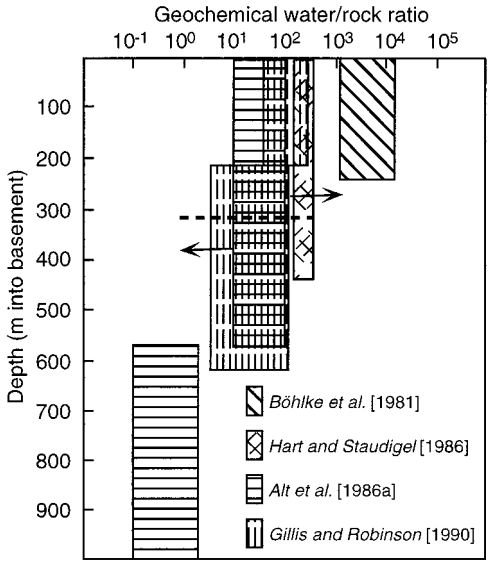

Figure 4. Summary of geochemical water/rock ratios estimated from products of basalt alteration in the upper oceanic crust, plotted versus depth into basement. Estimates are based on samples from DSDP Hole 396B [*Böhlke et al*., 1981], Hole 504B [*Alt et al*., 1986a], DSDP Sites 261 and 462 [*Hart and Staudigel*, 1986], and holes CY-1 and CY-1A in the Troodos ophiolite [*Gillis and Robinson*, 1990]. The dashed line at 320 m into basement, and the arrows to the right and left, indicate that water/rock ratios are likely somewhat higher than indicated above the depth of the line, and somewhat lower below the line [*Alt et al*., 1986a]. Note the similarity between distribution of geochemically estimated water/rock ratios and the distribution of bulk permeabilities determined with packer experiments and borehole temperature logs (Plate 1).

reflect absolute temperatures and pressures, the distribution of rock permeability, and fluid residence time [*Spooner et al*., 1977]. These calculations generally include assumptions of (1) initial compositions of both unaltered rock and circulating fluid, (2) rapid exchange between liquid and solid phases, and (3) the presence of either an infinite source of fluid (open system) or a finite source (closed system) [e.g., *Mottl*, 1983; *Thompson*, 1983]. Because chemically estimated water/rock ratios are integrated over the life of the flow systems, they reflect multiple stages (temperatures, chemistries) of flow, and values estimated using different tracers and systems tend to vary because of reaction kinetics [*Spooner et al*., 1977]. As a rule, chemically based estimates of water/rock ratios should be less than or equal to absolute (physical) ratios because fluid residence times may be too short for geochemical equilibrium, and fluids often pass through previously altered rock.

Water/rock ratios calculated in several studies of upper crustal alteration are summarized in Figure 4. These calculations are based on oxygen isotope, potassium, iron, and magnesium analyses of bulk rock from the upper kilometer of DSDP/ODP Hole 504B [*Alt and Emmermann*, 1985; *Alt et al*., 1985, 1986a, b]; phosphate and oxygen analyses of basalts from DSDP Hole 396B [*Böhlke et al*., 1981, 1984], Sr and Rb/Sr data from additional DSDP sites ranging in age from 80 to 160 Ma [*Hart and Staudigel*, 1986], and oxygen isotope and sodium and calcium contents of altered bulk rock samples from Troodos [*Gillis and Robinson*, 1990]. Collectively, these data illustrate vertical layering in upper crustal alteration, with greater water-rock interaction within the upper few hundred meters of basement (pillows, flows, breccias) and much less water-rock interaction within the lower extrusives and sheeted dikes [*Alt*, 1995]. While water/rock ratios have not been used to estimate quantitative values of basalt permeability, the combined profile of ratios versus depth are qualitatively similar to the bulk permeability versus depth profile compiled from borehole measurements (Plate 1), illustrating a possible influence of permeability on upper crustal evolution.

4. DISCUSSION

Estimates of permeability within the basaltic oceanic crust vary over orders of magnitude in different locations, with depth below the top of basement and the method of analysis (Tables 1 and 2, Plate 1, and Figure 5). Values for shallow oceanic basement are generally consistent with measurements and estimates from elsewhere in crystalline rock [*Clauser*, 1992]. Core measurements of centimeter-scale samples are generally close to 10^{-21} to 10^{-17} m^2, while packer data approach 10^{-12} m^2 in uppermost basement and drop to 10^{-17} m^2 in the deepest basaltic crust. Estimates of bulk permeability from borehole thermal data are somewhat more tightly constrained than packer data in their interval of measurement, but the range in estimated permeabilities is still large, varying over six orders of magnitude. Fracture analyses often indicate very high permeabilites ($\geq 10^{-12}$ m^2), but there is no way to test many of the assumptions upon which the interpretations are based. The few seafloor resistivity experiments conducted at the ridge crest indicate values of about 10^{-16} to 10^{-12} m^2 and are interpreted to apply to the upper kilometer of basaltic crust, but these permeabilities and depths are not well constrained. Heat flow and modeling studies have incorporated an enormous range of permeabilities and length scales, including the full extent of direct and indirect borehole measurements and seafloor resistivity experiments, but also extend to permeabilities several orders of magnitude greater than have been measured in the seafloor.

These permeability measurements and estimates illustrate several general trends. First, bulk values measured with a drill string packer and estimated with borehole thermal measurements suggest that the greatest permeabilities are found within the upper few hundred meters of crust (Plate 1). The detailed distribution of permeability within this region is not obvious from most of the borehole measurements themselves, as the inter-

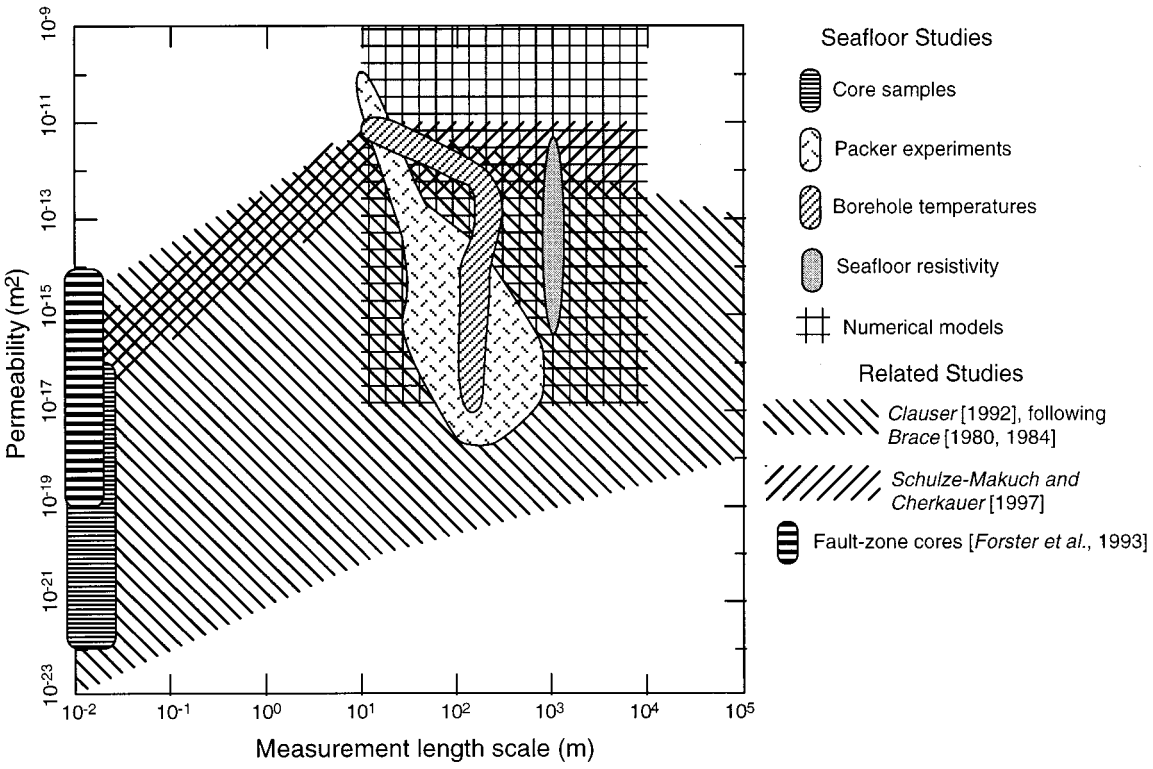

Figure 5. Summary of selected estimates of the permeability of basaltic oceanic basement (Tables 1 and 2) and estimates of formation permeability from related environments. See discussion in text regarding the length scale of the estimates.

pretations are based on assumptions of homogeneity and isotropy. Exceptions include the few estimates, based on both temperature logs and packer experiments, that allow assignment of the most significant transmissivity to relatively thin zones (tens of meters) in the upper crust. When combined with other geophysical, geochemical, and geological observations, it appears that the highest permeability values are often associated with lithologically and structurally distinct intervals (i.e., pillows, flows, faults, and breccia zones). Given that many geological transitions in the upper crust are abrupt and that permeability in this setting is intimately controlled by crustal lithology and structure, it seems likely that regions within the upper crust having very different hydrogeologic properties will often be sharply bounded. Because of this heterogeneity and because there are likely to be variations associated with crustal spreading rate, age, extent of alteration, and other geological parameters, defining a single permeability versus depth relationship for the basaltic oceanic crust is not possible at present and may never be possible.

The crude trend of the global oceanic data set, and of measurements of crystalline rocks in general, is for apparent permeability to increase with the length scale of measurement, at least over the interval of hand sample to borehole scales (10^{-2} m $\leq$ measurement length $\leq 10^{1}$ m) (Figure 5). In the case of borehole packer measurements and estimates based on borehole logs, there is an opposite trend embedded in the data (Plate 1). Because permeability in crystalline rocks tends to be concentrated along thin intervals, the inclusion of much wider zones around the most permeable intervals results in an overall underestimate of bulk permeability [e.g., *Black*, 1990; *Hufschmied et al.*, 1990]. If smaller intervals in DSDP and ODP boreholes containing fractures or breccia zones could be isolated and tested, the bulk permeabilities of these intervals would tend to be greater than those previously reported for the longer borehole intervals. Similarly, if Hole 1026B had been drilled another 50 m into basement and if the temperature log had been collected much later, after the less permeable zones in basement had thermally equilibrated, it might not have been possible to identify where in the upper 100 m of basement the greatest permeability was concentrated.

Apparent permeabilities in crystalline rocks in the global data set seem to peak and plateau once the measurement scale reaches some critical length of the order of tens to hundreds of meters [*Clauser*, 1992]. This interpretation is similar to that recently applied to three carbonate aquifers thought to contain both porous medium and fracture permeability [*Schulze-Makuch and Cherkauer*, 1997]. Bulk hydraulic conductivities estimated from packer and other well tests differed from basin-scale estimates in that study by only one order of magnitude or less. This observation is consistent with the global crystalline rock data set [*Clauser*, 1992], in which

bulk permeabilities were found to plateau at the borehole scale, although the wide range of measured values may contain different trends for individual regions (Figure 5).

Schulze-Makuch and Cherkauer [1997] also suggested that it is measurement volume, not measurement length, that should be used to examine scaling issues in heterogeneous aquifers. I have taken the cube root of the measurement volumes cited in their analysis to crudely convert from volume scale to length scale so that their results could be compared with those from crystalline rocks (Figure 5). The final plateau in permeability from *Schulze-Makuch and Cherkauer* [1997] is at the high end of the borehole measurements from upper oceanic basement, about 10^{-12} to 10^{-11} m^2, but the plateau length scale is similar. The oceanic values do not cluster neatly along a regular trend as a function of length scale, but this may reflect variations in geological parameters (age, spreading rate, alteration, etc.) as well as the need to consider rock volume of each test rather than interval length. A more appropriate comparison would include measurements made at the same location over a range of length and volume scales, but how is the scale of individual experiments to be properly assessed? What volumes of rock were actually tested?

This question can be addressed through calculation of the "radius of influence" for these tests, the distance into the formation at which there would be a negligible head change resulting from flow into or out of the borehole. The radius of influence of a free-flowing, overpressured well has been studied extensively within the petroleum industry [*Matthews and Russell*, 1967; *Hurst et al*., 1981], and similar calculations have been made for terrestrial aquifers to assist with resource development and capture zone analyses [e.g., *Sen and Sabtan*, 1992; *Guyonnet et al*., 1993; *Bakker and Strack*, 1996]. As with many other borehole calculations of hydrologic properties, these estimates are based on the assumption that the formation around the well behaves as a homogeneous, isotropic, porous medium.

Guyonnet et al. [1993] applied the *Cooper et al*. [1967] solution to calculate the radius of influence during slug testing as a function of the magnitude of the perturbation (relative to the original head change at the well), time, and well bore storage. The maximum radius of influence of a slug test at the 1% perturbation level ($r_{i-1\%}$) is $r_{i-1\%} = \omega\, r_w\, C_D^m$, where r_w is well radius, C_D is dimensionless well storage, and ω and m are coefficients derived from a least squares best fit of calculated values in log-log space. Application of this relation to slug tests in the upper oceanic crust [*Anderson and Zoback*, 1982; *Anderson et al*., 1985b, c; *Becker*, 1989, 1996] suggests a radial influence extending only 3–30 m from the borehole, and including 10^1–10^4 m^3 of rock.

A similar radius of investigation calculation was applied to injection tests using the *Cooper and Jacob* [1946] late-time approximation. For a test in which fluid is pumped into the formation at a steady rate, the radial distance from the well at which no pressure perturbation is expected is $r_{i-0} = 2.25\ Tt/S$. This relation applies only when $u = r^2S/4Tt \leq 0.01$, where r is the distance from a pumping well at which observations are made. In the case of seafloor pumping tests conducted thus far, there has been no observation well, making it difficult to estimate values for storativity (S) with confidence. We can bracket likely values for storativity through consideration of calculations made from slug test data [e.g., *Anderson and Zoback*, 1982; *Anderson et al*., 1985b, c; *Becker*, 1989, 1996], which suggest that appropriate values are of the order of 10^{-4} to 10^{-3} over a range of crustal settings and tested intervals.

Using these storativity values, measured transmissivities (T) from pumping tests, and typical test durations of 20–30 min, the radius of influence of pumping tests conducted in upper basement is of the order of 0.2–11 km, while the total volume of rock tested ranges from 10^4 to 10^6 m^3. The observation that slug and pumping tests conducted over the same depth intervals in single holes generally indicated similar bulk permeabilities [e.g., *Becker*, 1991] suggests that the differences in measurement scale did not involve significantly different flow systems.

A much greater volume of rock was tested during longer-term experiments associated with the flow of water into or out of upper crustal sections having natural pressures different from hydrostatic [*Becker et al*., 1983a; *Fisher et al*., 1997]. Assuming that the formation is incompressible, the radius of influence around a flowing well increases approximately with the square root of time [*Hurst et al*., 1981, p. 306]:

$$r_i = 2.6408\, r_w \left(\frac{kt}{n\mu\beta r_w^2} \right)^{0.4886} \tag{4}$$

where ϕ is porosity and β is fluid compressibility. Because it neglects aquifer compressibility, equation (4) provides an upper limit as to the length scale over which these calculations may apply. Application of this relation to the flow of fluid into the upper Hole 504B with appropriate parameters ($k = 10^{-13}$ m^2, $\phi = 0.1$, $r_w = 0.15$ m, β and μ appropriate for $T = 10°$–$60°$C) yields a radius of influence of 4–10 km as of DSDP Leg 70. Application of (4) to flow into 504B over the next 7–13 years (ODP Legs 111–148) yields radial distances of tens of kilometers. A similar analysis applied to flow out of Hole 1026B during the 10–20 days following drilling with appropriate physical parameters also suggests a radius of influence of several tens of kilometers, while flow into Hole 858G, 1.5 days following penetration of upper basement, would have a radius of influence of 0.5–5.0 km, depending on the thickness of the permeable zone.

Long-term borehole flow experiments can also be considered using the *Cooper and Jacob* [1946] method described earlier, although this requires application of a Neumann boundary condition at the borehole wall rather than the more appropriate Dirichlet boundary condition. Using the same parameters for analysis of the

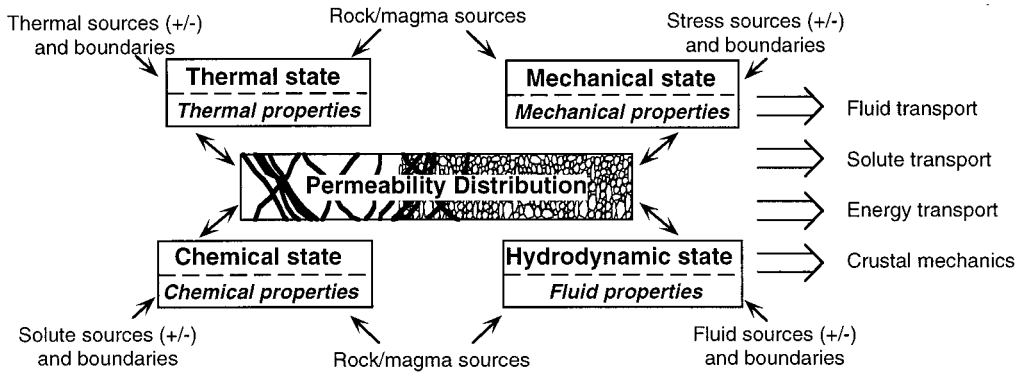

Figure 6. A conceptual illustration of how the distribution of permeability within the upper oceanic crust will influence, and be influenced by a wide range of properties and processes. This permeocentric view of coupled crustal processes (inspired by *Garven* [1995, Figure 4]) shows that no representation of permeability in the oceanic basement is free from fundamental assumptions. The permeability distribution acts as a transform between processes and products in the upper oceanic crust.

long-term flow experiments yields a radius of influence of 2–7 km for Hole 1026B after 20 days, 1–7 km for Hole 504B after 50 days, and 0.3–0.9 km for Hole 858G after 1.5 days of flow. These calculations are broadly consistent with upper crust in these areas hosting regionally significant hydrothermal circulation, although greater constraint would be provided by time series records of flow rates and formation pressures, particularly if the latter were available from more than one well, so that storativity could be determined with greater confidence. These calculations raise additional questions about the representation of permeability in coupled models and about our ability to use models to constrain quantitative permeability values for the upper oceanic crust. If the lateral scale of bulk permeability determined from borehole measurements on ridge flanks is several kilometers or more, are regional permeabilities in the uppermost kilometer of oceanic basement orders of magnitude greater than have been measured, as results of many numerical studies suggest (Table 2)? In order to accept such high regional permeabilities, we must surmise that all oceanic basement holes in which measurements have been made were drilled in kilometer-scale regions of hydrologically anomalous (low permeability) crust. An alternative explanation is that the horizontal bulk permeability values measured in oceanic basement boreholes are representative, but that most of this permeability is concentrated within relatively narrow zones. A highly layered lithologic and tectonic structure would lead to enormous permeability anisotropy within the upper crust. Efficient lateral heat transport might then take place without requiring deep convection or low-aspect-ratio convection cells on ridge flanks. Numerical models will not resolve this question, as a range of flow geometries can produce similar thermal and chemical results.

The situation at the ridge crest is more complex and less well constrained, as we have no direct measurements of permeability in very young, normal crust. But the bulk of the indirect evidence points to crust at the ridge crest having a heterogeneous permeability distribution as well. Hydrothermal vents and sulfide structures are commonly located along seafloor faults and fissures. If the upper crust at ridge crests is uniformally permeable to a depth of kilometers, how does fluid flow over a region of square kilometers (necessary to gather sufficient heat) become channeled to exit the seafloor at high velocities through a small number of vents, each tens of centimeters in diameter? The situation is made more complicated by the transient nature of magmatic, tectonic, and hydrothermal events. Different parts of the upper crust are likely to be involved in hydrothermal circulation at different times.

If permeability within the basaltic oceanic crust is distributed heterogeneously, can Rayleigh number calculations be applied to interpret hydrothermal systems? The presence of widely spaced, highly permeable zones violates several of the primary assumptions common to Rayleigh number analysis [e.g., *McKibben and O'Sullivan*, 1980; *Ormond and Genthon*, 1993], as do phase separation and extreme differences in fluid properties with temperature and pressure [*Bischoff and Rosebauer*, 1994, 1989; *Butterfield et al*., 1990], the presence of nonhorizontal boundaries at either the top or bottom of the convecting layer [*Palm*, 1990; *Criss and Hofmeister*, 1991], transient changes in formation properties over a range in timescales [e.g., *Cann and Strens*, 1989; *Lowell and Germanovich*, 1994; *Dutrow and Norton*, 1995], and the presence of heat sources (instabilities) along vertical boundaries [e.g., *Fehn et al*., 1983; *Travis et al*., 1991].

It has been implicit in many models of seafloor hydrothermal circulation incorporating the REV approach that in the absence of a detailed understanding of the permeability distribution in the upper crust, an isotropic and homogeneous (or smoothly varying with depth) representation is the most hydrologically "objective." But because of the relations between permeability distribution and numerous mechanical, chemical, and thermal processes, no representation of permeability in the oceanic crust is neutral (Figure 6). For example, the effi-

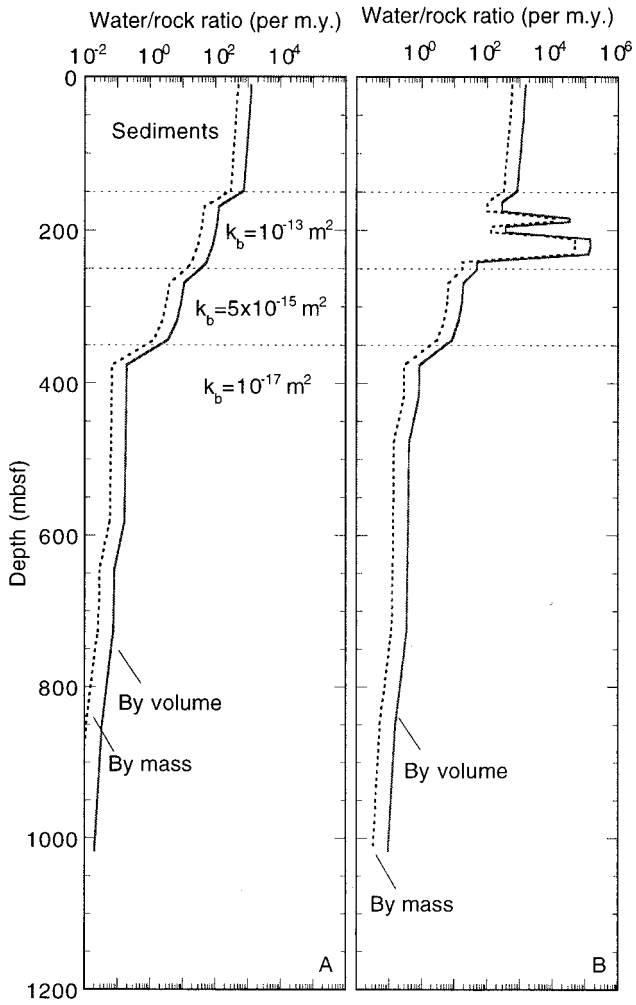

Figure 7. Physical (volume and mass) water/rock ratios per million years calculated for idealized simulations of coupled heat and fluid flow within the upper oceanic crust of a ridge flank, including basement and seafloor topography and variable sediment thickness. Values were calculated for a depth profile below the peak of a local basement high. (a) Simulation HIGHSEDK includes the listed permeability values distributed uniformally within the regions bounded by dotted lines. (b) Simulation THICBHIK includes the same formation values within the illustrated depth intervals, but with most of the permeability in the upper 100 m of basement concentrated within two zones 10 m and 30 m thick. Sediment permeability (and other properties) varied identically as a function of depth beneath the seafloor in both simulations [*Fisher et al*., 1994].

ciency of advective heat transport depends explicitly on whether permeability is uniformally distributed or concentrated along discrete conduits. Whether the crust behaves as a porous or fractured medium will greatly influence changes in hydrologic properties (and associated thermal and chemical processes) when fluid pressure changes following an intrusive or tectonic event. If the oceanic crust behaves chemically as a porous sponge, with evenly distributed and closely spaced pathways dominating water-rock interaction, then large volumes of rock will react with flowing fluid over relatively short timescales. If flow is restricted to narrow pathways, however, the walls of these zones may become altered at an early hydrothermal stage, isolating subsequent flows from continued interaction with the host rock except by diffusion. The historical approach has been to assume that permeability within discrete subdomains is uniformally distributed, but this should be recognized as a mathematical simplification rather than a geological necessity until observational justification is found.

As a semiquantitative example of the potential importance of permeability representation in hydrothermal models of the upper crust, water/rock ratios have been calculated for two numerical simulations of ridge-flank hydrothermal circulation (Figure 7). The parameters for the simulations are based on measured properties and known upper crustal geometries at Site 504, including basement relief and variable sediment thickness (cases HIGHSEDK and THICBHIK from *Fisher et al*. [1994]). Heat flow at the base of the crust was 200 mW m^{-2}, and the simulations were allowed to continue until steady state conditions were reached. Crustal permeability in both simulations was assigned to be 10^{-13} m^2 over the first 100 m into basement, 5×10^{-15} m^2 over the next 100 m into basement, and 10^{-17} m^2 over the greater depths in the upper crust. Water/rock ratios were calculated by tabulating the cumulative flux of fluid (by mass and volume) into and out of individual mesh elements along a column extending from the seafloor to the base of the simulation domain and comparing these values with the mass and volume of the rock within the same mesh elements. The calculated water/rock ratios are thus physical values and are expected to be considerably greater than chemical water/rock ratios calculated from fluid or solid geochemistry for a similar system.

The first simulation included permeability distributed evenly within each of the layers in upper basement (Figure 7a), while the second simulation had most of the permeability within shallowest basement concentrated in two zones having a combined thickness of 40 m (Figure 7b). Because the cumulative flux of water through any part of the model increases with time, the water/rock ratios were calculated per million years at steady state. Simulated water/rock ratios change abruptly by several orders of magnitude at the boundaries between layers having significantly different permeabilities (Figure 7). Similarly abrupt decreases with depth in chemical water/rock ratios were calculated from seafloor and ophiolite samples (Figure 4). Physical water/rock ratios can be many orders of magnitude greater within thin, extremely permeable layers (Figure 7b). The more vigorous convection caused by the inclusion of these thin layers also increased the physical water/rock ratios within underlying units, even when the permeability of these deeper layers was unchanged (Figure 7). Coupled processes in the upper oceanic crust will behave quite differently depending on how permeability is distributed.

5. CONCLUSIONS AND RECOMMENDATIONS

Several decades of observational, experimental, and mathematical studies confirm the importance of fluid flow within basaltic oceanic crust over a wide range of temperatures, pressures, chemistries, and crustal ages and settings. Significant advances have been made in determining where and how quickly fluids move through upper oceanic basement and what impact these fluids have on crustal and ocean properties. But much of our understanding is conceptual rather than specific: we know much more about the integrated effects of flow than we do about the mechanisms and rates by which many water-rock interactions are controlled. Gaps in our knowledge of fluid flow processes reflect, in large part, uncertainties regarding the distribution and evolution of permeability within the crust. Resolving these uncertainties is critical to understanding the nature of coupled physical and chemical processes that operate over the life of the oceanic crust. In the absence of a more complete picture of how permeability is distributed within the oceanic crust, we can not constrain predictive models incorporating fluid flow, crustal evolution, and global geochemical budgets.

The available data (observational, experimental, and inferential) support several generalizations regarding permeability within basaltic oceanic crust. Basement hydrogeology is intimately linked to crustal formation and modification at and close to the ridge crest. Differences in permeability are associated with primary stratigraphy and with lateral variations in the form of intrusive and extrusive basalt. The shallowest oceanic basement, comprising pillows, flows, and zones of brecciation, is likely to contain some of the greatest permeability in the upper crust, with a strong horizontal anisotropy resulting from crustal layering. While subvertical faults may provide important conduits between shallow and deeper crustal hydrothermal systems, significant lateral flow seems to be required within the upper kilometer of basement to explain seafloor heat flow anomalies and the apparent homogenization of temperatures near the sediment-basement contact on several ridge flanks. Additional subhorizontal conduits at depth, perhaps within and at the base of the sheeted dikes, may allow lateral energy and solute transport; such zones remain to be located and tested to determine their properties.

Further controls on upper crustal hydrogeology result from synmagmatic and postmagmatic tectonic modification. At the ridge crest, extensional faults are likely to provide conduits for fluids to move quickly between shallow-crust and deeper-crust hydrothermal reservoirs. Even if the remaining crust has a relatively high permeability, flow along subvertical conduits would allow large volumes of high-temperature hydrothermal fluid to move quickly from depth to the seafloor, where it can vent at relatively restricted and isolated sites. The formation of faults that strike subparallel to the ridge crest is also likely to result in large-scale permeability anisotropy, perhaps extending to great depth within the crust. These faults may remain seismically, structurally, and hydrologically important well after the crust leaves the ridge crest, but the relative importance of faults in influencing the geometry and intensity of off-axis hydrothermal flows remains to be determined. Understanding the hydrologic importance of faults within the shallow crust will require that we learn more about the formation and distribution of permeability in general, as it seems unlikely that either constructional layering or faulting alone can provide sufficient directional permeability to explain the observed patterns of fluid flow and water-rock interaction. It appears, instead, that the upper oceanic crust is permeable over a continuum of scales (spatial, temporal), with tectonically enhanced permeability along faults and fractures superimposed over a heterogeneous, layered system.

Idealized models of pervasively distributed permeability (isotropic, homogeneous) allow the estimation of equivalent properties for the crust, but these are representations of convenience. The geological record and numerous direct measurements of properties within the seafloor demonstrate that upper crustal properties are often heterogeneous and strongly anisotropic. In some cases, irregularly distributed properties can be effectively represented using a continuum approach, but the applicability and accuracy of such models will depend on the nature of the problem being addressed and the time and length scales of interest.

Given the difficulty of quantitatively describing upper crustal permeability in general, it is not possible at present to accurately predict changes in permeability as the crust ages. In some cases, permeability should be lost as fractures, breccia zones, and faults are closed by hydrothermal precipitation and mechanical compaction. In other cases, however, permeability may be enhanced by off-axis tectonic and geochemical mechanisms. Observations from seafloor over a wide range of ages suggest that the aggregate influence of these processes on crustal hydrogeology is neither monotonic nor linear. While there tends to be greater alteration as the crust ages, and seismic data and models suggest that this alteration leads to closure of cracks in the crust [e.g., *Wilkens et al*., 1991; *Shaw*, 1994], the available data do not demonstrate a concurrent permeability reduction (Plate 1).

After 30 years of deep ocean drilling there remain enormous gaps in our understanding of primary crustal evolution, and many of these issues will remain unresolved until additional direct measurements are completed in a variety of settings. Simply drilling, coring, and testing within upper basement (1–2 km) along several crustal aging profiles, through seafloor produced at different rates, would be very helpful. While additional measurements of bulk permeability in single holes will continue to be useful, particularly if measurements can be completed along crustal flow lines to quantify changes in bulk permeability as the crust ages, it is also necessary to attempt a new series of focused experiments. These

experiments will require the use of specialized methods in single boreholes (i.e., flow meter and tracer testing), as well as cross-hole experiments involving one or more observation wells completed at different depths. Multihole experiments will be particularly useful for exploring the importance of fracture-dominated flow, horizontal and vertical anisotropy, and the lateral scales of crustal heterogeneity. Multihole experiments will be facilitated through the use of long-term borehole observatories as well as long-term deployments of seafloor instruments to document relations between hydrologic properties and tectonic events, seafloor venting, and magmatic activity. One set of multihole and seafloor observations of hydrogeologic and geophysical processes was recently conducted during ODP Leg 169 to Middle Valley Juan de Fuca Ridge [*Shipboard Scientific Party*, 1998], and preliminary interpretations of these data should be available in the next year.

While we will not resolve the distribution of permeability within upper oceanic basement using coupled models, it would be worthwhile to explore the influences of fracture versus porous medium flow on a range of transport and reaction processes in the crust. New models incorporating highly anisotropic permeability distributions and multiporosity representations should be applied to seafloor hydrothermal systems. It is also time to merge key aspects of fracture loop and REV approaches and to create models that include the capability of gathering heat from a wide area and channeling vent fluids to flow through isolated conduits at the seafloor. Fractured rock might be treated as a percolation network [e.g., *Gueguen et al*., 1991] or a hierarchical, multiscale continuum [e.g., *Neuman*, 1990] rather than as an equivalent porous medium with a single set of properties. In the absence of a large data set of observations on subseafloor hydrologic properties (and the global data set is like to remain limited for some time), it would also be helpful to use stochastic methods to generate a range of plausible permeability distributions, and then evaluate how these representations influence fluid flow patterns, intensities, and water-rock interactions. For example, will the inclusion of discontinuous regions of greater and lesser permeability cause the formation of preferred flow channels, or will hydrothermal convection follow one or more "natural" patterns? Would the inclusion of preferential flow channels increase convection stability? Additional progress can be made through continued application of physically and chemically coupled models that allow properties and processes to change with time, but ultimately these models will require additional observational constraints to be applied with confidence.

Care must be taken in all simulation efforts to use as much observational (geological, geophysical, and geochemical) evidence as possible. While the vast array of information already collected on seafloor fluid flow, crustal character, and the transport of heat and solutes is sometimes contradictory and confusing, underlying it all must be consistent system behaviors, a primary set of relations between properties and processes that will provide the basis for a realistic understanding of oceanic crustal hydrogeology.

ACKNOWLEDGMENTS. This review is based on field, laboratory, and computer experiments generously supported over the last 8 years through grants from the National Science Foundation (OCE 9003486, OCE 9415762, and OCE 9502970), the Office of Naval Research (00014-92-J-1204), the United States Science Support Program (139-20606, 168-00421, and 168-00425), and the Petroleum Research Fund (23615-G2). The manuscript and my thinking were greatly clarified through reviews by K. Becker, J. Braun, C. Forster, C. Stein, and T. Torgersen, as well as discussions with many of the cited authors. This review would not exist without the officers, crews, and technical support staff of oceanographic research vessels, whose skill and dedication make field measurements and sample collection possible.

REFERENCES

Abbott, D. H., W. Menke, M. Hobart, R. N. Anderson, and R. W. Embley, Correlated sediment thickness, temperature gradient, and excess pore pressure in a marine fault block basin, *Geophys. Res. Lett*., *11*, 485–488, 1984.

Agar, S. M., Microstructural evolution of a deformation zone in the upper oceanic crust: Evidence from DSDP Hole 504B, *J. Geodyn*., *13*, 119–140, 1991.

Agar, S. M., Rheological evolution of the ocean floor: A microstructural view, *J. Geophys. Res*., *99*, 3175–3200, 1994.

Aksyuk, A. M., V. M. Vitovtova, A. A. Pustovoy, G. S. Kharin, and V. M. Shmonov, The permeability of oceanic basalts and some questions of the formation of hydrothermal springs in the rift zone of the Atlantic Ocean, *Oceanology*, *Engl. Transl*., *32*, 778–784, 1992.

Alt, J. C., Subseafloor processes in mid-ocean ridge hydrothermal systems, in *Seafloor Hydrothermal Systems: Physical, Chemical, Biological, and Geological Interactions*, *Geophys. Monogr. Ser*., vol. 91, edited by S. E. Humphris et al., pp. 85–114, AGU, Washington, D. C., 1995.

Alt, J. C., and R. Emmermann, Geochemistry of hydrothermally altered basalts, DSDP Hole 504B, Leg 83, *Initial Rep. Deep Sea Drill. Proj*., *83*, 249–262, 1985.

Alt, J. C., C. Laverne, and K. Muehlenbachs, Alteration of the upper oceanic crust: Mineralogy and processes in DSDP Hole 504B, Leg 83, *Initial Rep. Deep Sea Drill. Proj*., *83*, 217–247, 1985.

Alt, J. C., J. Honnorez, C. Laverne, and R. Emmermann, Hydrothermal alteration of a 1-km section through the upper oceanic crust, Deep Sea Drilling Project Hole 504B: Mineralogy, chemistry and evolution of seawater-basalt interactions, *J. Geophys. Res*., *91*, 10,309–10,335, 1986a.

Alt, J. C., K. Muehlenbachs, and J. Honnorez, An oxygen isotope profile through the upper kilometer of the oceanic crust, DSDP Hole 504B, *Earth. Planet. Sci. Lett*., *80*, 217–229, 1986b.

Alt, J. C., T. F. Anderson, L. Bonnell, and K. Muehlenbachs, The mineralogy, chemistry, and stable isotopic composition of hydrothermally altered sheeted dikes, DSDP Hole 504B, Leg 111, in *Proc. Ocean Drill. Program Sci. Res*., *111*, pp. 27–40, 1989.

Alt, J. C., D. A. H. Teagle, C. Laverne, D. A. Vanko, W. Bach, J. Honnorez, K. Becker, M. Ayadi, and P. A. Pezard, Ridge-flank alteration of upper oceanic crust in the eastern Pacific: Synthesis of results for volcanic rocks of Holes 504B and 896A, *Proc. Ocean Drill. Program Sci. Results*, *148*, 435–450, 1996.

Anderson, R., and M. Hobart, The relation between heat flow, sediment thickness, and age in the eastern Pacific, *J. Geophys. Res*., *81*, 2968–2989, 1976.

Anderson, R. N., and M. D. Zoback, Permeability, underpressures

and convection in the oceanic crust near the Costa Rica Rift, eastern equatorial Pacific, *J. Geophys. Res*., *87*, 2860–2868, 1982.

Anderson, R. N., and M. D. Zoback, The implications of fracture and void distribution from borehole televiewer imagery for the seismic velocity of the upper oceanic crust at Deep Sea Drilling Project Holes 501 and 504B, *Initial Rep. Deep Sea Drill. Proj*., *69*, 255–270, 1983.

Anderson, R., G. Moore, S. Schilt, R. Cardwell, A. Trehu, and V. Vaquier, Heat flow near a fossil ridge on the north flank of the Galapagos Spreading Center, *J. Geophys. Res*., *81*, 1828–1838, 1976.

Anderson, R., M. G. Langseth, and J. Sclater, The mechanisms of heat transfer through the floor of the Indian Ocean, *J. Geophys. Res*., *82*, 3391–3409, 1977.

Anderson, R., M. Hobart, and M. G. Langseth, Convective heat transfer in oceanic crust and sediment in the Indian Ocean, *Science*, *204*, 828–832, 1979.

Anderson, R. N., H. O'Malley, and R. L. Newmark, Use of geophysical logs for quantitative determination of fracturing, alteration, and lithostratigraphy in the upper oceanic crust, Deep Sea Drilling Project, Holes 504B and 556, *Initial Rep. Deep Sea Drill. Proj*., *83*, 443–478, 1985a.

Anderson, R. N., M. D. Zoback, S. H. Hickman, and R. L. Newmark, Permeability versus depth in the upper oceanic crust: In situ measurements in Deep Sea Drilling Project Hole 504B, eastern equatorial Pacific, *Initial Rep. Deep Sea Drill. Project*, *83*, 429–442, 1985b.

Anderson, R. N., M. D. Zoback, S. H. Hickman, and R. L. Newmark, Permeability versus depth in the upper oceanic crust: In situ measurements in DSDP Hole 504B, eastern equatorial Pacific, *J. Geophys. Res*., *90*, 3659–3669, 1985c.

Applegate, B., and R. W. Embley, Submarine tumuli and inflated tube-fed lava flows on axial volcano, Juan de Fuca Ridge, *Bull. Volcanol*., *54*, 447–458, 1992.

Ayadi, M., P. Pezard, and F. D. de Larouziere, Fracture distribution from downhole electrical images at the base of the sheeted dike complex in Hole 504B, *Proc. Ocean Drill. Program Sci. Results*, *148*, 307–315, 1996.

Baker, E. T., C. R. German, and H. Elderfield, Subseafloor processes in mid-ocean ridge hydrothermal systems, in *Seafloor Hydrothermal Systems: Physical, Chemical, Biological and Geological Interactions*, *Geophys. Monogr. Ser*., vol. 91, edited by S. E. Humphris et al., pp. 47–84, AGU, Washington, D. C., 1995.

Baker, P., P. Stout, M. Kastner, and H. Elderfield, Large-scale lateral advection of seawater through oceanic crust in the central equatorial Pacific, *Earth. Planet. Sci. Lett*., *105*, 522–533, 1991.

Bakker, M., and O. D. L. Strack, Capture zone delineation in two-dimensional groundwater flow models, *Water Resour. Res*., *32*, 1309–1315, 1996.

Barton, C., and D. Moos, Analysis of macroscopic fractures in the Cajon Pass scientific drillhole, *Geophys. Res. Lett*., *15*, 1013–1016, 1988.

Barton, C. A., M. D. Zoback, and D. Moos, Fluid flow along potentially active faults in crystalline rocks, *Geology*, *23*, 683–686, 1995.

Barton, C. A., S. Hickman, R. Morin, M. D. Zoback, T. Finkbeiner, J. Sass, and D. Benoit, Fracture permeability and its relationship to in situ stress in the Dixie Valley, Nevada, geothermal reservoir, in *International Symposium on Observation of the Continental Crust through Drilling*, vol. VIII, edited by I. Ikeda, pp. 210–215, Natl. Res. Inst. for Earth Sci. and Disaster Prev., Tsukuba, Japan, 1996.

Bear, J., Dynamics of fluids in porous media, Elsevier, New York, 1972.

Bear, J., Modeling flow and contaminant transport in fractured rock, in *Flow and Contaminant Transport in Fractured Rock*, edited by J. Bear, C.-F. Tsang, and G. de Marsily, pp. 1–37, Academic, San Diego, Calif., 1993.

Becker, K., Large scale electrical resistivity and bulk porosity of the oceanic crust, *Initial Rep. Deep Sea Drill. Proj*., *83*, 410–428, 1985.

Becker, K., Special report: Development and use of packers in ODP, *JOIDES J*., *12*, pp. 51–57, Joint Oceanogr. Inst., Washington, D. C., 1986.

Becker, K., Measurements of the permeability of the sheeted dikes in Hole 504B, ODP Leg 111, in *Proc. Ocean Drill. Program ODP*, *Sci. Results*, *111*, 317–325, 1989.

Becker, K., A guide to formation testing using ODP drillstring packers, *Tech. Note 14*, Ocean Drill. Program, College Station, Tex., 1990a.

Becker, K., Measurements of the permeability of the upper oceanic crust at Hole 395A, ODP Leg 109, *Proc. Ocean Drill. Program Sci. Results*, *106*/*109*, 213–222, 1990b.

Becker, K., Large-scale electrical resistivity and bulk porosity of the upper oceanic crust at Hole 395A, *Proc. Ocean Drill. Program Sci. Results*, *106*/*109*, 205–212, 1990c.

Becker, K., In-situ bulk permeability of oceanic gabbros in Hole 735B, ODP Leg 118, *Proc. Ocean Drill. Program Sci. Results*, *118*, 333–347, 1991.

Becker, K., Permeability measurements in Hole 896A and implications for the lateral variability of upper crustal permeability at Sites 504 and 896, *Proc. Ocean Drill. Program Sci. Results*, *148*, 353–363, 1996.

Becker, K., et al., In situ electrical resistivity and bulk porosity of the oceanic crust, Costa Rica Rift, *Nature*, *300*, 594–598, 1982.

Becker, K., M. G. Langseth, R. P. Von Herzen, and R. Anderson, Deep crustal geothermal measurements, Hole 504B, Costa Rica Rift, *J. Geophys. Res*., *88*, 3447–3457, 1983a.

Becker, K., M. G. Langseth, and R. P. Von Herzen, Deep crustal geothermal measurements, Hole 504B, Deep Sea Drilling Project Legs 69 and 70, *Initial Rep. Deep Sea Drill. Proj*., *69*, 223–236, 1983b.

Becker, K., M. G. Langseth, and R. D. Hyndman, Temperature measurements in Hole 395A, Leg 78B, *Initial Rep. Deep Sea Drill. Proj*., *78B*, 689–698, 1984.

Becker, K., M. Langseth, R. Anderson, and M. Hobart, Deep crustal geothermal measurements, Hole 504B, Costa Rica Rift, Legs 69, 70, 83, and 92, *Initial Rep. Deep Sea Drill. Proj*., *83*, 405–418, 1985.

Becker, K., et al., Deep drilling into young oceanic crust, Hole 504B, Costa Rica Rift, *Rev. Geophys*., *27*, 79–102, 1989.

Becker, K., R. H. Morin, and E. E. Davis, Permeabilities in the Middle Valley hydrothermal system measured with packer and flow meter experiments, *Proc. Ocean Drill. Program Sci. Results*, *139*, 613–626, 1994.

Becker, K., R. P. Von Herzen, J. Kirklin, R. Evans, D. Kadko, M. Kinoshita, O. Matsubayashi, R. Mills, A. Schultz, and P. Rona, Conductive heat flow at the TAG active hydrothermal mound: Results from 1993–1995 submersible surveys, *Geophys. Res. Lett*., *23*, 3463–3466, 1996.

Birch, F., Low values of oceanic heat flow, *J. Geophys. Res*., *72*, 2261–2262, 1967.

Bischoff, J. L., and R. J. Rosenbauer, The critical point and two phase boundary of seawater, 200–500°C, *Earth. Planet. Sci. Lett*., *68*, 162–170, 1984.

Bischoff, J. L., and R. J. Rosenbauer, Salinity variations in submarine hydrothermal systems by layered double-diffusive convection, *J. Geology*, *97*, 613–623, 1989.

Black, J. H., Focussed packer testing: A structured approach to save time and improve results, in *Field Testing in Engineering Geology*, vol. 6, edited by F. G. Bell et al., pp. 313–321, Golder Assoc., Bridgford House, Trent Bridge, Nottingham, England, 1990.

Bodvarsson, G., and R. P. Lowell, Ocean-floor heat flow and the circulation of interstitial waters, *J. Geophys. Res*., *77*, 4472–4475, 1972.

Böhlke, J. K., J. Honnorez, B. J. Honnorez-Guerstein, K. Muehlenbachs, and N. Peterson, Heterogeneous alteration of the upper oceanic crust: Correlation of rock chemistry, magnetic properties, and O isotope ratios with alterations in basalts from Site 396b, DSDP, *J. Geophys. Res*., *86*, 7935–7950, 1981.

Böhlke, J. K., J. Alt, and K. Muehlenbachs, Oxygen isotope-water relations in altered deep-sea basalts, *Can. J. Earth Sci*., *21*, 67–77, 1984.

Bonatti, E., and C. G. A. Harrison, Eruption styles of basalt in oceanic spreading ridges and seamounts: The effect of magma temperature and viscosity, *J. Geophys. Res*., *93*, 2967–2980, 1988.

Brace, W. F., Permeability of crystalline and argillaceous rocks, *Int. J. Rock Mech. Min. Sci*., *17*, 241–251, 1980.

Brace, W. F., Permeability of crystalline rocks: New in-situ measurements, *J. Geophys. Res*., *89*, 4327–4330, 1984.

Bredehoeft, J. D., and S. S. Papadopulos, A method for determining the hydraulic properties of tight formations, *Water Resour. Res*., *16*, 223–238, 1980.

Brikowski, T., and D. L. Norton, Influence of magma chamber geometry on hydrothermal activity at mid-ocean ridges, *Earth Planet. Sci. Lett*., *93*, 241–255, 1989.

Broglia, C., and D. Moos, In-situ structure and properties of 110-Ma crust from geophysical logs in DSDP Hole 418A, *Proc. Ocean Drill. Program Sci. Results*, *102*, 29–47, 1988.

Brown, S. R., Fluid flow through rock joints: The effect of surface roughness, *J. Geophys. Res*., *92*, 1337–1347, 1987.

Bruhn, R. L., Fracturing in normal fault zones: Implications for fluid transport and fault stability, in *The Mechanical Involvement of Fluids in Faulting*, edited by S. H. Hickman, R. Sibson, and R. Bruhn, *U.S. Geol. Surv. Open File Rep*., *94-228*, 231–246, 1994.

Bryan, W. B., S. E. Humphris, G. Thompson, and J. F. Casey, Comparative volcanology of small axial eruptive centers in the MARK area, *J. Geophys. Res*., *99*, 2973–2984, 1994.

Butterfield, D. A., G. J. Massoth, R. E. McDuff, J. E. Lupton, and M. D. Lilley, Geochemistry of hydrothermal vent fluids from Axial Seamount hydrothermal emission study vent field, Juan de Fuca Ridge: Subseafloor boiling and subsequent fluid-rock interactions, *J. Geophys. Res*., *95*, 12,895–12,921, 1990.

Butterfield, D. A., R. E. McDuff, M. J. Mottl, M. D. Lilley, J. E. Lupton, and G. J. Massoth, Gradients in the composition of hydrothermal fluids from the Endeavour segment vent field: Phase separation and brine loss, *J. Geophys. Res*., *99*, 9561–9583, 1994.

Caine, J. S., J. P. Evans, and C. B. Forster, Fault zone architecture and permeability structure, *Geology*, *24*, 1025–1028, 1996.

Calvert, A., Seismic evidence for a magma chamber beneath the slow spreading Mid-Atlantic Ridge, *Nature*, *377*, 410–414, 1995.

Campbell, A., et al., Chemistry of hot springs on the Mid-Atlantic Ridge, *Nature*, *335*, 514–519, 1988.

Cann, J. R., A layered model for oceanic crust developed, *Geophys. J. R. Astron. Soc*., *39*, 169–187, 1974.

Cann, J. R., and M. R. Strens, Black smokers fuelled by freezing magma, *Nature*, *298*, 147–149, 1982.

Cann, J. R., and M. R. Strens, Modeling periodic megaplume emissions by black smoker systems, *J. Geophys. Res*., *94*, 12,227–12,237, 1989.

Cann, J. R., M. R. Strens, and A. Rice, A simple magma-driven thermal balance model for the formation of volcanogenic massive sulfides, *Earth. Planet. Sci. Lett*., *76*, 123–134, 1985.

Carbotte, S. M., J. C. Mutter, and L. Xu, Contribution of volcanism and tectonism to axial and flank morphology of the southern East Pacific Rise, 17°10′–17°40′S, from a study of layer 2A geometry, *J. Geophys. Res*., *102*, 10,465–10,184, 1997.

Caress, D., M. S. Burnett, and J. A. Orcutt, Tomographic image of the axial low-velocity zone at 12°50′N on the East Pacific Rise, *J. Geophys. Res*., *97*, 9243–9263, 1992.

Carlson, R. L., and C. N. Herrick, Densities and porosities in the oceanic crust and their variations with depth and age, *J. Geophys. Res*., *95*, 9153–9170, 1990.

Carlson, R., and R. Jacobson, Comment on "Upper crustal structure as a function of plate age" by Robert Houtz and John Ewing, *J. Geophys. Res*., *99*, 3135–3138, 1994.

Carlson, R. L., K. R. Snow, and R. H. Wilkens, Density of old oceanic crust: An estimate derived from downhole logging on ODP Leg 102, in *Proc. Ocean Drill. Program Sci. Results*, *102*, 63–68, 1988.

Cathles, L., Scales and effects of fluid flow in the upper crust, *Science*, *248*, 323–329, 1990.

Cathles, L., A capless 350°C flow zone model to explain megaplumes, salinity variations, and high-temperature veins in ridge axis hydrothermal systems, *Econ. Geol*., *88*, 1977–1988, 1993.

Chen, Y. J., Oceanic crustal thickness versus spreading rate, *Geophys. Res. Lett*., *19*, 753–756, 1992.

Choukroune, L., Structural study of basaltic rocks showing brittle deformation (Deep Sea Drilling Project Legs 51, 52, and 53, Sites 417 and 418), *Initial Rep. Deep Sea Drill. Proj*., *51*, *52*, *53*, 1491–1498, 1980.

Christensen, N. I., and R. Ramananantoandro, Permeability of the oceanic crust based on experimental studies of basalt permeability at elevated pressures, *Tectonophysics*, *149*, 181–186, 1988.

Christeson, G. L., G. M. Purdy, and G. J. Fryer, Seismic constraints on shallow crustal emplacement processes at the fast spreading East Pacific Rise, *J. Geophys. Res*., *99*, 17,957–17,973, 1994.

Clauser, C., Permeability of crystalline rocks, *Eos Trans. AGU*, *73*(21), 233, 237–238, 1992.

Cooper, H. H., Jr., and C. E. Jacob, A generalized graphical method for evaluating formation constraints and summarizing well-field history, *Eos Trans. AGU*, *27*, 526–534, 1946.

Cooper, H. H., Jr., J. D. Bredehoeft, and I. S. Papadopulos, Response of a finite diameter well to an instantaneous charge of water, *Water Resour. Res*., *3*, 267–269, 1967.

Costa Rica Rift Unified Scientific Team (CRRUST), Geothermal regimes of the Costa Rica Rift, east Pacific, investigated by drilling, DSDP-IPRD legs 68, 69, and 70, *Geol. Soc. Am. Bull*., *93*, 862–875, 1982.

Coyle, B. J., and M. D. Zoback, In situ permeability and fluid pressure measurements at ~2 km depth in the Cajon Pass research well, *Geophys. Res. Lett*., *15*, 1029–1032, 1988.

Criss, R. E., and A. M. Hofmeister, Application of fluid dynamics principles in tilted permeable media to terrestrial hydrothermal systems, *Geophys. Res. Lett*., *18*, 199–202, 1991.

Curray, J. R., and D. G. Moore, *Initial Reports of the Deep Sea Drilling Project*, vol. 64, parts 1 and 2, U.S. Govt. Print. Off., Washington, D. C., 1982.

Darcy, H., *Les Fontaines Publiques de la Ville de Dijon*, 647 pp., Victor Dalmont, Paris, 1856.

David, C., Geometry of flow paths for fluid transport in rocks, *J. Geophys. Res*., *98*, 12,267–12,278, 1993.

Davis, E. E., and K. Becker, Formation temperatures and pressures in a sedimented rift hydrothermal system: 10 months of CORK observations, Holes 857D and 858G, *Proc. Ocean Drill. Proj. Sci. Results*, *139*, 649–666, 1994a.

Davis, E. E., and K. Becker, Thermal and tectonic structure of Escanaba Trough: New heat flow measurements and seismic reflection profiles, in *Geologic, Hydrothermal, and Biologic Studies at Escanaba Trough, Gorda Ridge, Offshore Northern California*, edited by J. L. Morton, R. A. Zierenberg and C. A. Reiss, *U.S. Geol. Surv. Bull*., *2022*, 45–64, 1994b.

Davis, E. E., and D. S. Chapman, Problems with imaging cellular hydrothermal convection in oceanic crust, *Geophys. Res. Lett*., *24*, 3551–3554, 1996.

Davis, E. E., and C. R. B. Lister, Fundamentals of ridge crest topography, *Earth. Planet. Sci. Lett*., *21*, 405–413, 1974.

Davis, E. E., and H. Villinger, Tectonic and thermal structure of the Middle Valley sedimented rift, northern Juan de Fuca Ridge, *Proc. Ocean Drill. Program Initial Rep*., *139*, 9–41, 1992.

Davis, E. E., C. R. B. Lister, U. S. Wade, and R. D. Hyndman, Detailed heat flow measurements over the Juan de Fuca Ridge system, *J. Geophys. Res*., *85*, 299–310, 1980.

Davis, E. E., D. S. Chapman, C. Forster, and H. Villinger, Heat-flow variations correlated with buried basement topography on the Juan de Fuca Ridge flank, *Nature*, *342*, 533–537, 1989.

Davis, E. E., et al., FlankFlux: An experiment to study the nature

of hydrothermal circulation in young oceanic crust, *Can. J. Earth Sci*., *29*(5), 925–952, 1992a.
Davis, E. E., M. J. Mottl, and A. T. Fisher (Eds.), *Proceedings of the Ocean Drilling Program*, *Initial Reports*, vol. 139, 1026 pp., Ocean Drill. Program, College Station, Tex., 1992b.
Davis, E. E., D. S. Chapman, and C. B. Forster, Observations concerning the vigor of hydrothermal circulation in young volcanic crust, *J. Geophys. Res*., *101*, 2927–2942, 1996.
Davis, E. E., A. T. Fisher, and J. Firth, *Proceedings of the Ocean Drilling Program*, *Initial Reports*, vol. 168, 470 pp., Ocean Drill. Program, College Station, Tex., 1997a.
Davis, E. E., K. Wang, J. He, D. S. Chapman, H. Villinger, and A. Rosenberger, An unequivocal case for high Nusselt-number hydrothermal convection in sediment-buried igneous oceanic crust, *Earth. Planet. Sci. Lett*., *146*, 137–150, 1997b.
Davison, C. C., and E. T. Kozak, Hydrogeologic characteristics of major fracture zones in a large granite batholith of the Canadian shield, in *Fourth Canadian-American Conference on Hydrogeology*, edited by B. Hitchton and S. Bachu, pp. 52–59, Natl. Water Well Assoc., Dublin, Ohio, 1988.
Delaney, J. R., V. Robigou, R. McDuff, and M. Tivey, Geology of a vigorous hydrothermal system on the Endeavor segment, Juan de Fuca Ridge, *J. Geophys. Res*., *97*, 19,663–19,682, 1992.
Dershowitz, W., and I. Miller, Dual porosity fracture flow and transport, *Geophys. Res. Lett*., *22*, 1441–1444, 1995.
Detrick, R. S., P. Buhl, E. Vera, J. Mutter, J. Orcutt, J. Madsen, and T. Brocher, Multi-channel seismic imaging of a crustal magma chamber along the East Pacific Rise, *Nature*, *326*, 61–64, 1987.
Detrick, R., J. Collins, R. Steven, and S. Swift, In situ evidence for the nature of the seismic layer 2/3 boundary in oceanic crust, *Nature*, *370*, 288–290, 1994.
Dick, H. J. B., P. S. Meyer, S. Bloomer, S. Kirby, D. Stakes, and C. Mawer, Lithostratigraphic evolution of an in-situ section of oceanic layer 3, *Proc. Ocean Drill. Program Sci. Results*, *118*, 439–515, 1991.
Dutrow, B., and D. Norton, Evolution of fluid pressure and fracture propagation during contact metamorphism, *J. Metamorph. Geol*., *13*, 677–686, 1995.
Elder, J. W., Physical processes in geothermal areas, in *Terrestrial Heat Flow*, *Geophys. Monogr. Ser*., vol. 8, edited by W. H. K. Lee, pp. 211–239, AGU, Washington, D. C., 1965.
Elderfield, H., and A. Schultz, Mid-ocean ridge hydrothermal fluxes and the chemical composition of the ocean, *Annu. Rev. Earth Planet. Sci*., *24*, 191–224, 1996.
Embley, R. W., and W. W. Chadwick, Jr., Volcanic and hydrothermal processes associated with a recent phase of seafloor spreading at the northern Cleft segment, Juan de Fuca Ridge, *J. Geophys. Res*., *99*, 4741–4760, 1994.
Embley, R. W., M. A. Hobart, R. N. Anderson, and D. Abbott, Anomalous heat flow in the northwest Atlantic, A case for continued hydrothermal circulation in 80-m.y. crust, *J. Geophys. Res*., *88*, 1067–1074, 1983.
Embley, R. W., I. R. Jonasson, M. R. Perfit, J. M. Franklin, M. A. Tivey, A. Malahoff, M. F. Smith, and T. J. G. Francis, Submersible investigation of an extinct hydrothermal system on the Galapagos Ridge: Sulfide mounds, stockwork zone, and differentiated lavas, *Can. Mineral*., *26*, 517–540, 1988.
Evans, R. L., Constraints on the large-scale porosity and permeability structure of young oceanic crust from velocity and resistivity data, *Geophys. J. Int*., *119*, 869–879, 1994.
Evans, R. L., S. C. Constable, M. C. Sinha, C. S. Cox, and M. J. Unsworth, Upper crustal resistivity structure of the East Pacific Rise near 13°N, *Geophys. Res. Lett*., *18*, 1917–1920, 1991.
Fehn, U., The evolution of low-temperature convection cells near spreading centers: A mechanism for the formation of the Galapagos Mounds and similar manganese deposits, *Econ. Geol*., *81*, 1396–1407, 1986.
Fehn, U., and L. Cathles, Hydrothermal convection at slow-spreading midocean ridges, *Tectonophysics*, *55*, 239–260, 1979.
Fehn, U., and L. Cathles, The influence of plate movement on the evolution of hydrothermal convection cells in the oceanic crust, *Tectonophysics*, *125*, 289–312, 1986.
Fehn, U., K. Green, R. P. Von Herzen, and L. Cathles, Numerical models for the hydrothermal field at the Galapagos Spreading Center, *J. Geophys. Res*., *88*, 1033–1048, 1983.
Fisher, A. T., and K. Becker, The reduction in heat flow with depth: Evidence for borehole convection?, *Sci. Drill*., *2*, 34–40, 1991.
Fisher, A. T., and K. Becker, The correlation between heat flow and basement relief: Observational and numerical examples and implications for upper crustal permeability, *J. Geophys. Res*., *100*, 12,641–12,657, 1995.
Fisher, A. T., K. Becker, T. N. Narasimhan, M. G. Langseth, and M. J. Mottl, Passive, off-axis convection on the southern flank of the Costa Rica Rift, *J. Geophys. Res*., *95*, 9343–9370, 1990.
Fisher, A. T., K. Becker, and T. N. Narasimhan, Off-axis hydrothermal circulation: Parametric tests of a refined model of processes at Deep Sea Drilling Project/Ocean Drilling Program Site 504, *J. Geophys. Res*., *99*, 3097–3121, 1994.
Fisher, A. T., E. E. Davis, J. Grigel, D. Pribnow, K. Becker, and J. Stein, On the lateral and vertical scale of ridge-flank hydrothermal circulation (abstract), *Eos Trans. AGU*, *77*(46), Fall Meet. Suppl., 755, 1996.
Fisher, A. T., K. Becker, and E. E. Davis, The permeability of young oceanic crust east of Juan de Fuca Ridge determined using borehole thermal measurements, *Geophys. Res. Lett*., *24*, 1311–1314, 1997.
Floyd, P., and P. Castillo, Geochemistry and petrogenesis of Jurassic ocean crust basalts, Site 801, *Proc. Ocean Drill. Program Sci. Results*, *129*, 361–388, 1992.
Fornari, D., and R. W. Embley, Tectonic and volcanic controls on hydrothermal processes at the mid-ocean ridge: An overview based on near-bottom and submersible studies, in *Seafloor Hydrothermal Systems: Physical, Chemical, Biological and Geological Interactions*, *Geophys. Monogr. Ser*., vol. 91, edited by S. E. Humphris *et al*., pp. 1–46, AGU, Washington, D. C., 1995.
Forster, C. B., and J. P. Evans, Hydrogeology of thrust faults and crystalline thrust sheets: Results of combined field and modeling studies, *Geophys. Res. Lett*., *18*, 979–982, 1991.
Forster, C. B., J. V. Goddard, and J. P. Evans, Permeability structure of a thrust fault, in *The Mechanical Involvement of Fluids in Faulting*, edited by S. H. Hickman, R. Sibson, and R. Bruhn, *U.S. Geol. Surv. Open File Rep*., *94-228*, 216–223, 1994.
Fournier, R. O., The transition from hydrostatic to greater than hydrostatic fluid pressure in presently active continental hydrothermal systems in crystalline rocks, *Geophys. Res. Lett*., *18*, 955–958, 1991.
Francheteau, J., R. Armijo, J. L. Cheminee, R. Hekinian, P. Lonsdale, and N. Blum, Dyke complex of the East Pacific Rise exposed in the walls of Hess Deep and the structure of upper oceanic crust, *Earth. Planet. Sci. Lett*., *111*, 109–121, 1992.
Freeze, R. A., and J. A. Cherry, *Groundwater*, 604 pp., Simon and Schuster, New York, 1979.
Gable, R., R. Morin, and K. Becker, Geothermal state of Hole 504B: ODP Leg 111 overview, *Proc. Ocean Drill. Program Sci. Results*, *111*, 87–96, 1989.
Gable, R., R. H. Morin, and K. Becker, Geothermal state of DSDP Holes 333A, 395A and 534A: Results from the DIANAUT program, *Geophys. Res. Lett*., *19*, 505–508, 1992.
Gable, R., R. Morin, K. Becker, and P. Pezard, Heat flow in the upper part of the oceanic crust: Synthesis of in-situ temperature measurements in Hole 504B, *Proc. Ocean Drill. Program Sci. Results*, *137*/*140*, 321–326, 1995.
Gale, J. E., and K. G. Raven, Effect of sample size on stress-permeability relationship for natural fractures, *Tech. Inf. Rep. 48*, *LBL-11865*, Lawrence Berkeley Lab., Berkeley, Calif., 1980.
Gallahan, W. E., and R. A. Duncan, Spatial and temporal variability in crystallization of celadonites within the Troodos ophiolite, Cyprus: Implications for low-temperature alteration of the oceanic crust, *J. Geophys. Res*., *99*, 3147–3161, 1994.
Garven, G., Continental-scale groundwater flow and geologic processes, *Annu. Rev. Earth Planet. Sci*., *23*, 89–117, 1995.
Germanovich, L. N., and R. P. Lowell, Percolation theory, ther-

moelasticity, and discrete hydrothermal venting in the Earth's crust, *Science*, *255*, 1564–1567, 1992.

Gillis, K., and P. T. Robinson, Distribution of alteration zones in the upper oceanic crust, *Geology*, *16*, 262–266, 1988.

Gillis, K. M., and P. T. Robinson, Patterns and processes of alteration in the lavas and dikes of the Troodos ophiolite, Cyprus, *J. Geophys. Res*., *95*, 21,523–21,548, 1990.

Gillis, K., and G. Thompson, Metabasalts from the Mid-Atlantic Ridge: New insights into hydrothermal systems in slow-spreading crust, *Contrib. Mineral. Petrol*., *113*, 502–523, 1993.

Ginster, U., M. J. Mottl, and R. P. Von Herzen, Heat flux from black smokers on the Endeavor and Cleft segments, Juan de Fuca Ridge, *J. Geophys. Res*., *99*, 4937–4950, 1994.

Glover, P. W. J., K. Matsuki, R. Hikima, and K. Hayashi, Fluid flow in fractally rough synthetic fractures, *Geophys. Res. Lett*., *24*, 1803–1806, 1997.

Goldberg, D., C. Broglia, and K. Becker, Fracture permeability and alteration in gabbro from the Atlantis II fracture zone, in *Geologic Applications of Wireline Logs II*, edited by A. Hurst, C. M. Griffiths and P. F. Worthington, *Geol. Soc. Spec. Publ*., *65*, 199–210, 1992.

Goldfarb, M. S., and J. R. Delaney, Response of two-phase fluids to fracture configurations within submarine hydrothermal systems, *J. Geophys. Res*., *93*, 4585–4594, 1988.

Green, K. E., R. P. Von Herzen, and D. L. Williams, The Galapagos Spreading Center at 86°W: A detailed geothermal field study, *J. Geophys. Res*., *86*, 979–986, 1981.

Gregg, T. K. P., and W. W. Chadwick Jr., Submarine lava-flow inflation: A model for the formation of lava pillars, *Geology*, *24*, 981–984, 1996.

Gregory, R. T., and H. P. Taylor, An oxygen isotope profile in a section of Cretaceous oceanic crust, Samail Ophiolite, Oman: Evidence for $\delta^{18}O$ buffering of the oceans by deep (>5 km) seawater-hydrothermal circulation at mid-ocean ridges, *J. Geophys. Res*., *86*, 2737–2755, 1981.

Gueguen, Y., C. David, and P. Gavrilenko, Percolation networks and fluid transport in the crust, *Geophys. Res. Lett*., *18*, 931–934, 1991.

Gueguen, Y., P. Gavrilenko, and M. Le Ravalec, Scales of rock permeability, *Surv. Geophys*., *17*, 245–263, 1996.

Guerin, G., K. Becker, R. Gable, and P. Pezard, Temperature measurements and heat-flow analysis in Hole 504B, *Proc. Ocean Drill. Program Sci. Results*, *148*, 291–296, 1996.

Guyonnet, D., S. Mishra, and J. McCord, Evaluating the volume of porous medium investigated during slug tests, *Groundwater*, *31*, 627–633, 1993.

Haar, L., J. S. Gallagher, and G. S. Kell, *NBS/NRC Steam Tables*, 316 pp., Hemisphere, Bristol, Pa., 1984.

Hamano, Y., Physical properties of basalts from Holes 417D and 418A, *Initial Rep. Deep Sea Drill. Proj*., *51*, *52*, *53*, 1457–1466, 1980.

Hannington, M. D., I. R. Jonasson, P. M. Herzig, and S. Petersen, Physical and chemical processes of seafloor mineralization at mid-ocean ridges, in *Seafloor Hydrothermal Systems: Physical, Chemical, Biological and Geological Interactions*, *Geophys. Monogr. Ser*., vol. 91, edited by S. E. Humphris et al., pp. 115–157, AGU, Washington, D. C., 1995.

Harding, A. J., J. A. Orcutt, M. E. Kappus, E. E. Vera, J. C. Mutter, P. Buhl, R. S. Detrick, and T. M. Brocher, Structure of young oceanic crust at 13°N on the East Pacific Rise from expanding spread profiles, *J. Geophys. Res*., *94*, 12,163–12,196, 1989.

Harding, A. J., G. M. Kent, and J. A. Orcutt, A multichannel seismic investigation of upper oceanic crust at 9°N on the East Pacific Rise: Implications for crustal accretion, *J. Geophys. Res*., *98*, 13,925–13,944, 1993.

Harper, G. D., J. R. Bowman, and R. Kuhns, A field, chemical, and stable isotope study of subseafloor metamorphism of the Josephine ophiolite, California–Oregon, *J. Geophys. Res*., *93*, 4625–4656, 1988.

Hart, S. R., and H. Staudigel, Ocean crust vein mineral deposition: Rb/Sr ages, U-Th-Pb geochemistry, and duration of circulation at DSDP Sites 261, 462, and 516, *Geochim. Cosmochim. Acta*, *50*, 2751–2761, 1986.

Hartline, B. K., and C. R. B. Lister, Topographic forcing of supercritical convection in a porous medium such as the oceanic crust, *Earth. Planet. Sci. Lett*., *55*, 75–86, 1981.

Haymon, R. M., R. A. Koski, and M. J. Abrams, Hydrothermal discharge zones beneath massive sulfide deposits mapped in the Oman ophiolite, *Geology*, *17*, 531–535, 1989.

Haymon, R. M., D. J. Fornari, M. H. Edwards, S. Carbotte, D. Wright, and K. C. Macdonald, Hydrothermal vent distribution along the East Pacific Rise crest (9°09′–54′N) and its relationship to magmatic and tectonic processes on fast-spreading mid-ocean ridges, *Earth. Planet. Sci. Lett*., *104*, 513–534, 1991.

Haymon, R. M., et al., Volcanic eruption of the mid-ocean ridge along the East Pacific Rise at 9°45–52′N: Direct submersible observations of seafloor phenomena associated with an eruption in April 1991, *Earth. Planet. Sci. Lett*., *119*, 85–101, 1993.

Head, J. W., III, L. Wilson, and D. K. Smith, Mid-ocean ridge reuptive vent morphology and substructure: Evidence for dike widths, eruption rates, and evolution of eruptions and axial volcanic ridges, *J. Geophys. Res*., *101*, 28,265–28,280, 1996.

Hey, R., R. K. Duennebier, and W. J. Morgan, Propogating rifts on mid-ocean ridges, *J. Geophys. Res*., *85*, 3647–3658, 1980.

Hickman, S. H., M. G. Langseth, and J. F. Svitek, In-situ permeability and pore-pressure measurements near the Mid-Atlantic Ridge, Deep Sea Drilling Project Hole 395A, *Initial Rep. Deep Sea Drill. Proj*., *78B*, 699–708, 1984a.

Hickman, S. H., J. F. Svitek, and M. G. Langseth, Borehole televiewer log of Hole 395A, *Initial Rep. Deep Sea Drill. Proj*., *78B*, 709–715, 1984b.

Hobart, M., M. Langseth, and R. N. Anderson, A geothermal and geophysical survey of the south flank of the Costa Rica Rift, sites 504 and 505, *Initial Rep. Deep Sea Drill. Proj*., *83*, 379–404, 1985.

Holmes, M. L., and H. P. Johnson, Upper crustal densities derived from seafloor gravity measurements: Northern Juan de Fuca Ridge, *Geophys. Res. Lett*., *17*, 1871–1874, 1993.

Horne, R. N., and M. J. O'Sullivan, Oscillatory convection in a porous medium heated from below, *J. Fluid Mech*., *64*, 1–15, 1974.

Horner, D. R., Pressure build-up in wells, in *Proc. World Pet. Congr*., *3rd*, *Sect. II*, vol. 2, 501–521, 1951.

Houtz, R., and J. Ewing, Upper crustal structure as a function of plate age, *J. Geophys. Res*., *81*, 2490–2498, 1976.

Hubbert, M. K., The theory of groundwater motion, *J. Geology*, *48*, 785–944, 1940.

Hufschmied, P., M. Thury, S. Vomvoris, R. W. Andrews, and F. Herzog, Hydrologic investigations of low permeability rock in the NAGRA program: From methods development to site characterization, in *Hydrogeology of Low Permeability Environments*, vol. 2, edited by S. P. Neuman and I. Neretnieks, pp. 83–113, H. Heise, Hannover, Germany, 1990.

Humphris, S. E., R. A. Zierenberg, L. S. Mullineaux, and R. E. Thompson (Eds.), *Seafloor Hydrothermal Systems: Physical, Chemical, Biological, and Geological Interactions*, *Geophys. Monogr. Ser*., vol. 91, 466 pp., AGU, Washington, D. C., 1995.

Humphris, S. E., et al., *Proceedings of the Ocean Drilling Program*, *ODP*, *Initial Reports*, vol. 158, 384 pp., Ocean Drill. Program, College Station, Tex., 1996.

Hurst, W. H., O. K. Haynie, and R. N. Walker, Some problems in pressure buildup, in *Advances in Petroleum Engineering*, edited by W. H. Hurst, pp. 296–312, PennWell Books, Tulsa, Okla., 1981.

Hyndman, R. D., and M. J. Drury, The physical properties of oceanic basement rocks from deep drilling on the Mid-Atlantic Ridge, *J. Geophys. Res*., *81*, 4042–4052, 1976.

Hyndman, R. D., and M. H. Salisbury, The physical nature of young upper oceanic crust on the Mid-Atlantic Ridge, Deep Sea Drilling Project Hole 395A, *Initial Rep. Deep Sea Drill. Proj*., *78B*, 839–848, 1984.

Jacobson, R. S., Impact of crustal evolution on changes of the

seismic properties of the uppermost oceanic crust, *Rev. Geophys.*, *30*, 23–42, 1992.
Jarrard, R. D., and C. Broglia, Geophysical properties of oceanic crust at Sites 768 and 770, *Proc. Ocean Drill. Program Sci. Results*, *124*, 75–90, 1991.
Jarrard, R. D., R. L. Larson, A. T. Fisher, and L. J. Abrams, Geophysical aging of oceanic crust: Evidence from Hole 801C, *Proc. Ocean Drill. Proj.*, *ODP*, *Sci. Results*, *144*, 649–662, 1995.
Johnson, D. M., Crack distribution in the upper oceanic crust and its effects upon seismic velocity, seismic structure, formation permeability, and fluid circulation, *Initial Rep. Deep Sea Drill. Proj.*, *51–53*, 1479–1490, 1980a.
Johnson, D. M., Fluid permeability of oceanic basalts, *Initial Rep. Deep Sea Drill. Proj.*, *51–53*, 1473–1477, 1980b.
Johnson, H. P., and M. Hutnak, Conductive heat flow measured in unsedimented regions of the seafloor, *Eos Trans. AGU*, *77*(33), 321, 324, 1996.
Johnson, H. P., K. Becker, and R. P. V. Herzen, Near-axis heat flow measurements on the northern Juan de Fuca Ridge: Implications for fluid circulation in oceanic crust, *Geophys. Res. Lett.*, *20*, 1875–1878, 1993.
Kadko, D., J. Baross, and J. C. Alt, The magnitude and global implications of hydrothermal flux, in *Seafloor Hydrothermal Systems: Physical, Chemical, Biological, and Geological Interactions*, *Geophys. Monogr. Ser.*, vol. 91, edited by S. E. Humphris et al., pp. 446–466, AGU, Washington, D. C., 1995.
Kappus, M. E., A. J. Harding, and J. A. Orcutt, A baseline for upper crustal velocity variations along the East Pacific Rise at 13°N, *J. Geophys. Res.*, *100*, 6143–6161, 1995.
Karato, S., Physical properties of basalts from Deep Sea Drilling Project Hole 504B, *Initial Rep. Deep Sea Drill. Proj.*, *69*, 687–695, 1983a.
Karato, S., Physical properties of basalts from the Galapagos, Leg 70, *Initial Rep. Deep Sea Drill. Proj.*, *70*, 423–428, 1983b.
Karson, J. A., and H. J. B. Dick, Tectonics of ridge-transform intersections at the Kane Fracture Zone, *Mar. Geophys. Res.*, *6*, 51–98, 1983.
Karson, J. A., and P. A. Rona, Block-tilting, transfer faults, and structural control of magmatic and hydrothermal processes in the TAG area, mid-Atlantic 26° North, *Geol. Soc. Am. Bull.*, *102*, 1635–1645, 1990.
Keller, A. A., P. V. Roberts, and P. K. Kitanidis, Prediction of single phase transport properties in a variable aperature fracture, *Geophys. Res. Lett.*, *22*, 1425–1428, 1995.
Kent, G. M., S. A. Swift, R. S. Detrick, J. A. Collins, and R. A. Stephen, Evidence for active normal faulting on 5.9 Ma crust near Hole 504B on the southern flank of the Costa Rica Rift, *Geology*, *24*, 83–86, 1996.
Kirkpatrick, R. J., The physical state of the oceanic crust: Results of downhole geophysical logging in the Mid-Atlantic Ridge at 23°N, *J. Geophys. Res.*, *84*, 178–188, 1979.
Kohl, T., and R. J. Hopkirk, "FRACTure"—a simulation code for forced fluid flow and transport in fractured, porous rock, *Geothermics*, *24*, 333–343, 1995.
Kopietz, J., K. Becker, and Y. Hamano, Temperature measurements at Site 395, ODP Leg 109, in *Proc. Ocean Drill. Program Sci. Results*, *106/109*, 197–203, 1990.
Langseth, M., and K. Becker, Structure of igneous basement at sites 857 and 858 based on Leg 139 downhole logging, *Proc. Ocean Drill. Program Sci. Results*, *139*, 573–583, 1994.
Langseth, M. G., and B. Herman, Heat transfer in the oceanic crust of the Brazil Basin, *J. Geophys. Res.*, *86*, 10,805–10,819, 1981.
Langseth, M. G., and E. A. Silver, The Nicoya convergent margin—A region of exceptionally low heat flow, *Geophys. Res. Lett.*, *23*, 891–894, 1996.
Langseth, M. G., J. Cann, J. Natland, and M. Hobart, Geothermal phenomena at the Costa Rica Rift, Background to objectives for drilling at Deep Sea Drilling Project sites 501, 504, 505, *Initial Rep. Deep Sea Drill. Proj.*, *69*, 5–29, 1983.
Langseth, M. G., R. D. Hyndman, K. Becker, S. H. Hickman, and M. H. Salisbury, The hydrogeological regime of isolated sediment ponds in mid-oceanic ridges, *Initial Rep. Deep Sea Drill. Proj.*, *78B*, 825–837, 1984.
Langseth, M. G., M. J. Mottl, M. A. Hobart, and A. T. Fisher, The distribution of geothermal and geochemical gradients near Site 501/504, Implications for hydrothermal circulation in the oceanic crust, *Proc. Ocean Drill. Program Initial Rep.*, *111*, 23–32, 1988.
Langseth, M. G., K. Becker, R. P. Von Herzen, and P. Schultheiss, Heat and fluid flux through sediment on the western flank of the Mid-Atlantic Ridge: A hydrogeological study of North Pond, *Geophys. Res. Lett.*, *19*, 517–520, 1992.
Lapwood, E., Convection of a fluid in a porous media, *Proc. Cambridge Philos. Soc.*, *44*, 508–521, 1948.
Larson, R., et al., *Proceedings of the Ocean Drilling Program*, *Initial Reports*, vol. 129, 488 pp., Ocean Drill. Program, College Station, Tex., 1992.
Larson, R. L., A. T. Fisher, and R. Jarrard, Highly layered and permeable Jurassic oceanic crust in the western Pacific, *Earth. Planet. Sci. Lett.*, *119*, 71–83, 1993.
Lee, C.-H., and I. Farmer, *Fluid Flow in Discontinuous Rocks*, 169 pp., Chapman and Hall, New York, 1993.
Lee, T.-C., On terrain corrections in terrestrial heat flow, *Pure Appl. Geophys.*, *135*(1), 1–13, 1991.
Lee, W. H. K., and S. Uyeda, Review of heat flow data, in *Terrestrial Heat Flow*, *Geophys. Monogr. Ser.*, vol. 8, edited by W. H. K. Lee, pp. 87–190, AGU, Washington, D. C., 1965.
Le Pichon, X., and M. G. Langseth, Heat flow from mid-ocean ridges and sea-floor spreading, *Tectonophysics*, *8*, 319–344, 1969.
Lichtner, P. C., Continuum model for simultaneous chemical reactions and mass transport in hydrothermal systems, *Geochim. Cosmochim. Acta*, *49*, 779–800, 1985.
Lister, C. R. B., Heat flow of the Juan de Fuca Ridge, *J. Geophys. Res.*, *75*, 2648–2654, 1970.
Lister, C. R. B., On the thermal balance of a mid-ocean ridge, *Geophys. J. R. Astron. Soc.*, *26*, 515–535, 1972.
Lister, C. R. B., On the penetration of water into hot rock, *Geophys. J. R. Astron. Soc.*, *39*, 465–509, 1974.
Lister, C. R. B., Qualitative models of spreading center processes, including hydrothermal penetration, *Tectonophysics*, *37*, 203–218, 1977.
Lister, C. R. B., Heat flow and hydrothermal circulation, *Annu. Rev. Earth Planet. Sci.*, *8*, 95–117, 1980.
Lister, C. R. B., Active and passive hydrothermal systems in the oceanic crust: Predicted physical conditions, in *The Dynamic Environment of the Ocean Floor*, edited by K. A. Fanning and F. T. Mannheim, pp. 441–470, D. C. Heath, Lexington, Mass., 1981.
Logan, J. M., and C. L. Decker, Cyclic flow along faults, in *The Mechanical Involvement of Fluids in Faulting*, edited by S. H. Hickman, R. Sibson, and R. Bruhn, *U.S. Geol. Surv. Open File Rep.*, *94-228*, 190–203, 1994.
Lonsdale, P., Deep-tow observations at the mound abyssal hydrothermal field, Galapagos Rift, *Earth. Planet. Sci. Lett.*, *36*, 92–110, 1977.
Lonsdale, P., and K. Becker, Hydrothermal plumes, hot springs, and conductive heat flow in the southern trough of Guaymas Basin, *Earth. Planet. Sci. Lett.*, *73*, 211–225, 1985.
Lowell, R. P., Circulation in fractures, hot springs, and convective heat transport on mid-ocean ridge crests, *Geophys. J. R. Astron. Soc.*, *40*, 351–365, 1975.
Lowell, R. P., Topographically driven subcritical hydrothermal convection in the oceanic crust, *Earth. Planet. Sci. Lett.*, *49*, 21–28, 1980.
Lowell, R. P., Thermoelasticity and the formation of black smokers, *Geophys. Res. Lett.*, *17*, 709–712, 1990.
Lowell, R. P., Modeling continental and submarine hydrothermal systems, *Rev. Geophys.*, *29*, 457–476, 1991.
Lowell, R. P., and L. N. Germanovich, On the temporal evolution of high-temperature hydrothermal systems at ocean ridge crests, *J. Geophys. Res.*, *99*, 565–575, 1994.
Lowell, R. P., and L. N. Germanovich, Dike injection and the

formation of megaplumes at ocean ridges, *Science*, *267*, 1804–1807, 1995.

Lowell, R. P., and P. A. Rona, Hydrothermal models for the generation of massive sulfide deposits, *J. Geophys. Res*., *90*, 8769–8783, 1985.

Lowell, R. P., P. Van Chappellen, and L. N. Germanovich, Silica precipitation in fractures and the evolution of permeability in hydrothermal upflow zones, *Science*, *260*, 192–194, 1993.

Lowell, R. P., P. A. Rona, and R. P. Von Herzen, Seafloor hydrothermal systems, *J. Geophys. Res*., *100*, 327–352, 1995.

Macdonald, K., Mid-ocean ridges: Fine-scale tectonic, volcanic, and hydrothermal processes within the plate boundary zone, *Annu. Rev. Earth Planet. Sci*., *10*, 155–190, 1982.

Macdonald, K. C., P. J. Fox, L. J. Perram, M. F. Eisen, R. M. Haymon, S. P. Miller, C. M. Carbotte, M.-H. Cormier, and A. N. Shor, A new view of the mid-ocean ridge from the behavior of ridge-axis discontinuities, *Nature*, *335*, 217–225, 1988.

Macdonald, K. C., R. Haymon, and A. Shor, A 220 km^2 recently erupted lava field on the East Pacific Rise near lat 8°S, *Geology*, *17*, 212–216, 1989.

Macdonald, K. C., P. J. Fox, R. T. Alexander, R. Pockalny, and P. Gente, Volcanic growth faults and the origin of Pacific abyssal hills, *Nature*, *380*, 125–129, 1996.

Matthews, C. S., and D. G. Russell, *Pressure Build-up and Flow Tests in Wells*, *Henry L. Doherty Ser*., vol. 1, 172 pp., Soc. Pet. Eng., Richardson, Tex., 1967.

Matthews, M., M. Salisbury, and R. Hyndman, Basement logging on the Mid-Atlantic Ridge, Deep Sea Drilling Project Hole 395A, *Initial Rep. Deep Sea Drill. Proj*., *78B*, 717–730, 1984.

Mattisson, C., M. A. Knackstedt, and T. J. Sneden, Transport in fractured porous solids, *Geophys. Res. Lett*., *24*, 495–498, 1997.

McClain, J. S., J. Orcutt, and M. Burnett, The East Pacific Rise in cross section: A seismic model, *J. Geophys. Res*., *90*, 8627–8639, 1985.

McClain, J. S., C. Chin, and E. M. Moores, Seismic velocities in young ocean crust; Constraints on models for the development of permeablity and water penetration, in *Ophiolites: Oceanic Crustal Analogues*; "*Troodos 1987*," edited by J. Malpas et al., pp. 577–581, Min. of Agric. and Nat. Resour., Nicosia, Cyprus, 1990.

McConnell, C., Double porosity well testing in the fractured carbonate rocks of the Ozarks, *Ground Water*, *31*, 75–83, 1993.

McDonald, M. A., S. C. Webb, J. A. Hildebrand, and B. D. Cornuelle, Seismic structure and anisotropy of the Juan de Fuca Ridge at 45°N, *J. Geophys. Res*., *99*, 4857–4873, 1994.

McKenzie, D., Some remarks on heat flow and gravity anomalies, *J. Geophys. Res*., *72*, 6261–6273, 1967.

McKibbin, R., and M. J. O'Sullivan, Onset of convection in a layered porous medium heated from below, *J. Fluid Mech*., *96*, 375–393, 1980.

Moench, A. F., Double-porosity models for a fissured groundwater reservoir with fracture skin, *Water Resour. Res*., *7*, 831–846, 1984.

Moores, E. M., and F. J. Vine, The Troodos massif, Cyprus, and other ophiolites as oceanic crust: Evaluations and implications, *Philos. Trans. R. Soc. London*, *Ser. A*, *268*, 443–466, 1971.

Moos, D., Petrophysical results from logging in DSDP Hole 395A, ODP Leg 109, *Proc. Ocean Drill. Program Sci. Results*, *106/109*, 237–253, 1990.

Moos, D., and D. Marion, Morphology of extrusive basalts and its relationship to seismic velocities in the shallow oceanic crust, *J. Geophys. Res*., *99*, 2985–2994, 1994.

Morin, R. H., R. N. Anderson, and C. A. Barton, Analysis and interpretation of the borehole televiewer log: Information on the state of stress and the lithostratigraphy at Hole 504B, in *Proc. Ocean Drill. Program Sci. Results*, *111*, 109–118, 1989.

Morin, R. H., A. E. Hess, and K. Becker, In situ measurements of fluid flow in DSDP Holes 395A and 534A: Results from the DIANAUT program, *Geophys. Res. Lett*., *19*, 509–512, 1992a.

Morin, R. H., D. Moos, and A. E. Hess, Analysis of the borehole televiewer log from DSDP 395A: Results from the DIANAUT program, *Geophys. Res. Lett*., *19*, 501–504, 1992b.

Mottl, M. J., Metabasalts, axial hot springs, and the structure of hydrothermal systems at mid-ocean ridges, *Geol. Soc. Am. Bull*., *89*, 161–180, 1983.

Mottl, M. J., Hydrothermal convection, reaction and diffusion in sediments on the Costa Rica Rift flank, Pore water evidence from ODP Sites 677 and 678, *Proc. Ocean Drill. Program ODP*, *Sci. Results*, *111*, 195–214, 1989.

Mottl, M. J., and C. G. Wheat, Hydrothermal circulation through mid-ocean ridge flanks: Fluxes of heat and magnesium, *Geochim. Cosmochim. Acta*, *58*, 2225–2237, 1994.

Muehlenbachs, K., The alteration and aging of the basaltic layer of the sea floor: Oxygen isotope evidence from DSDP/IPOD Legs 51, 52, and 53, *Initial Rep. Deep Sea Drill. Proj*., *51–53*, 1159–1167, 1980.

Natland, J. H., Comparison of chemical and magnetic stratigraphy of Holes 396 and 396B, *Initial Rep. Deep Sea Drill. Proj*., *46*, 425–430, 1979.

Nehlig, P., Fracture and permeability analysis in magma-hydrothermal transition zones in the Samail ophiolite (Oman), *J. Geophys. Res*., *99*, 589–601, 1994.

Nehlig, P., and T. Juteau, Deep crustal seawater penetration and circulation at ocean ridges: Evidence from the Oman Ophiolite, *Mar. Geol*., *84*, 209–228, 1988a.

Nehlig, P., and T. Juteau, Flow porosities, permeabilities and preliminary data on fluid inclusions and fossil thermal gradients in the crustal sequence of the Sumail ophiolite (Oman), *Tectonophysics*, *151*, 199–221, 1988b.

Neuman, S. P., Universal scaling of hydraulic conductivities and dispersivities in geologic media, *Water Resour. Res*., *26*, 1749–1758, 1990.

Neuzil, C. E., How permeable are clays and shales?, *Water Resour. Res*., *30*, 145–150, 1994.

Newmark, R. L., R. N. Anderson, D. Moos, and M. D. Zoback, Sonic and ultrasonic logging of Hole 504B and its implications for the structure, porosity and stress regime of the upper 1 km of the oceanic crust, *Initial Rep. Deep Sea Drill. Proj*., *83*, 479–510, 1985a.

Newmark, R. L., R. N. Anderson, D. Moos, and M. D. Zoback, Structure, porosity, and stress regime of the upper oceanic crust: Sonic and ultrasonic logging of DSDP Hole 504B, *Tectonophysics*, *118*, 1–42, 1985b.

Nield, D. A., Onset of thermohaline convection in a porous medium, *Water Resour. Res*., *4*, 553–560, 1968.

Nobes, D. C., L. K. Law, and R. N. Edwards, The determination of resistivity and porosity of the sediment and fractured basalt layers near the Juan de Fuca Ridge, *Geophys. J. R. Astron. Soc*., *86*, 289–317, 1986.

Noel, M., and M. W. Hounslow, Heat flow evidence for hydrothermal convection in Cretaceous crust of the Madiera Abyssal Plain, *Earth. Planet. Sci. Lett*., *90*, 77–86, 1988.

Norton, D., Metasomatism and permeability, *Am. J. Sci*., *288*, 604–618, 1988.

Norton, D., and R. Knapp, Transport phenomena in hydrothermal systems: The nature of porosity, *Am. J. Sci*., *277*, 913–936, 1977.

Oreskes, N., K. Shrader-Frechette, and K. Belitz, Verification, validation, and confirmation of numerical models in the Earth sciences, *Science*, *263*, 641–646, 1994.

Ormond, A., and P. Genthon, 3-D thermoconvection in an anisotropic inclined sedimentary layer, *Geophys. J. Int*., *11*, 257–263, 1993.

Ortoleva, P., E. Marino, C. Moore, and J. Chadham, Geochemical self-organization, I, Reaction-transport feedbacks and modeling approach, *Am. J. Sci*., *287*, 979–1007, 1987.

Palm, E., Rayleigh convection, mass transport, and change in porosity in layers of sandstone, *J. Geophys. Res*., *95*, 8675–8679, 1990.

Papadopulos, S. S., J. D. Bredehoeft, and H. H. Cooper, On the analysis of "slug" test data, *Water Resour. Res*., *9*, 1087–1089, 1973.

Parker, R. L., and D. W. Oldenberg, Thermal model of ocean ridges, *Nature Phys. Sci*., *242*, 137–139, 1973.

Parsons, B., and J. G. Sclater, An analysis of the variation of ocean

floor bathymetry and heat flow with age, *J. Geophys. Res*., *82*, 803–829, 1977.
Person, M., J. R. Raffensperger, S. Ge, and G. Garven, Basin-scale hydrogeologic modeling, *Rev. Geophys*., *34*, 61–87, 1996. (Correction, *Rev. Geophys*., *34*, 307–309, 1996.)
Peterson, C., R. Duncan, and K. F. Scheidegger, Sequence and longevity of basalt alteration in Deep Sea Drilling Project Site 597, *Initial Rep. Deep Sea Drill. Proj*., *92*, 509–515, 1986.
Pezard, P. A., Electrical properties of mid-ocean ridge basalt and implications for the structure of the upper oceanic crust in Hole 504B, *J. Geophys. Res*., *95*, 9237–9264, 1990.
Pezard, P. A., R. N. Anderson, W. B. F. Ryan, K. Becker, J. C. Alt, and P. Gente, Accretion, structure and hydrology of intermediate spreading-rate oceanic crust from drillhole experiments and seafloor observations, *Mar. Geophys. Res*., *14*, 93–123, 1992.
Pezard, P., K. Becker, A. Revil, M. Ayadi, and P. K. Harvey, Fractures, porosity, and stress in the dolerites of Hole 504B, *Proc. Ocean Drill. Program Sci. Results*, *148*, 317–329, 1996.
Pezard, P. A., M. Ayadi, A. Revil, G. Bronner, and R. Wilkens, Detailed structure of an oceanic normal fault: A multiscalar approach at DSDP/ODP Site 504, *Geophys. Res. Lett*., *24*, 337–340, 1997.
Pinder, G. F., P. S. Huyakorn, and E. A. Sudicky, Simulation of flow and transport in fractured porous media, in *Flow and Contaminant Transport in Fractured Rock*, edited by J. Bear, C.-F. Tsang and G. de Marsily, pp. 385–435, Academic, San Diego, Calif., 1993.
Pringle, M., Radiometric ages of basaltic basement recovered at Sites 800, 801, and 802, ODP Leg 129, western Pacific Ocean, in *Proc. Ocean Drill. Program Sci. Results*, *129*, 389–404, 1992.
Purdy, M., and R. Detrick, Crustal structure of the Mid-Atlantic Ridge at 23°N from seismic refraction studies, *J. Geophys. Res*., *91*, 3739–3762, 1986.
Raitt, R. W., The crustal rocks, in *The Sea*, vol. 3, *The Earth Beneath the Sea*, edited by M. N. Hill, pp. 85–102, Wiley-Interscience, New York, 1963.
Ribando, R., K. Torrence, and D. Turcotte, Numerical models for hydrothermal circulation in the oceanic crust, *J. Geophys. Res*., *81*, 3007–3012, 1976.
Rohr, K. M. M., and U. Schmidt, Seismic structure of Middle Valley near sites 855-858, leg 139, Juan de Fuca Ridge, *Proc. Ocean Drill. Program Sci. Results*, *139*, 3–17, 1994.
Rohr, K., U. Schmidt, C. Lowe, and B. Milkereit, Multichannel seismic reflection data across Endeavour segment, Juan de Fuca Ridge, *Rep. 2847*, Geol. Surv. of Can., Sidney, B. C., 1994.
Rona, P. A., and D. A. Trivett, Discrete and diffuse heat transfer at ASHES vent field, *Earth. Planet. Sci. Lett*., *109*, 57–71, 1992.
Rona, P. A., R. P. Denlinger, M. R. Fisk, K. J. Howard, G. L. Taghon, K. D. Klitgord, J. S. McClain, G. R. McMurray, and J. C. Wiltshire, Major off-axis hydrothermal activity on the northern Gorda Ridge, *Geology*, *18*, 493–496, 1990.
Rosenberg, N. D., and F. J. Spera, Role of anisotropic and/or layered permeability in hydrothermal convection, *Geophys. Res. Lett*., *17*, 235–238, 1990.
Rosenberg, N. D., F. J. Spera, and R. M. Haymon, The relationship between flow and permeability field in seafloor hydrothermal systems, *Earth. Planet. Sci. Lett*., *116*, 135–153, 1993.
Salisbury, M., T. Donnelly, and J. Francheteau, Geophysical logging in Deep Sea Drilling Project Hole 417D, in *Initial Rep. Deep Sea Drill. Proj*., *51–53*, 705–713, 1980.
Salisbury, M. H., N. I. Christensen, and R. H. Wilkens, Nature of the layer 2/3 transition from a comparison of laboratory and logging velocities and petrology at the base of Hole 504B, in *Proc. Ocean Drill. Program Sci. Results*, *148*, 353–363, 1996.
Schultz, A., J. R. Delaney, and R. E. McDuff, On the partitioning of heat flux between diffuse and point source seafloor venting, *J. Geophys. Res*., *97*, 12,299–12,315, 1992.
Schulze-Makuch, D., and D. S. Cherkauer, Method developed for extrapolating scale behavior, *Eos Trans. AGU*, *78*(1), 3, 1997.
Sclater, J. G., and J. Francheteau, The implications of terrestrial heat flow observations on current tectonic and geochemical models of the crust and upper mantle of the Earth, *Geophys. J. R. Astron. Soc*., *20*, 509–542, 1970.
Sclater, J. G., R. P. Von Herzen, D. L. Williams, R. N. Anderson, and K. Klitgord, The Galapagos Spreading Center: Heat flow on the north flank, *Geophys. J. R. Astron. Soc*., *38*, 609–626, 1974.
Sclater, J. G., J. Crowe, and R. Anderson, On the reliability of oceanic heat flow averages, *J. Geophys. Res*., *81*, 2997–3006, 1976.
Sclater, J. G., C. Jaupart, and D. Galson, The heat flow through oceanic and continental crust and the heat loss of the Earth, *Rev. Geophys*., *18*, 269–311, 1980.
Sen, Z., and A. A. Sabtan, Straight-line intercept method in aquifer volume calculations, *Ground Water*, *30*, 569–573, 1992.
Shaw, P., Age variations of oceanic crust Poisson's ratio: Inversion and a porosity inversion model, *J. Geophys. Res*., *99*, 3057–3066, 1994.
Shipboard Scientific Party, Site 735, *Proc. Ocean Drill. Program*, *Initial Rep*., *118*, 89–212, 1989.
Shipboard Scientific Party, Site 858, *Proc. Ocean Drill. Program Initial Rep*., *139*, 431–572, 1992.
Shipboard Scientific Party, Introduction and summary: Hydrothermal circulation in the oceanic crust and its consequences on the eastern flank of the Juan de Fuca Ridge, *Proc. Ocean Drill. Program*, *Initial Rep*., *168*, 7–21, 1997a.
Shipboard Scientific Party, Middle Valley: Dead Dog area (Site 1036), *Proc. Ocean Drill. Program*, *Initial Rep*., *169*, in press, 1998.
Shor, G. G., Jr., W. H. Menard, and R. W. Raitt, Structure of the Pacific basin, in *The Sea*, vol. 4, *New Concepts of Sea Floor Evolution*, edited by A. E. Maxwell, pp. 3–27, Wiley-Interscience, New York, 1971.
Smith, D. K., and J. R. Cann, The role of seamount volcanism in crustal construction along the Mid-Atlantic Ridge, *J. Geophys. Res*., *97*, 1645–1658, 1992.
Smith, L., C. B. Forster, and J. P. Evans, Interaction of fault zones, fluid flow and heat transfer at the basin scale, in *Hydrogeology of Low Permeability Environments*, vol. 2, edited by S. P. Neuman and I. Neretnieks, pp. 41–67, H. Heise, Hannover, Germany, 1990.
Snelgrove, S. H., and C. B. Forster, Impact of seafloor sediment permeability and thickness on off-axis hydrothermal circulation: Juan de Fuca Ridge eastern flank, *J. Geophys. Res*., *101*, 2915–2925, 1996.
Snow, D. T., Rock fracture spacings, openings, and porosities, *J. Soil Mech. Found. Div. Am. Soc. Civ. Eng*., *94*, 73–91, 1968.
Sohn, R. A., S. C. Webb, J. A. Hildebrand, and B. C. Cornuelle, Three-dimensional tomographic velocity structure of upper crust, CoAxial segment, Juan de Fuca Ridge: Implications for on-axis evolution and hydrothermal circulation, *J. Geophys. Res*., *102*, 17,679–17,695, 1997.
Spooner, E. T. C., H. J. Chapman, and J. D. Smewing, Strontium isotopic contamination and oxidation during ocean floor hydrothermal metamorphism of the ophiolitic rocks of the Troodos massif, Cyprus, *Geochim. Cosmochim. Acta*, *41*, 873–890, 1977.
Staudigel, H., S. R. Hart, and S. H. Richardson, Alteration of oceanic crust: Processes and timing, *Earth. Planet. Sci. Lett*., *52*, 311–327, 1981.
Stein, C., and S. Stein, A model for the global variation in oceanic depth and heat flow with lithospheric age, *Nature*, *359*, 123–129, 1992.
Stein, C., and S. Stein, Constraints on hydrothermal heat flux through the oceanic lithosphere from global heat flow, *J. Geophys. Res*., *99*, 3081–3095, 1994.
Stephen, R., Seismic anisotropy observed in upper oceanic crust, *Geophys. Res. Lett*., *8*, 865–868, 1981.
Stephen, R., Seismic anisotropy observed in upper oceanic crust, *J. Geophys. Res*., *90*, 11,383–11,396, 1985.
Stern, C., and D. Elthon, Vertical variations in the effects of hydrothermal metamorphism in Chilean ophiolites: Their implications for ocean floor metamorphism, *Tectonophysics*, *55*, 179–213, 1979.

Stevenson, J. M., J. A. Hildebrand, M. A. Zumberge, and C. G. Fox, An ocean bottom gravity study of the southern Juan de Fuca Ridge, *J. Geophys. Res*., *99*, 4875–4888, 1994.

Strens, M. R., and J. R. Cann, A model of hydrothermal circulation in fault zones at mid-ocean ridge crests, *Geophys. J. R. Astron. Soc*., *71*, 225–240, 1982.

Strens, M. R., and J. R. Cann, A fracture-loop thermal balance model of black smoker circulation, *Tectonophysics*, *122*, 307–324, 1986.

Su, W., C. Mutter, J. C. Mutter, and W. R. Buck, Some theoretical predictions on the relationships among spreading rate, mantle temperature, and crustal thickness, *J. Geophys. Res*., *99*, 3215–3227, 1994.

Swift, S. A., H. Hoskins, and R. Stephen, Vertical seismic profile into the upper oceanic crust in Hole 504B, *Proc. Ocean Drill. Program Sci. Results*, *148*, 339–347, 1996.

Tamaki, K., K. Pisciotto, and J. Allan, *Proceedings of the Ocean Drilling Program*, *Initial Reports*, vol. 127, Ocean Drill. Program, College Station, Tex., 1990.

Theis, C. V., The lowering of the piezometer surface and the rate and discharge of a well using ground-water storage, *Eos Trans. AGU*, *16*, 519–524, 1935.

Thompson, G., Basalt-seawater interaction, in *Hydrothermal Processes at Seafloor Spreading Centers*, edited by P. A. Rona *et al*., pp. 225–278, Plenum, New York, 1983.

Travis, B. J., D. R. Janecky, and N. D. Rosenberg, Three-dimensional simulation of hydrothermal circulation at mid-ocean ridges, *Geophys. Res. Lett*., *18*, 1441–1444, 1991.

Tsang, Y. W., The effect of tortuosity on fluid flow through a single fracture, *Water Resour. Res*., *20*, 1209–1215, 1984.

Tsang, Y. W., and P. A. Witherspoon, Hydromechanical behavior of a deformable rock fracture subject to normal stress, *J. Geophys. Res*., *86*, 9287–9298, 1981.

Valsami-Jones, E., and J. R. Cann, Controls on the Sr and Nd isotopic compositions of hydrothermally altered rocks from the Pindos ophiolite, Greece, *Earth. Planet. Sci. Lett*., *125*, 39–54, 1994.

van Everdingen, D. A., Fracture characteristics of the sheeted dike complex, Troodos ophiolite, Cyprus: Implications for permeability of oceanic crust, *J. Geophys. Res*., *100*, 19,957–19,972, 1995.

Vanko, D., Temperature, pressure, and composition of hydrothermal fluids with their bearing on the magnitude of tectonic uplift at mid-ocean ridges, inferred from fluid inclusions in oceanic layer 3 rocks, *J. Geophys. Res*., *93*, 4595–4611, 1988.

Varga, R. J., and E. M. Moores, Spreading structure of the Troodos ophiolite, Cyprus, *Geology*, *13*, 846–850, 1985.

Von Damm, K. L., Controls on the chemistry and temporal variability of seafloor hydrothermal fluids, in *Seafloor Hydrothermal Systems: Physical, Chemical, Biological and Geological Interactions*, *Geophys. Monogr. Ser*., *91*, edited by S. E. Humphris et al., pp. 222–247, AGU, Washington, D. C., 1995.

Von Herzen, R. P., and A. E. Maxwell, The measurement of thermal conductivity of deep-sea sediments by a needle probe method, *J. Geophys. Res*., *64*, 1557–1563, 1959.

Von Herzen, R., and S. Uyeda, Heat flow through the eastern Pacific floor, *J. Geophys. Res*., *68*, 4219–4250, 1963.

Von Herzen, R. P., T. J. G. Francis, and K. Becker, In situ large-scale electrical resistivity of ocean crust, Hole 504B, *Initial Rep. Deep Sea Drill. Proj*., *69*, 237–244, 1983.

Von Herzen, R. P., H. J. B. Dick, and P. T. Robinson, Downhole measurements and physical properties, Hole 735B: Summary and tectonic relationships, *Proc. Ocean Drill. Program Sci. Results*, *118*, 553–556, 1991.

Walsh, J. B., and W. F. Brace, The effect of pressure on porosity and the transport properties of rocks, *J. Geophys. Res*., *89*, 9425–9431, 1984.

Wang, K., J. He, and E. E. Davis, Influence of basement topography on hydrothermal circulation in sediment-buried oceanic crust, *Earth. Planet. Sci. Lett*., *146*, 151–164, 1997.

Wells, J. T., and M. S. Ghiorso, Coupled fluid flow and reaction in mid-ocean ridge hydrothermal systems: The behavior of silica, *Geochim. Cosmochim. Acta*, *55*, 2467–2481, 1991.

White, D. J., and R. M. Clowes, Shallow crustal structure beneath the Juan de Fuca Ridge from 2-D seismic refraction tomography, *Geophys. J. Int*., *100*, 349–367, 1990.

White, D. J., and R. M. Clowes, Seismic attenuation structure beneath the Juan de Fuca Ridge from tomographic inversion of amplitudes, *J. Geophys. Res*., *99*, 3043–3056, 1994.

Wilcock, W. S. D., A model for the formation of transient event plumes above mid-ocean ridge hydrothermal systems, *J. Geophys. Res*., *102*, 12,109–12,121, 1997.

Wilcock, W. S. D., and J. R. Delaney, Mid-ocean ridge sulfide deposits: Evidence for heat extraction from magma chambers or cracking fronts, *Earth. Planet. Sci. Lett*., *145*, 49–64, 1996.

Wilcock, W. S. D., and A. McNabb, Estimates of crustal permeability on the Endeavour segment of the Juan de Fuca mid-ocean ridge, *Earth. Planet. Sci. Lett*., *138*, 83–91, 1996.

Wilcock, W. S. D., S. C. Soloman, G. M. Purdy, and D. R. Toomey, The seismic attenuation structure of a fast-spreading mid-ocean ridge, *Science*, *258*, 1470–1474, 1992.

Wilkens, R. H., G. J. Fryer, and J. Karsten, Evolution of porosity and seismic structure of upper oceanic crust: Importance of aspect ratios, *J. Geophys. Res*., *96*, 17,981–17,995, 1991.

Williams, C. F., T. N. Narasimhan, R. N. Anderson, M. D. Zoback, and K. Becker, Convection in the oceanic crust, Simulation of observations from Deep Sea Drilling Project Hole 504B, Costa Rica Rift, *J. Geophys. Res*., *91*, 4877–4889, 1986.

Williams, D. L., and R. P. Von Herzen, Heat loss from the Earth: New estimate, *Geology*, *2*, 327–328, 1974.

Williams, D. L., R. P. Von Herzen, J. G. Sclater, and R. N. Anderson, The Galapagos Spreading Centre, Lithospheric cooling and hydrothermal circulation, *Geophys. J. R. Astron. Soc*., *38*, 587–608, 1974.

Williams, D. L., K. Green, T. H. van Andel, R. P. Von Herzen, J. R. Dymond, and K. Crane, The hydrothermal mounds of the Galapagos Rift: Observations with DSRV *Alvin* and detailed heat flow studies, *J. Geophys. Res*., *84*, 7467–7484, 1979.

Wolery, T. J., and N. H. Sleep, Hydrothermal circulation and geochemical flux at mid-ocean ridges, *J. Geology*, *84*, 249–275, 1976.

Wyckoff, R. D., H. G. Boset, M. Muskat, and D. W. Reed, Measurement of permeability of porous media, *Am. Assoc. Pet. Geol. Bull*., *18*, 161–190, 1934.

Yang, J., R. N. Edwards, J. W. Molson, and E. A. Sudicky, Three-dimensional numerical simulation of the hydrothermal system within TAG-like sulfide mounds, *Geophys. Res. Lett*., *23*, 3475–3478, 1996.

Zimmerman, R. W., and G. S. Bodvarsson, Hydraulic conductivity of rock fractures, *Transp. Porous Media*, *23*, 1–30, 1996.

Zoback, M. D., and R. N. Anderson, Permeability, underpressures, and convection in the oceanic crust at Deep Sea Drilling Project Hole 504B, *Initial Rep. Deep Sea Drill. Proj*., *69*, 245–254, 1983.

A. T. Fisher, Earth Sciences Department, Earth and Marine Sciences Building, Room A232, University of California, Santa Cruz, CA 95064. (e-mail: afisher@earthsci.ucsc.edu)